Statistical Analysis of Abnormal Phase Shift Quiet Days (APQDs) in Low-/Mid-Latitudes for Solar Cycle 24 (2008–2019)

A thesis submitted to the Department of Physics and
Electronics in fulfillment
of the requirements for the degree of

MASTERS OF SCIENCE

OF

Rhodes University, Grahamstown

BY

Muneeza Ali
(0009-0006-2646-6070)

29 September 2025

DECLARATION

I, Muneeza Ali (23M3644) declare that the thesis entitled

Statistical Analysis of Abnormal Phase Shift Quiet Days (APQDs) in Low/Mid-Latitudes for Solar Cycle 24 (2008-2019)

submitted to the Department of Physics and Electronics, Rhodes University, Makhanda, for the degree of Masters of Science is the work of original research done by myself. I also declare that no material present in the thesis has been published earlier in any manner.

Dedication

This thesis is dedicated foremost to my mother, Mrs. Noor Jehan Muhammad Ali, whose unwavering support, encouragement, and prayers have been a constant source of strength throughout my journey.

I also dedicate this work to my late brother, Moiz Muhammad Ali. His passing during the course of this research was an immeasurable loss, yet by the grace of Allah, I found the strength and perseverance to continue.

To my son, Wafi Salman, your presence has been a guiding light. The joy and inspiration you bring have sustained me and reminded me to move forward with resilience.

I extend this dedication to my aunts, Mrs. Noorbano Shalwani (late), Mrs. Farzana Kabani (late), and Mrs. Yasmin Siddiqui, and to my uncles, Mr. Jamal Hooda and Mr. Farid Kabani, whose kindness and unconditional support have been invaluable and instrumental for reaching this milestone.

To my husband, Mr. Ghulam Murtaza, whose patience, counsel, and steadfast care have been central to my well-being during this journey. I am deeply grateful for your guidance and support, both personal and professional.

I also acknowledge my mentors and inspirational authors — Ms. Ali, Mr. Khan, Dr. Peterson, and Elif Shafak — for their wisdom and guidance, which have enriched both my academic and personal growth.

Finally, I dedicate this work to my dear friends, Dr. Mehwish Shafi Khan, Mrs. Esra Aman, Mrs. Salma Khan and Ms. Arefa Khan, whose thoughtful conversations and shared reflections have deepened my understanding of faith, values, and heritage.

Acknowledgements

All praise to almighty Allah who provided us with the capabilities to progress in our lives and thrive through the lifelong learning process. I humbly express innumerable gratitude for His uncountable blessings and protection upon me throughout my life.

I would like to express my sincere gratitude to all those who contributed, directly or indirectly, to the completion of this project.

First and foremost, I am deeply indebted to my supervisors, Drs. Zama Katamzi-Joseph, Emmanuel Nahayo and Mpho Tshisaphungo, for their encouragement, insightful critiques, patience, and unwavering support throughout this research journey. I am equally grateful to Drs. John Bosco Habarulema, Tshimangadzo Matamba, and Rendani Nndanganeni, for their invaluable guidance, constructive suggestions, and willingness to provide both administrative and intellectual support despite their demanding schedules. Their mentorship has greatly enriched this thesis. I am profoundly thankful to my supervisors and to SANSA for granting me the opportunity to remain at the organization until the completion of my work, to train alongside space weather forecasters, and to witness the professionalism and dedication of the experts. Learning from their knowledge, commitment, and values has been an inspiring and motivating experience.

My sincere thanks also go to my sponsoring officers, Mr. Ghulam Murtaza and Mr. Muhammad Ayyaz Ameen, for their confidence in me and their constant support. I am grateful to SUPARCO/PSWC for providing the funding necessary to pursue my Master's degree, and to Rhodes University for granting me the opportunity to undertake this study. I also wish to acknowledge the cooperation of the Finance Directorate, Academic Office, International Office, Student Fees Office, and the International Student Council.

I extend heartfelt thanks to Mrs. Hester Olivier, Mrs. Sandra Marais, Mrs. Anita Engelbrecht, Ms. Juchelle Ontong, Mr. Keenan Janneker, Dr. Pierre Cilliers and Mr. Clint Fouché. Their warmth, generosity, and thoughtful conversations have left a lasting impact. I am especially grateful to Ms. Juchelle Ontong for her assistance with administrative matters related to Rhodes University, and to Mrs. Hester Olivier for her support with library resources, research papers, and book recommendations, as well as for our enriching and insightful discussions.

Finally, I wish to express my gratitude and appreciation for the friendship and support of Mr. Lehlogonolo Arnold Phasha, Mrs. Salma Khan and family and Ms. Nondumiso Khumalo, whose kindness, hospitality, and companionship sustained me during my stay in South Africa.

Abstract

The solar quiet (Sq) focus position of normal quiet current systems is usually around $\pm 30^{\circ}$ from the magnetic equator. Deformed Sq current vortices observed away from this position may contribute to abnormal phase-shift quiet days (APQDs). Moreover, regional variations, hemispheric asymmetries of neutral winds, conductivities, and non-migrating tides may influence the APQDs. To understand this phenomenon, a statistical analysis of APQDs was conducted for Solar Cycle 24 (SC24: 2008-2019). The study used 1-min magnetic field data from 43 INTERMAGNET geomagnetic observatories between -60° and $+60^{\circ}$ magnetic latitudes in three longitudinal sectors: American, Africa-European, and Asia-Australian. Quiet days were identified by a |SYM-H| $\leq$ 10nT threshold. APQDs were identified in low- and mid-latitudes to shed light on regional, global, and seasonal occurrence rates. Results showed high global and regional APQD occurrences during D season across solar cycle phases in all longitudinal sectors. Moreover, the highest occurrence rate of regional and global APQDs was observed in the Northern Hemisphere's low-latitudes (43.4% & 36.7%) and in the Southern Hemisphere's mid-latitudes (31% and 31.4%), respectively. For hourly distribution of APQDs occurrence rates, mostly in the D season, high rates were observed in the morning (6:30-9:30 SLT) for low latitudes in the Northern Hemisphere and in the afternoon (15:30-16:30 SLT) for mid-latitudes in the Southern Hemisphere. The results showed that the sudden stratospheric warming (SSW) event might have influenced the ionospheric current system on 23 January 2009, most likely shifting Sq foci latitudes to 55°N and 54°S, and causing APQDs at mid-latitude observatories and equatorial observatory MBO.

Key words: solar quiet (Sq) variations, abnormal phase shift quiet days (APQDs), Sq focus, geomagnetic observations.

Acronyms

APQDs	Abnormal Phase Shift Quiet Days
AQDs	Abnormal Quiet Days
BL	Night-time baseline value covering the initial 2 or the last 2 hours centered around local midnight
B_x	X-component of the Solar Wind in the Geocentric Solar Model (GSM)
B_y	Y-component of the Solar Wind in the Geocentric Solar Model (GSM)
B_z	Z-component of the Solar Wind in the Geocentric Solar Model (GSM)
B_t	Total amplitude of the Solar Wind in the Geocentric Solar Model (GSM)
EEJ	Equatorial Electrojet
FAC	Field-Aligned Currents
H	Horizontal component of geomagnetic Field
HSSW	High Speed Solar Wind
ICME	Interplanetary Coronal Mass Ejections
IHFACs	Inter-Hemispheric Field Aligned Currents
IMF	Inter-Planetary Magnetic Field
INTERMAGNET	International Real-time MAGnetic observatories NETwork
LL	Low Latitudes
LT	Solar Local Time

ML	Mid Latitudes
NH	Northern Hemisphere
NQDs	Normal Quiet Days
PSWC	Pakistan Space Weather Centre
QDs	Quiet Days found in individual years of the study
R_E	Radius of the Earth
SC	Solar Cycle
SCV	Single Current Vortex
SH	Southern Hemisphere
SPNF	Super-posed Northward Field
SPSF	Super-posed Southward Field
Sq (H)	Solar Quiet hourly values calculated from the Horizontal component of the geomagnetic field
Sq	Solar Quiet Variations
SUPARCO	Pakistan Space and Upper Atmosphere Research Commission
SYM-H	Symmetric-H Index, which gives a measure of quiet or disturbed levels of the 1-minute geomagnetic field variations
X	Geographic True North component of the geomagnetic field
Y	Geographic True East component of the geomagnetic Field

Table of Contents

List of Tables

List of Figures

Chapter 1

Introduction

The geomagnetic field is a complex and ever-changing phenomenon that plays a vital role in numerous geophysical processes, with profound implications for both scientific research and practical applications. The Earth's magnetic field has two main components: the core field, which originates from the chaotic motion of molten iron within the Earth's outer core, (Mandea et al., 2007), and the external field, primarily generated by dynamic activity within the upper layers of the Earth's atmosphere. The ionosphere (a region of the atmosphere that is ionized by solar radiation) contributes to the variations of the external magnetic field through electric currents engendered by the interplay of charged particles in motion with the Earth's magnetic field. Furthermore, the magnetosphere contributes to the external field variations via magnetospheric currents driven by the solar wind and various space weather phenomena (Heilig & Lühr, 2018). The measured internal field contributes a minor 2-3% derived from the magnetized lithospheric rocks located 10 to 70 kilometers beneath the Earth's surface (Vervelidou, 2013). The complex interplay between the Earth's internal and external magnetic field components culminates in a magnetic environment that is not only fascinating in its intricacy but also vital for a multitude of applications, such as navigation, space weather forecasting, and shielding humanity from the adverse effects of space weather.

In the E-region of the ionosphere (90-150 km), lies a sophisticated dynamo, resulting primarily from extreme ultraviolet radiation (EUV). The energy flux from the EUV drives the atmospheric tides and neutral winds by inducing a transport of ionospheric ions via collisions across the Earth's magnetic field (Olsen & Stolle, 2017; Le Sager & Huang, 2002). This system of currents comprises two vortices, which are centered at $\pm 30^{\circ}$ magnetic latitude and are situated around local noon, exhibiting anticlockwise circulation in the Northern Hemisphere and clockwise circulation in the Southern Hemisphere when observed from an overhead perspective of the ionosphere. These currents manifest in the ground magnetic field data, mainly horizontal (H)/northward (X) component as maximum variation in solar quiet conditions, i.e. $Sq(H)$ or $Sq(X)$ for observatories in low-latitudinal region (magnetic latitude $\leq \pm 30^{\circ}$), and minimum variation in solar quiet conditions, i.e. $Sq(H)$ or $Sq(X)$, for observatories in mid-latitudinal region (magnetic latitude$> \pm 30^{\circ}$) (Olsen & Stolle, 2017). This configuration represents the

ideal Sq schema (Anad et al., 2016). The $Sq(H)$ variations are referred to as Sq throughout the thesis, unless explicitly mentioned when using the X, eastward (Y) and declination (D) components.

Phase shifts of solar quiet (Sq) variations are anomalies in geomagnetic field variation that were reported for the deep minimum phase of solar cycle 24, 2008-2009. The first study to report on these anomalies in regular quiet diurnal geomagnetic variation was conducted by Chapman and Stagg (1929). Subsequent studies on these anomalies were carried out in the years following the International Geophysical Year (IGY) of July 1957 - December 1958 (Price, 1963; Cardus & Romana, 1962; Yacob & Sen, 1974; Rourke, 1964; Takeda & Yamada, 1989; Malin & Gupta, 1977; Matsushita & Maeda, 1965; Campbell et al., 1989; Feldstein & Zaitzev, 1968). During the International Quiet Solar Years (IQSY) between 1964 and 1965, some studies reported anomalies in the magnetic field variations, especially on days when the magnetic activity was very quiet, due to perturbations in the ionospheric dynamo region (McKenna, 1965; Price, 1963; Pomerantz, 1964).

Such anomalies in the magnetic field as reported by the earlier studies were further analyzed in the decades following the IQSY. Brown and Williams (1969) conducted an initial study that reported on the anomalous variations in the H- or X-component of the quiet geomagnetic field in the mid-latitudinal region. This study laid the foundation for the study of abnormal quiet days both in phase shifts and amplitude variations, coining the phrase abnormal quiet days (AQDs). Abnormal phase-shift quiet days (APQDs) are the phase shifts observed outside the time range of the regular or normal quiet-day (NQD) variations of the H-component of the geomagnetic field data (Butcher, 1989; Vichare et al., 2012). In this study, only days with phase shifts observed one hour outside NQD variations were considered as APQDs. APQDs are attributed to many mechanisms, such as the complex interchange and coupling of the different layers of the atmosphere due to neutral winds and plasma motions. The atmospheric migrating and non-migrating tides, planetary waves, sudden stratospheric warmings (SSWs), counter electrojets (CEJ), singular current vortex (SCV), superposed northward/southward fields (SPNF/SPSF) were initially reported by Campbell (2012) and the references therein. A compendium of the studies of the past 75 years, featuring all possible causes of the E-region current abnormalities impacting the geomagnetic field variations, was compiled in Yamazaki and Maute (2017). In the decades following IQSY, limited, yet notable, research was undertaken to distinguish such phase-shifts and anomalous amplitude variations of the quiet daily variation from the geomagnetic field data in the low- and mid-latitudinal region. These pertained to anomalies in E-region conductivity and used focused phases of the solar cycle (Anad et al., 2016; Santos et al., 2017; Erick et al., 2016; Hwang et al., 2012). Some abnormal phase-shifts have been reported for some selected longitude sectors (Bello et al., 2014; Bolaji et al., 2015; Shinbori et al., 2017; Archana & Arora, 2022; Archana et al., 2023). Similarly, APQDs have been studied

for specific seasonal or yearly trends (Bhardwaj et al., 2015; Echer et al., 2011; Ugwu & Okeke, 2021; Falayi, 2014; Shinbori et al., 2014; Santos et al., 2022; Morozova et al., 2020; Schnepf et al., 2018; Vichare et al., 2012; Love & Rigler, 2014).

The magnetic meridian effects and the invasion of the Southern Hemisphere in the Northern Hemisphere during the quietest days are anomalous irregularities reported by Mayaud and IAGA (1967). The synopsis, titled 'Atlas of K-indices', was the guiding aid for the derivation of the K-indices for local observatories. This guide elaborates on how such irregularities can affect the accuracy of calculations for the local observatory's magnetic activity levels in the form of K-indices, thus causing errors in the calculation of Sq variations. Knowledge of such irregularities and the ability to recognize such irregular features from magnetograms were crucial for absolute measurement observers and geomagnetic observatory custodians who calculated the K-indices by means of analogue geomagnetic field records. This study led to different research attempts to explain such irregularities. They were attributed to asymmetry in heating and conductivities in the E-region of the ionosphere, diurnal and semi-diurnal tides, neutral winds, and electric fields, longitudinal differences in sunrises and sunsets, and seasonal inequality, which caused additional mid-latitudinal currents to flow between both hemispheres (Van Sabben, 1970; Wagner et al., 1980; Richards & Torr, 1986). However, the overall solar cycle and seasonal trends of APQDs have not been studied extensively for solar cycle 24, and specifically not for the categorization of local, regional, and global variations of such abnormal phase shifts. It was suggested by Stening (1989) that APQDs may be caused by asymmetry of hemispheres in the solstices and equinoxes. While the north-south asymmetry in the Sq current system is well-documented, it is important to consider the broader context of solar and geomagnetic influences. The asymmetry is not only a result of current solar and geomagnetic conditions, but also reflects long-term solar cycles and the inherent asymmetries in the Earth's magnetic field. Therefore, this study attempts to conduct a statistical analysis of APQDs with respect to seasons, different longitudinal sectors, and hemispheres for all years of solar cycle 24 (2008-2019). Moreover, analyses of magnetically conjugate stations having a relatively higher number of APQDs have been undertaken for different phases of the solar cycle in order to understand the seasonal asymmetry of the hemispheres during different phases of the solar cycle.

There is currently no clear definition of and methodology to characterize these APQDs and determine seasonal and solar cycle trends with respect to latitudinal/longitudinal and hemispheric variations. This study aims to clearly devise and adopt a consistent method to identify the APQDs in low- and mid-latitudinal regions and to discover global characteristics of their trends and behaviors during the different phases of the solar cycle.

1.1 Research Motivation

According to Soloviev et al. (2019), under quiet regular geomagnetic conditions, the Sq foci appear mostly at positions of around positions of $\pm 30^{\circ}$ magnetic latitude. Earlier studies on APQDs revealed major deviations from standard Sq foci positions (Hasegawa, 1960; Butcher, 1982) because these abnormal periods of phase-shifts display variations in the current dynamics of the ionospheric and atmospheric systems, as observed in geomagnetic field records near Sq foci positions (Campbell, 2012; Bhardwaj et al., 2015; Morozova et al., 2020).

The Sq pattern fails to demonstrate any form of predictability during quiet geomagnetic days. According to statistical analysis by Chen et al. (2007), the daily range of meridian chain ground magnetic field measurements more than doubles for successive days, especially in the low-latitudinal region, which responds to small E-region wind changes. 70–80% of the total variability now originates from lower-atmospheric forces, including tides, non-migrating tides, planetary waves, and gravity waves that modify the dynamo electric field as they ascend through the atmosphere. The remaining portion of the variance is caused by small fluctuations in solar EUV radiation that influence daytime conductivity. Some portion of the influence of the equatorial electrojet (EEJ) on Sq was first analyzed by Forbes (1981), followed by statistical studies by Stening (1995), which confirmed that these controlling factors influence the Sq variation. Recent modeling demonstrates that meteorological input also creates randomness in the daily Sq morphology (Yamazaki et al., 2016; Takeda, 2016).

The Sq current vortex shows an asymmetric pattern in the quiet-time ionospheric dynamo that positions its foci at different latitudes between the solstice months of the summer and winter hemispheres. The north–south difference in Sq patterns was found to cause the southern Sq vortex to lag behind the northern vortex by as much as 60° (Van Sabben, 1964). It was first documented by Van Sabben (1966) that meridional currents dominate from south to north in the low- and mid-latitudinal regions due to potential difference at the Sq foci in both hemispheres. These currents were later named as inter-hemispheric field-aligned currents (IHFACs) (Fukushima, 1979). Satellite and magnetometer-chain reconstructions show that the intensity and latitude of the foci follow the E-region conductivity peaks that occur during seasonal solar illumination and neutral-wind tidal alignment. The Sq amplitude reaches its highest value near the June and December solstices before decreasing during equinox periods in most longitudinal sectors, yet its pattern depends on local time and longitude, because tides produce time-dependent changes in dynamo efficiency (Pedatella et al., 2011). The observed seasonal changes in Sq amplitude and phase are explained by tidal effects, in addition to Hall-to-Pedersen conductivity variations, especially in the SAA region, according to spherical harmonic analysis (Takeda, 1990; Yamazaki & Maute, 2017; Owolabi et al., 2022).

The Sq system expands and contracts over an 11-year period during the solar cycle. Observations at 69 sites from 1947 to 2013 showed that Sq daily variation expands by 30-50% throughout solar minimum to solar maximum, while the peak occurs two years after F10.7 flux reaches its highest point (Shinbori et al., 2014). The increased ionospheric electron density and conductivity, which result from higher EUV irradiance during solar maxima, drive these changes along with stronger thermospheric winds. The dynamo exhibits only weak longitude-dependent changes in current foci latitude, while solar activity has a minimal effect (Shinbori et al., 2017). The solar quiet reference field (SQRF) model has been used as an empirical tool to study observed amplitude changes, while demonstrating the problem of limited solar cycle data for distinguishing between solar and Earth's main field variations (Chen et al., 2021).

The different methodologies to calculate solar quiet variation often missed non-cyclic corrections. The incorrect selection of baselines to subtract hourly values and medians instead of corrected averages often resulted in inaccurate calculation of Sq variation. The application of smoothing techniques resulted in imprecise statistical variations due to erroneous calculations of the times of phase-shifts. The selection of quiet days was often determined by popular usage of international quiet days (IQDs) and the use of different thresholds of planetary indices may not have been successful in determining extremely quiet days when APQD phenomena were more likely to occur.

The statistical investigation of seasonal effects on APQDs throughout a complete solar cycle across the Northern and Southern Hemispheres and longitudinal sectors remains insufficiently explored, as is the influence of EEJ on APQDs. Moreover, it is hard to find in the existing literature, seasonal, hemispheric, latitudinal and longitudinal trends of APQD occurrences for an entire solar cycle. APQDs can also be explained by the impact of distortion of Sq current vortices (Chen et al., 2007); however, the extent of the impact of this mechanism has not been fully quantified for different phases of the solar cycle.

1.2 Aims and Objectives of the Study

The aim of this study is to statistically analyze APQDs in each phase of solar cycle 24, using global ground-based magnetic observatory data. In addition, the study investigates the extent to which the quiet time ionospheric or magnetospheric currents play a role in causing or influencing APQDs. The comprehensive objectives emanating from the stated aims are:

1. To establish an accurate methodology to identify APQDs from ground-based magnetometer data;

2. To report occurrence rates at an equal number of observatories in each hemisphere and,

statistical results of longitudinal and global occurrences of APQDs based on Lloyd's seasons for solar cycle phases;

3. To establish seasonal occurrence rates of time distributions of APQDs in comparison with NQDs, by using conjugate magnetic observatories in both hemispheres for every solar cycle phase;

4. To report APQD occurrence rates in every solar cycle phase for magnetic latitude and geographic longitude observatories at an equal number of observatories in both hemispheres (low- and mid-latitudinal regions);

5. To calculate Sq foci positions during minimum and maximum phases of solar cycle 24 in order to compare and ascertain the variational trends of APQDs and statistical determination of Sq foci position offsets from ideal Sq schema for both hemispheres;

6. To report on examples of deformations in the Sq current systems and IHFACs that contribute to APQDs observed in Sq field at highest Sq foci positions during minimum and maximum phases of solar cycle 24, as well as on normal Sq foci latitudes at $\pm 30^{\circ}$ in both hemispheres.

1.3 Thesis Layout

This thesis consists of 5 chapters. Chapter 2 offers a literature review of space weather and solar activity, its phases, solar cycle 24, the solar wind, the ionosphere, the current systems generated by the E-region dynamo (Sq and EEJ) and their driving mechanisms, the magnetosphere and its impact on ionospheric currents, the IHFACs, the geomagnetic field and the self-sustaining dynamo mechanism, normal Sq variations and the abnormal behavior of the quiet magnetic field variations. Deformation types in the Sq current system and irregular movement of the Sq foci, which particularly influence the APQDs, are also discussed in Chapter 2. Chapter 3 describes the geomagnetic field components, instruments used for the monitoring of magnetic field variations, INTERMAGNET and data selection from various observatories. Geomagnetic indices, particularly the SYM-H index, its derivation and usage are briefly described. The method that was used to define and quantify APQDs by means of geomagnetic observatory data is explained in detail. Furthermore, the distribution of longitudinal sectors and the separation of solar cycle phases, the use of the SYM-H Index in the determination of quiet days, and methods for statistical analyses of the solar cycle phases are also mentioned. Chapter 4 presents the main results of the statistical analysis. The analyses of significant findings are discussed in Chapter 5 alongside conclusions and recommendations for future work.

Chapter 2

Literature Review

2.1 Introduction

The purpose of this comprehensive literature survey is to examine the complex interactions between solar activity, ionospheric dynamics, and geomagnetic parameters. The focus will be on the role of the E-region dynamo in generating electric currents, on the various perturbations in the dynamo of the ionospheric current system caused by a variety of factors, and on their manifestation in ground magnetic observatory data. It evaluates the effect of solar phenomena under quiet conditions on quiet-time Sq currents, uncovering both typical and atypical variations. The normal and abnormal quiet day variations are introduced with examples, and the influence of Sq foci positions is evaluated. The influence of external factors such as tidal forces and magnetospheric processes on geomagnetic behavior is also briefly addressed. A brief historical overview of advancements in this field is provided, along with contemporary modeling techniques that were used in earlier studies to predict current variation as observed in ground observations.

2.2 Space Weather

"Space weather" refers to conditions on the Sun and in the solar wind, magnetosphere, ionosphere, and thermosphere that can influence the performance and reliability of spaceborne and ground-based technological systems and can endanger human life or health. Adverse conditions in the space environment can cause disruption of satellite operations, communication, navigation, and electric power distribution grids, leading to a variety of socio-economic losses (Moldwin, 2008).

Space weather encompasses a variety of phenomena resulting from solar activity that can significantly impact Earth's geomagnetic environment. The interaction between solar wind and Earth's magnetosphere plays a crucial role in shaping space weather events. Variations in the interplanetary magnetic field (IMF), along with changes in the velocity and density of the

solar wind, are key factors controlling geomagnetic field fluctuations, especially in high-latitude zones such as the polar cap (Levitin et al., 1982). These interactions can lead to geomagnetic disturbances, which are particularly pronounced during periods of heightened solar activity.

Space weather effects, most notably geomagnetic storms, are primarily driven by solar activity such as solar flares, interplanetary coronal mass ejections (ICMEs) and high speed solar wind (HSSW), which influence the ionosphere and geomagnetic fields. ICMEs are large-scale magnetized plasma expulsions in interplanetary space that correspond to coronal mass ejections launched from the solar corona and measured by spacecraft in situ (Temmer, 2021). Coronal mass ejections that become ICMEs are frequently associated with filament/prominence eruptions, coronal restructuring, and sometimes flares; their solar origins determine composition and initial kinematics (Kilpua et al., 2017). HSSW are fast solar wind flows that originate from open magnetic-field regions (coronal holes) on the Sun and propagate into the heliosphere, often persisting for multiple solar rotations and corotating with the Sun (Cranmer, 2009; Temmer, 2021). When these fast streams overtake preceding slower wind, they produce stream interaction regions (SIRs) that can steepen into corotating interaction regions (CIRs) with enhanced density, magnetic field strength, and wave activity (Cranmer, 2009; Richardson, 2018). Open-field regions in the solar corona (coronal holes) are the principal sources of high-speed streams; the geometry and expansion of open flux determine stream speed and structure (Cranmer, 2009; Temmer, 2021; Richardson, 2018).

The impact of these space weather events varies with latitude, affecting ionospheric electron densities, electric fields, and geomagnetic currents. In low-latitudinal regions, effects such as ionospheric disturbances, variations in the equatorial electrojet (EEJ) and prompt penetration electric fields (PPEF) and disturbance dynamo electric field (DDEF) are observed. PPEF is a key driver of ionospheric disturbances at low-latitudinal regions. These fields can cause rapid increases in ionospheric plasma during daytime, with opposite effects at night (Vasyliūnas, 1970; Blanc & Richmond, 1980; Shahzad et al., 2023; Calabia et al., 2022). Geomagnetic storms can cause both positive and negative ionospheric storms at low-latitudinal regions, characterized by increases or decreases in electron density. These changes are influenced by electric fields penetrating from the magnetosphere, which can alter the F-region density profiles due to recombination rate variations with altitude (Veenadhari & Alex, 2006). The strength of the EEJ, a current flowing eastward in the equatorial ionosphere, is affected by storm-time electric field changes. This can lead to significant ionospheric responses, such as the expansion of the equatorial ionization anomaly (EIA) crest to higher latitudes during the main and recovery phases of storms (Shahzad et al., 2023).

Overall, space weather's impact on Earth is multifaceted, involving complex interactions between solar activity, ionospheric dynamics, and geomagnetic field parameters. Understanding

these interactions from baseline effects of tranquil terrestrial conditions is crucial for predicting and mitigating adverse effects on technological systems and human activities reliant on stable geomagnetic conditions.

2.3 Solar Activity

Solar activity and the solar cycle are fundamental aspects of space weather that significantly influence the ground geomagnetic field parameters and ionospheric dynamics. Solar activity is primarily driven by the solar cycle, an approximately 11-year cycle characterized by changes in the number of sunspots on the Sun's surface. Sunspots are regions of intense magnetic activity that are found in greater numbers during the maximum phase of the solar cycle. Sunspots are mostly associated with ICMEs, solar flares, and highly energetic particles such as protons or electrons that can interact with the Earth's magnetosphere and affect the ionosphere. In the minimum phase, the sunspots tend to be fewer to none (Moldwin, 2008).

The solar cycle is defined as a quasi-periodic variation with an average period of about 11 years, most easily observed by means of sunspots. The cycle is characterized by a sharp rise from solar minimum to maximum, followed by a gradual decline, with the rise phase typically lasting 3-6 years and the decline phase 5-8 years (Javaraiah et al., 2012; Hathaway, 2015). During the ~11-year solar cycle, the polarity of the Sun's magnetic field reverses. As the magnetic reversal takes place twice in two solar cycles, the Sun's full magnetic cycle is 22 years long. It is known as the "Hale" cycle, when the Sun's large-scale magnetic field configuration is repeated. The solar cycle consists of 4 phases, namely, minimum, ascending, maximum, and descending phases, with each phase lasting approximately 2 to 4 years (Krainev & Webber, 2004; Driel-Gesztelyi & Owens, 2020; Martin, 2024).

2.3.1 Phases of the Solar Cycle (SC)

The phases of the solar cycle are briefly described in the following subsections.

2.3.1.1 Solar Minimum

The solar minimum marks the beginning and end of a solar cycle and is characterized by a minimum number of sunspots and less solar flare activity, confined mostly to the B and C-class (Chertok & Belov, 2017) flares. The magnetic field of the Sun is very stable at this time, and the frequency of solar flares and ICMEs are typically at a minimum. The heliospheric current sheet flattens, leading to a more uniform solar wind. Despite the dominance of solar quietness, space weather can still be affected by HSSW from coronal holes (Hathaway, 2015; Owens &

Forsyth, 2013).

2.3.1.2 Ascending Phase

The increasing or rising phase is a period of intensifying solar activity. The number of sunspots increases as the solar magnetic field grows more complex and dynamic. The interplanetary magnetic field strengthens, and geomagnetic storms become more frequent on Earth. This period shows a change in solar dynamism, with magnetic flux emerging more forcefully across the solar surface (Pesnell, 2008).

2.3.1.3 Solar Maximum

The solar maximum is when activity in the cycle peaks. It is the period when the number of sunspots are at a maximum with frequent solar flares and ICMEs. This results in the formation of intensely magnetically active regions, with flare intensity increasing to M and X-class (Hady et al., 2015). The Sun's magnetic poles reverse during this period, a characteristic of the magnetic dynamo process. The strong ultraviolet and X-ray emissions profoundly affect the upper Earth's atmosphere, resulting in ionospheric disturbances and enhanced satellite drag. Solar radiation storms are also more dangerous for space-based systems and astronauts (Hathaway, 2015; Schwenn, 2006).

2.3.1.4 Descending Phase

After the maximum, the declining or decreasing phase is characterized by the continuous decrease in sunspot numbers and solar activity. The occurrence and magnitude of flares and ICMEs decrease, and the Sun's magnetic field starts organizing towards the next polarity reversal. Coronal holes again become the main source of solar wind. Nevertheless, the decreasing geomagnetic activity is still high because of continuous HSSW (Gopalswamy, 2006; Owens & Forsyth, 2013).

2.3.2 Solar Cycle 24

The numbering of solar cycles began with the work of Rudolf Wolf in the mid-19th century. Wolf, a Swiss astronomer, was instrumental in establishing a systematic approach to recording the number of sunspots, which is a key indicator of solar activity. He introduced the concept of the relative sunspot number and organized regular observations, which allowed for the identification and numbering of solar cycles. He analyzed historical data and established the 11-year periodicity of solar activity, which is now known as the Schwabe cycle (Clette et al.,

2014).

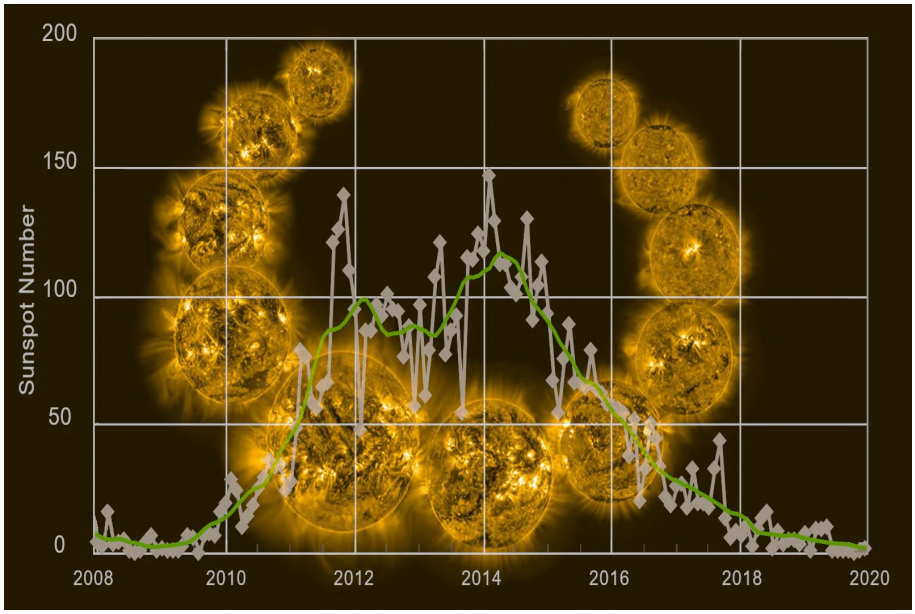

Figure 2.1: The image shows how solar cycle 24 progressed, with respect to increasing sunspot numbers, towards maximum phase and the gradual decline towards minimum phase. In the background, Europe's PROBA2 satellite (payload: SWAP extreme UV imager) took 11 snapshots of the progression of solar cycle phases corresponding to sunspot numbers. Source: https://www.theweathernetwork.com/en/news/science/space/what-are-the-northern-lights-what-causes-them-and-where-can-they-be-seen.

The first numbered cycle, solar cycle 1, was identified to have started in 1755 and prevailed till 1766. This retrospective identification was based on Wolf's analysis of historical sunspot records (Vasiljeva & Pishkalo, 2021). This systematic approach to numbering solar cycles has continued to the present, allowing for a clearer understanding of solar activity (Wickramasinghe et al., 2017).

Figure 2.1 shows the progression of solar cycle 24, which commenced in December 2008 and concluded in December 2019. The maximum phase of solar cycle 24 occurred in April 2014, when the maximum number of sunspots was 121 per day. The minimum number of sunspots was 4 per day in December 2019 (Kaplan, 2024). The criteria and distribution of the solar cycle 24 into phases for undertaking this study has been elaborated in Chapter 3 and depicted in Figure 3.7 .

2.4 Solar Wind and Interplanetary Magnetic Field (IMF)

Solar wind is a stream of charged particles released from the upper atmosphere of the Sun, known as the corona (Raouafi et al., 2021). This plasma consists primarily of electrons, protons, and alpha particles with kinetic energies ranging from 0.5 to 10 keV (Schwenn, 2006). The

outflow occurs because the high coronal temperatures above one million K provide sufficient kinetic energy to allow particles to escape the Sun's gravitational pull, (Parker, 1958). The solar wind plays a crucial role in shaping the heliosphere and influencing space weather phenomena.

The interaction between solar wind and Earth's magnetosphere results in various geomagnetic effects. The magnetic field components on Earth's surface can be quantitatively related to solar wind plasma parameters by means of regression analysis methods (Feldstein & Levitin, 1986). These interactions are vital for understanding geomagnetic storms and their impacts on technological systems.

The interplanetary magnetic field (IMF) extends the influence of the solar magnetic field throughout the solar system through the solar wind. The IMF exists as three components, which the scientific community describes by means of B_x, B_y, and B_z measurements in geocentric solar magnetospheric (GSM) or geocentric solar ecliptic (GSE) coordinates. The B_x component is the radial component, which represents the magnetic field strength of the IMF in the direction away from or towards the Sun. The B_y, east-west component, exists within the ecliptic plane because it shows the spiral structure that solar rotation creates in the IMF. The north-south component, B_z, plays a crucial role in geomagnetic activity because a southward (negative B_z) direction enables magnetic field reconnection with Earth, which can lead to geomagnetic storms. The total magnetic field strength (B_t) can be defined as:

$$\mathrm{B_t} = \sqrt{\mathrm{B_x^2} + \mathrm{B_y^2} + \mathrm{B_z^2}}.$$

B_t functions as an indicator of the total magnetic field strength that the solar wind transports.

The solar wind interacts with the magnetic field of Earth through its magnetic field components, B_x, B_y, B_z and B_t components. During calm intervals, the IMF maintains its stable spiral structure as IMF B_z shows minimal fluctuations around zero while B_t remains at low values of 4 and 6 nT near the Earth, which leads to stable geomagnetic conditions (Gonzalez et al., 1994). The IMF B_z shifts to a southward direction during disturbed periods, which includes high-speed stream arrivals and ICMEs, thus enabling solar wind plasma to connect better with Earth's magnetosphere through magnetopause magnetic reconnection (Gonzalez et al., 1994; Tsurutani et al., 1988). The northward orientation of the IMF B_z results in reduced geomagnetic activity because reconnection rates are suppressed (Tenfjord et al., 2017). The increase in B_t (10 to 20 nT or more) generates plasma convection, increasing geomagnetic disturbances (Tenfjord et al., 2017). B_x and B_y variations control the entry directions of the solar wind structures upon interaction with the magnetosphere, which determine space weather outcomes and affect radiation belt dynamics and ionospheric current behavior (Tsurutani & Lakhina, 1997). The

accurate prediction of geomagnetic storm intensity depends on understanding how IMF vector components modulate solar wind dynamics.

2.5 Ionosphere

The ionosphere is an ionized plasma region of Earth's upper atmosphere, extending from about 50 km to 1,000 km above the surface of the Earth. It plays a significant role in atmospheric electricity and affects radio wave propagation. The solar radiation, particularly the ultraviolet (UV) and the X-rays, ionize the neutral atmospheric gases, forming the positive ions and free electrons (Chemin, 2023). Different layers are formed due to altitude-specific ionization processes. The D-region (50 to 90 km) is the lowest layer formed by the solar X-rays. The E-(Kennelly-Heaviside Layer) and F-regions extend from 90 to 150 km and 150 to about 500 km, respectively. Both regions are primarily affected by the UV radiation (Nicholls, 1993; Eshtemirovich et al., 2023).

2.5.1 Current Systems in the Ionosphere

Ionospheric currents are the main source of the regular geomagnetic field variation of a few tens of nT as discerned from ground observations. There are different current systems within the ionosphere, as shown by Figure 2.3. These systems are the EEJ, Sq currents, auroral electrojets, and field-aligned currents (FACs). The amplitude and phase variations are characterized by the solar quiet (Sq) variations, which depend on solar local time (SLT). Sq is a quiet diurnal variation because it is only prominent in geomagnetic field records when disturbances driven by the solar wind are absent. The Sq variations are also known as solar regular (Sr) variations. (Yamazaki & Maute, 2017).

Ionospheric currents are generated when there is a disparity in drift velocities between electrons and positive ions when these charged particles collide with neutral gas molecules. This process leads to an accumulation of space charge with polarization electric field ($\vec{\mathbf{E}}$), resulting in a total electric field $\vec{\mathbf{E}}_t = \vec{\mathbf{E}} + \frac{\vec{\mathbf{U}}\times\vec{\mathbf{B}}}{c}$, where $\vec{\mathbf{U}}$ is the velocity of neutral gas, $\vec{\mathbf{B}}$ is the Earth's magnetic field and c is the speed of light (Hall, 1966).

The ionospheric wind dynamo is responsible for the generation mechanism of Sq variations. Yamazaki and Maute (2017) describes the ionospheric wind dynamo theory. The ionosphere's dynamo region spans the area at an altitude between 90 and 150 km (E-region), where ion-neutral collision rates match or exceed ion gyro-frequency, but electron-neutral collisions remain much slower than electron gyro-frequency. The magnetic field lines trap electrons, while ions follow neutral wind movements. The plasma bulk motion results from ion-neutral collisions. The

ionospheric wind dynamo, also known as the E-region dynamo, operates primarily through the interaction between solar radiation and neutral particles. Solar activity influences the ionosphere by increasing ionization levels during daylight hours, which enhances conductivity. This increased conductivity is essential for sustaining the dynamo as it facilitates the generation of currents within the ionosphere (Baker & Martyn, 1953).

Assuming a magnetized plasma at steady state (under consideration of only origins of aeronomic or external processes, which dismiss local dynamical terms), the neutral particles collide with plasma to drive electric currents under the influence of the geomagnetic field (**B**), flowing with a plasma flow velocity (**V**). The electric field (**E**) generated is defined by equation 2.1:

$$\mathbf{E} = -\mathbf{V} \times \mathbf{B}. \tag{2.1}$$

As **E** is not curl-free, then according to Faraday's law, the curl of the field according to magnetic perturbations b arising from the main field of Earth is:

$$\nabla \times \mathbf{E} = \frac{-\delta \mathrm{b}}{-\delta \mathrm{t}}. \tag{2.2}$$

Magnetic perturbations related to ionospheric currents (**J**) can also be expressed in the form of Ampere's law:

$$\nabla \times \mathrm{b} = \mu_0 \, \mathbf{J}. \tag{2.3}$$

where μ_0 is the vacuum permeability.

The steady state assumption can be valid for a global ionospheric model. Ohm's law for steady state current density **J** is shown in equation 2.4:

$$\mathbf{J} = \sigma\big(\mathbf{E} + \mathbf{U} \times \mathbf{B}\big). \tag{2.4}$$

where **U** is the neutral wind velocity, **E** is the electric field, **B** is the Earth's magnetic field, and σ is a finite anisotropic conductivity tensor in partially ionized plasma with abundant collisions depicting the terrestrial ionosphere.

The ionospheric region has anisotropic conductivity tensors. The one parallel to the geomagnetic field is called parallel conductivity ($\sigma_{||}$) and is driven by the parallel electric field component ($\mathbf{E}_{||}$). The perpendicular currents ($\mathbf{E}_{\perp}$) in the orthogonal direction to **B** is called Pederson's conductivity (σ_P), while Hall's conductivity (σ_H) is perpendicular to both **B** and **E**. Parallel conductivity is of much greater magnitude than perpendicular conductivities. This causes electric currents to organize and distribute according to the geomagnetic field.

Ohm's law thus can be re-stated as:

$$\mathbf{J} = \sigma_{||}\mathbf{E}_{||} + \sigma_P(\mathbf{E}_\perp + \mathbf{U}\times\mathbf{B}) + \sigma_H\frac{\mathbf{B}}{|\mathbf{B}|}\times(\mathbf{E}_\perp + \mathbf{U}\times\mathbf{B}). \tag{2.5}$$

Equation 2.5 is central to describing the ionospheric wind dynamo, associating winds, electric currents, electric fields, conductivities, and relevant current systems. The dynamo model can be used to depict wind distributions by calculating electric fields and currents, and can further predict upper atmospheric properties.

The above-mentioned process is illustrated by Figure 2.2 adapted from Vasyliūnas (2012).

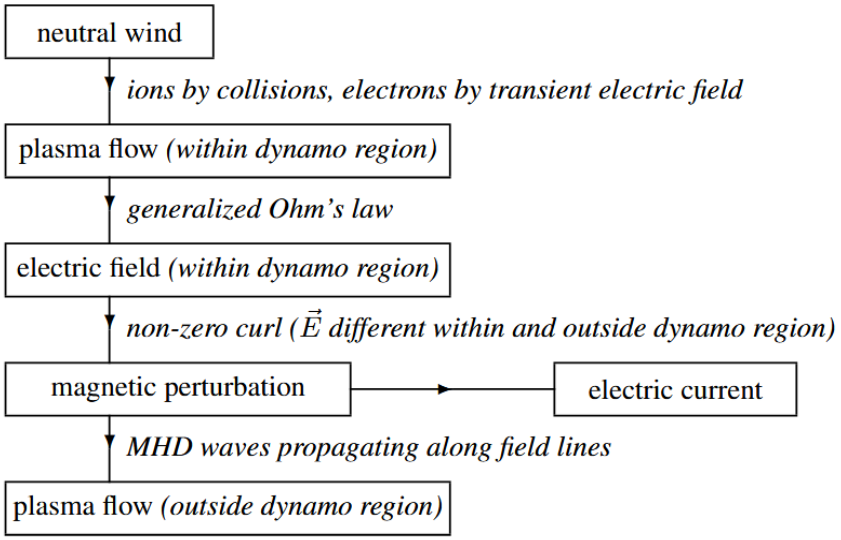

Figure 2.2: The diagram shows the development of the neutral wind ionospheric dynamo. Diagram source: Vasyliūnas (2012).

2.5.2 Solar Quiet (Sq) Current System

Sq current variations are a significant current system of the ionospheric E-region dynamo in the low- and mid-latitudinal regions. The amplitude and phase variations of the geomagnetic horizontal component on a quiet day result from the current system in the E-region dynamo.

Despite the limited studies on Sq anomalies, in-depth research on Sq variations has significantly improved the understanding of baseline determination for geomagnetic indices (Gjerloev, 2012), the electrodynamics of the ionosphere, ionospheric interaction of the lower atmosphere with the magnetosphere (Richmond, 1995), solar radiation monitoring (Svalgaard, 2016), and internal electrical conductivity (Campbell et al., 1998; Okeke & Obiora, 2016; Abbas et al.,

2019).

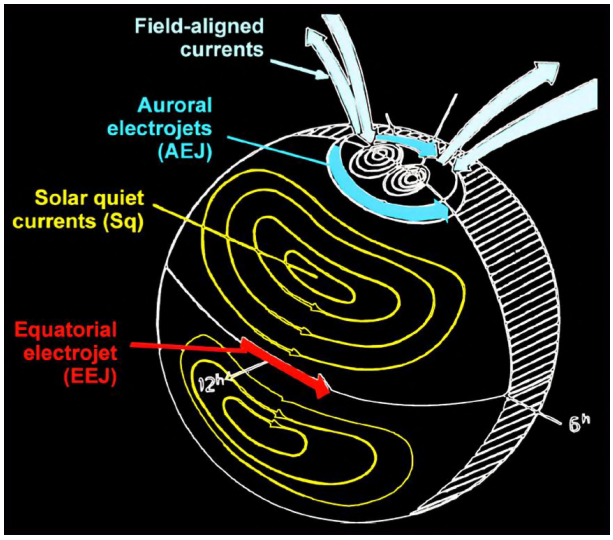

Figure 2.3: Illustration of all ionospheric currents. The simple geometry of the Sq current system is depicted, which is the source of the regular or normal quiet variations of the geomagnetic field. The direction of the Sq currents in each hemisphere is shown by arrows. Image source: Maus (2016), https://cedarscience.org/sites/default/files/workshops/2016/igrf-2016.pdf.

Understanding a two-dimensional equivalent current system flowing in a spherical thin shell at 110 km is pertinent to interpreting the diurnal quiet variations recorded in ground magnetometer data. The thin shell configuration in Figure 2.3 depicts the horizontal span of the Sq current system as being approximately 20,000 km (size of the dayside Earth), while the vertical span is close to 100 km (Yamazaki & Maute, 2017). Figure 2.4 depicts the shape of the Sq current systems that form two vortices, counterclockwise and clockwise in the Northern and Southern Hemispheres, respectively, for solar minima and maxima. The central point of the Sq current systems forms the focus, which records the least variations in Sq, such that ΔH (similar to calculation of $Sq(H)$) crosses the zero value axis before changing direction. This shows that the observatory is either close to the Sq focus or directly underneath it. The Sq current system can be derived from observed Sq diurnal variations on the Earth's surface using geomagnetic field measurements and potential theory (Shiraki, 1973).

The E-region dynamo, which depends on direct solar irradiation, powers these cells; thus, the current systems are concentrated on the day-side. The Sq currents receive strong modulation from atmospheric tides because they are coupled to the neutral atmosphere in the dynamo region. The Sq currents experience their primary control from the 24-hour tide, which operates as the main driver among the global-scale oscillations that include 24 hours, 12 hours, 8 hours, 6 hours, and their subsequent harmonics (Maeda, 1955; Kato, 1957; Lindzen & Chapman, 1969). The tropospheric infrared radiation absorption, together with stratospheric ozone absorption, leads to upward-propagating tides through latent heat release. These waves grow exponentially as they propagate upwards until they reach the dynamo region, where they develop horizontal

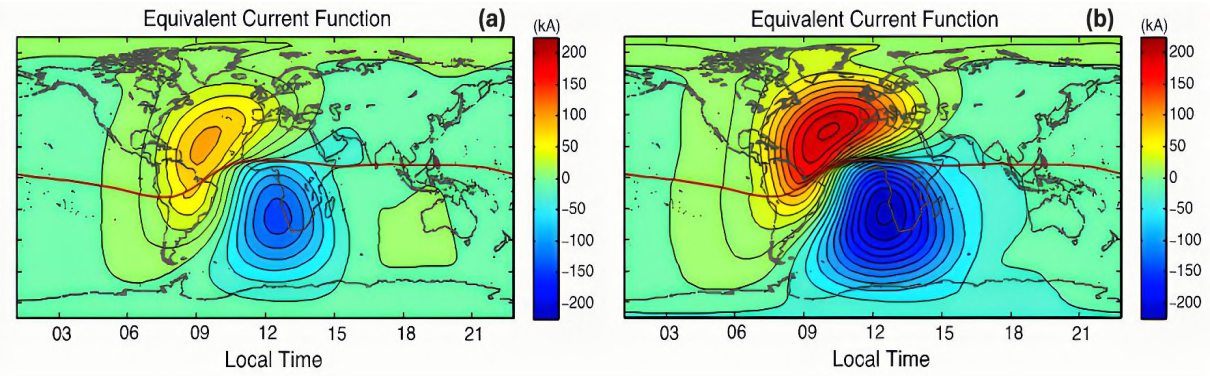

Figure 2.4: Sq current systems are depicted with equivalent current functions at 110 km altitude, forming two vortices counterclockwise and clockwise, in the Northern and Southern Hemispheres, respectively, in kA, as simulated by the TIE-GCM model for a magnetically quiet ($K_p = 0$) equinox condition at 12:00 UT for (a) solar minimum (b) and solar maximum phases. Image source: Yamazaki and Maute (2017).

wind amplitudes exceeding several tens of meters per second. The upward propagating tides generate one-third of the total Sq currents (Yamazaki and Richmond, 2013; and Yamazaki et al., 2014). The Sq current system produces distinct spectral peaks at 24h, 12h, 8h, and 6h, which can be observed in the magnetometer measurements of the mid-latitudinal regions (Campbell, 2003).

Sq current systems exhibit considerable day-to-day fluctuations in shape, amplitude, and phase. For instance, in the mid-latitudinal regions, the amplitude during a period of low solar activity can vary up to 30 percent from the average amplitude during a period of intense solar activity (Butcher & Brown, 1981b). The shape of the day-to-day variation for a number of observatories in the Northern and Southern Hemispheres indicates the magnetic observatory's location in relation to the Sq foci (underneath the Sq focus or at low- or mid-latitudinal regions). More detail is given in Section 2.8. The highly variable Sq amplitudes on consecutive quiet days seem to be dependent on winds and tides in the neutral atmosphere. For more information, studies by Kawano-Sasaki and Miyahara (2008), Jin et al. (2011), Fang et al. (2013), and Yamazaki et al. (2014) may be consulted.

The ionosphere shows a direct correlation between its conductivity levels and solar activity. This affects the amplitude and the focus position of the Sq current cells. The Sq amplitudes and conductivity are typically two times larger during solar maximum than during minimum (Takeda, 1999) as shown by Figure 2.4. In fact, the amplitude is linearly correlated with solar proxies like F10.7 (Yamazaki & Maute, 2017). Furthermore, the 24h, 12h and 8h Fourier components of the amplitude show a strong dependence on F10.7. The same relationship exists for the phase of the 24h and 12h components, which determines the focus position that moves to later local times with increasing solar activity (Olsen, 1993; Yamazaki & Maute, 2017).

The Sq amplitude reaches higher levels during summer months than winter months at mid-latitudinal regions because of extended solar irradiation. Peak amplitudes occur during both equinoxes in low- and equatorial latitudes because of the equatorial electrojet and possible equinoctial effects. The amplitudes during summer are around three times higher than during winter, especially during the solar minimum phase (Takeda, 1999; Yamazaki & Maute, 2017). The currents reach such low levels during winter that the Sq current cell may disappear and the Sq focus vanishes (Campbell et al., 1993; Rastogi & Crandra, 1996; Stening & Winch, 2013). The season exerts a substantial influence on the position of the foci latitudes. The foci latitudes move to earlier local times during summer months as compared to the winter months in both hemispheres (Campbell & Schiffmacher, 1987, 1988).

2.5.3 Equatorial Electrojet (EEJ)

Another dominant current system generated by the ionospheric dynamo is the EEJ as seen in Figure 2.3. EEJ is a strong zonal current (east to west) flowing at the magnetic equator where the two Sq current systems meet on the dayside. It is characterized by its strong jet-like current stream, which significantly enhances the geomagnetic field near the magnetic equator (Chapman, 1951). The EEJ receives its driving electric fields from the ionospheric dynamo system. The interaction between the global neutral wind system and Earth's magnetic field generates eastward zonal (E_y) and vertical (E_z) electric fields in the ionosphere (Moro et al., 2016). The generation mechanism is the Cowling conductivity effect, which facilitates the Hall current driven by the vertical DC electric field. This creates a secondary polarization electric field due to the accumulation of charges at the conductance boundaries of the ionospheric wind dynamo. This secondary polarization electric field enhances the current flow, which generates the Cowling conductivity that drives the EEJ (Pfaff et al., 1997; Amm et al., 2011). Figure 2.5 depicts the electric fields and current sources generating the equatorial electrojet. The EEJ reaches its peak intensity at local noontime and is more stable than other ionospheric current systems (Casey, 2005). Its strength depends on the eastward electric field strength which can be influenced by two-stream and gradient-drift instabilities. The current strength shows changes mainly for high electric field values because of these instabilities (Alken & Maus, 2010).

The EEJ exists as a part of the Sq current system but operates as an equatorial extension of this larger current system. Its connection to Sq currents exhibits complex behavior which is dependent on the region of the Earth (MacDougall, 1979). It interacts with the Sq current system by creating westward return currents on the flanks of the dip equator. The three primary sources that contribute to the return currents are the curvature of the field lines in the dynamo region, divergence of the east-west currents near the magnetic dip equator and the altitude variation of local neutral winds peaking around 5° magnetic latitude (Onwumechili, 1992). The EEJ operates independently from the Sq current because it exists as a self-contained system with

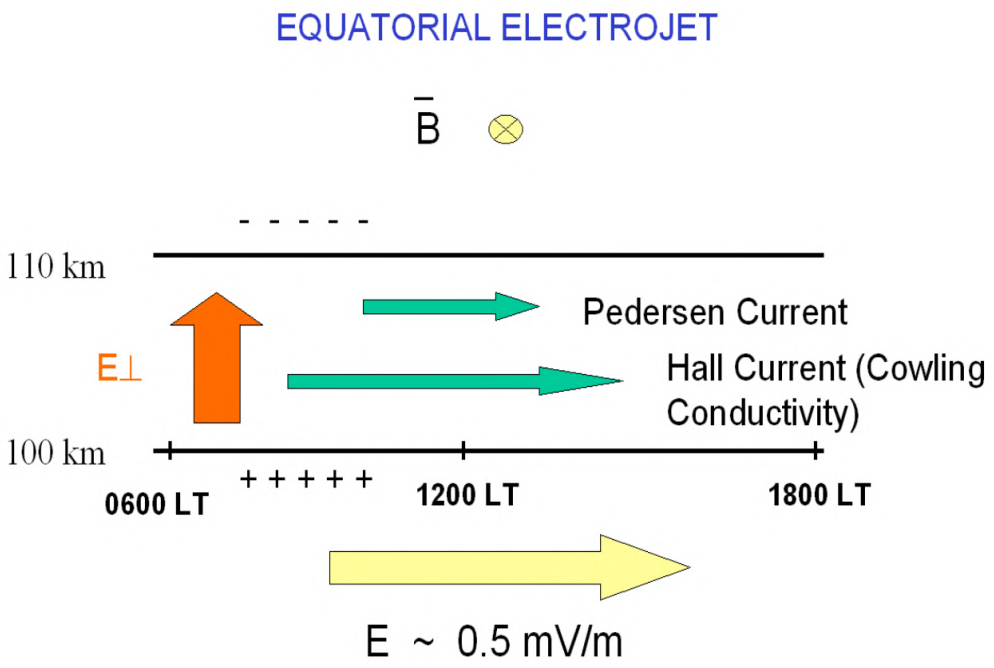

Figure 2.5: An illustration depicting the equatorial electrojet electric fields and current sources. Image source: Anderson et al. (2004).

complex operational dynamics. The EEJ-Sq relationship shows different patterns in various regions because local conditions, like geomagnetic conditions and atmospheric processes, affect these current systems (Bespalov & Savina, 2012). Its response to atmospheric waves, in addition to external electromagnetic effects, creates additional complexity in its relationship with the Sq current system (Onwumechili, 1992). The EEJ causes substantial geomagnetic field changes at the dip equator which is attributed to Sq current system interactions (Hamid et al., 2013). It shows a weak relationship with Sq currents and various longitudinal sector differences; for example, the Southeast Asian sector demonstrates a weak positive relationship, while the South American and Indian sectors show negative relationships (Hamid et al., 2014). However, Rabiu et al. (2025) used the transfer entropy approach to show that the EEJ-Sq current coupling demonstrates significant information exchange between these two systems, involving directional flow between the current systems.

2.6 Inter-Hemispheric Field-Aligned Currents (IHFACs)

Inter-hemispheric field-aligned currents (IHFACs) play a crucial role in understanding the geomagnetic field variations and their underlying mechanisms. These currents are primarily driven by asymmetries in ionospheric conductivity, influenced by solar radiation and seasonal variations. During summer-winter conditions, when one hemisphere is in the summer season and the other in the winter season, the conductivity contrast is most pronounced, leading to

significant IHFACs (Lyatskaya et al., 2014b, 2014a). Seasonal variations play a crucial role in modulating IHFACs; for instance, during the June solstice, currents flow from the summer hemisphere (Northern Hemisphere) to the winter hemisphere (Southern Hemisphere), while during the December solstice, the flow reverses (Lühr et al., 2019; Yamashita & Iyemori, 2002). The dynamo action within the ionosphere leads to vertical electric charge separation on the

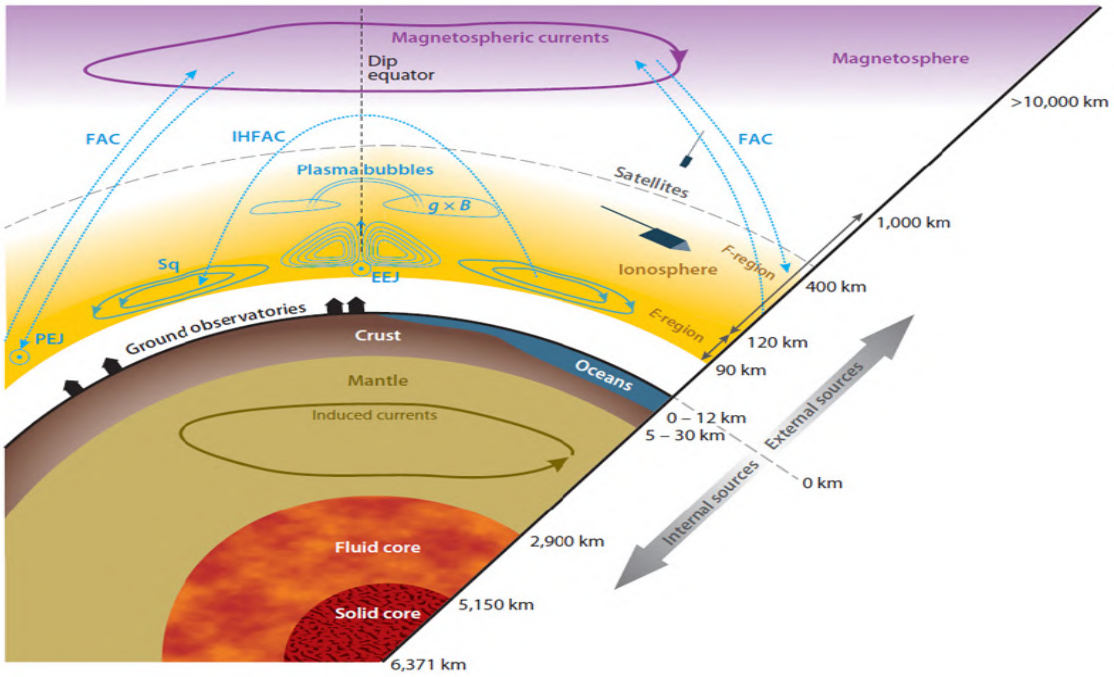

Figure 2.6: An illustration depicting the current systems of the magnetosphere, plasmasphere, and ionosphere. The IHFACs influence and connect the Sq current systems of both hemispheres. Image source: Olsen and Stolle (2017).

dayside, further impacting the geomagnetic field (Fukushima, 1979). On quiet days, ionospheric currents generate global perturbation magnetic potential patterns at ground level. Approximately 50 kA of current flows overhead in the ionosphere between each pair of contours, moving counterclockwise in the Northern Hemisphere and clockwise in the Southern Hemisphere. These effects are concentrated in the daylit hemisphere due to higher daytime ionospheric conductivities (Richmond, 1979).

The formation of IHFACs is closely tied to the solar quiet (Sq) current system, since this system generates currents in both hemispheres, and IHFACs act as a bridge between these hemispheric current systems, ensuring the closure of currents on a global scale (Lühr et al., 2015, 2019). The connection between IHFACs and the Sq system is evident in their diurnal and seasonal variations; for example, the amplitude of IHFACs is modulated by solar activity, with higher amplitudes observed during periods of higher solar radiation (Archana & Arora, 2024; Ranasinghe et al., 2021). Additionally, the longitudinal dependence of IHFACs, influenced by the SAA and non-migrating tides, further highlights their intricate relationship with the Sq system (Park et al., 2011; Liu et al., 2024).

At low-latitudinal regions, zonal winds drive ionization across magnetic field lines in the E-region, producing electric fields that map into the F-region and result in vertical drifts of ionization. These drifts are pivotal to forming features such as the equatorial anomaly (Titheridge, 1995). Additionally, meridional winds facilitate an inter-hemispheric flow of ionization, which can modify the size of equatorial anomaly peaks. This interplay between wind-driven ionization and field-aligned currents is fundamental to understanding normal and abnormal variations in Sq currents.

Furthermore, Van Sabben (1966) suggested that divergence-free anti-symmetrical currents confined to the ionosphere might contribute to equinoctial asymmetry. This hypothesis highlights another layer of complexity in understanding inter-hemispheric current systems and their effects on geomagnetic field parameters. The IHFAC interaction with the Sq currents of the Northern Hemisphere and Southern Hemisphere is depicted in Figure 2.6, showing the internal and external current systems alongside the heights of the Sq currents (80-110 km), FACs (90 km and altitudes > 10000 km) in the polar latitudes of the Northern and Southern Hemisphere and IHFACs (90-1000 km).

Above an altitude of ~150 km, partial cancellation of ionospheric currents due to complex wind structures can alter height-integrated current amplitudes by up to 25% (Rees, 1979). This variability is crucial for investigating correlations between data samples and variations as manifested in the ground-based magnetograms, potentially supporting or rejecting existing hypotheses about electric field models.

Overall, these insights collectively underscore the importance of IHFACs in shaping our understanding of geomagnetic field variations during quiet times. By refining models and considering various contributing factors such as solar wind parameters, interplanetary magnetic fields, and ionospheric conductivity, researchers have developed a more comprehensive picture of how these currents influence geomagnetic phenomena across different latitudes and seasons. Studies by Rastogi and Patil (1992), Baker (1953) and Schmucker (1999) greatly advanced our understanding, as did studies which integrated satellite data with ground measurements (Park et al., 2011; Bolaji et al., 2012; Owolabi et al., 2018; Park et al., 2020; Ranasinghe et al., 2021; Fillion et al., 2023; Wang et al., 2023).

The existence of field-aligned currents above the ionosphere in high latitudes was first hypothesized by Van Sabben (1966). Subsequently, several numerical calculations were undertaken which anticipated the local time dependence of IHFACs (Van Sabben, 1969, 1970; Schieldge et al., 1973; Maeda, 1974; Stening, 1977; Takeda, 1982).

Fukushima (1994) devised a foundational framework for understanding ionospheric currents and field-aligned currents (FACs) in the Earth's magnetosphere. It emphasizes the role of the

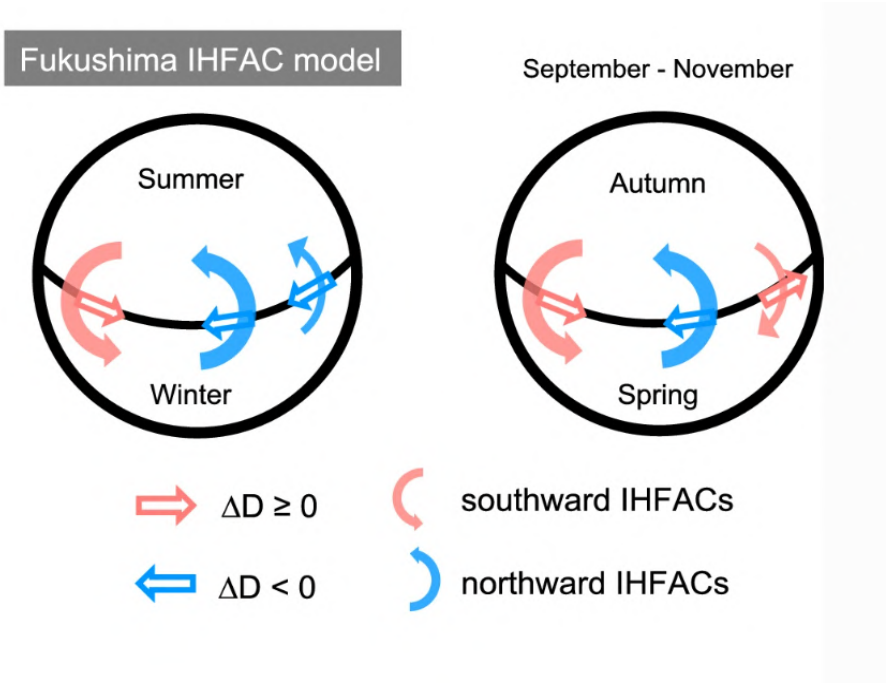

Figure 2.7: The illustration indicates the polarity of the IHFACs for different seasons according to Fukushima (1994). The magnetic field data of Davao (geographical latitude 7°N, geographical longitude 124.5°E) for the period August 2008 to July 2020 was utilized. The declination (D) component (east-west) of the magnetic field was used after computing the daily variation relative to the baseline. Image source: Ranasinghe et al. (2021).

geomagnetic field configuration in shaping large-scale ionospheric electrodynamics. The model incorporates the effects of the Earth's asymmetrical magnetic field, which deviates from a pure dipole configuration, and its impact on ionospheric currents and FACs (Le Sager & Huang, 2002). The Fukushima model underscores the importance of geomagnetic field asymmetry, which arises from non-dipolar components of the Earth's magnetic field. This asymmetry significantly affects the distribution and intensity of FACs and ionospheric currents (Le Sager & Huang, 2002; Gasda & Richmond, 1998). Seasonal movement of IHFACs derived from ground magnetic field data is depicted in Figure 2.7. During solstices, the eastward currents (indicated in red) flow from the Northern Hemisphere to the Southern Hemisphere at dawn (06:00 till 08:00 SLT), and westward currents (indicated in blue) from the Southern Hemisphere to the Northern Hemisphere at noon (11:00 till 13:00 SLT) and dusk (14:00 till 16:00 SLT) (Ranasinghe et al., 2021). During the autumnal equinox, the eastward currents flow from the Northern Hemisphere to the Southern Hemisphere at dawn and dusk, but the noontime currents remain the same as the solstices (Ranasinghe et al., 2021). The incorporation of this phenomenon is essential for comprehending the seasonal variations observed in geomagnetic parameters at low- and mid-latitudinal regions. The intensity and distribution of IHFACs vary with geomagnetic activity, solar wind conditions, and the orientation of the geomagnetic field. These variations are particularly pronounced during the equinoxes and solstices (Tsunomura, 1999; Aruliah et al., 1996).

Simulation studies were undertaken by Richmond and Roble (1987) and Takeda (1990) to illustrate how the IHFACs transit across the equator. The presence of IHFACs was observationally detected by satellite observations by the MAGSAT, Ørsted, CHAMP and Swarm satellites. These satellite observations led to the identification of climatological details according to latitude, longitude, atmospheric heights and seasons (Olsen, 1997; Yamashita & Iyemori, 2002; Park et al., 2011; Lühr et al., 2015; Wang et al., 2023). This discovery laid the foundation for further investigations of the behavior and effects of these currents.

2.7 The Earth's Magnetic Field

The Earth produces a vast magnetic field that extends from the interior of the Earth into space and interacts in space with the solar wind. The invisible geomagnetic field around Earth has the vital life-supporting function of protecting the planet from dangerous space and solar radiation. The geomagnetic field forms a dipole configuration that resembles a bar magnet, which is tilted by about 10° from the rotation axis of the Earth (Courtillot et al., 1992). The geomagnetic field deviates from simple dipole behavior, since it displays multiple temporal and spatial variations (Kivelson & Russell, 1995).

Many essential applications are derived from Earth's geomagnetic field and its operation thus requires a thorough understanding. It is produced deep inside the Earth and affects a broad spectrum of phenomena, such as the polar auroras, which are visible manifestations of the interaction between the solar wind and the Earth's magnetic field (Jault et al., 1999). The magnetic field plays a crucial role in navigation, as it influences the orientation of compass needles, and has thus provided a reliable means of direction-finding for centuries (Herrmann & Vorbach, 2020). Navigation systems on spacecraft and submarines rely on the geomagnetic field to determine their position. Scientists studying space weather use the geomagnetic field as a primary tool to forecast the effect of solar storms on communication systems, satellites, and power grids (Pulkkinen, 2007). Geophysicists employ magnetic data to conduct mineral exploration and archaeological dating, and to understand plate tectonics and Earth's internal processes (Jacobs, 1987).

2.7.1 Structure of the Earth's Interior

The Earth consists of four concentric shells, the crust and the mantle, the outer core and the inner core, as can be seen in Figure 2.8. The outermost layer of the Earth is the crust, which is thin and solid and forms the continents and ocean floors. Beneath the Earth's crust lies the solid, but plastic mantle, which reaches depths of approximately 2,900 kilometers. The core beneath the mantle consists of two parts: the liquid outer core and the solid inner core. The

outer core functions as an electrically conductive molten iron-nickel mixture which is subject to vigorous convection as it generates the magnetic field (Stacey & Davis, 2008).

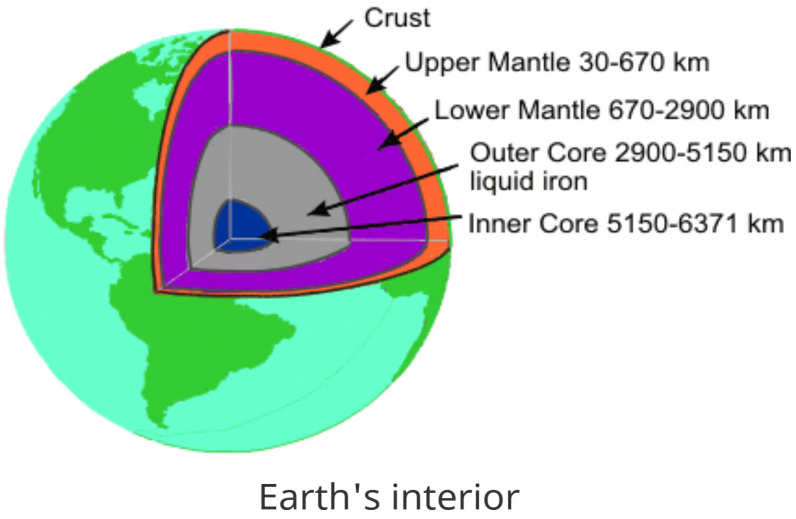

Figure 2.8: The layers of the Earth's interior are defined according to their depth. Image credit: NRCan; source: https://geomag.nrcan.gc.ca/mag_fld/fld-en.php.

2.7.2 Geodynamo Theory

The geodynamo theory explains how electrically conducting fluids moving within the outer core, generate and sustain the Earth's magnetic field. Gradual inner core solidification along with radioactive decay produces heat, which creates convective motions within the outer core. The combination of molten metal currents with Earth's rotation-generated Coriolis effect creates spiral patterns of fluid movement, as depicted in Figure 2.9. The cylindrical columns twisted by the Coriolis effect (indicated by blue arrows) organize the magnetic field lines into a dipolar field — one that has a distinct north pole and a distinct south pole represented by white lines.

The movement of an electrically conducting fluid through an existing magnetic field produces electric currents. According to Faraday's law of electromagnetic induction (Sreenivasan, 2010), these currents produce their own magnetic fields as defined by the following equation:

$$\frac{\partial \mathbf{B}}{\partial t} = \nabla \times (\mathbf{u} \times \mathbf{B}) + \eta \nabla^2 \mathbf{B} \tag{2.6}$$

where, B represents the magnetic field, u is the velocity of the fluid, η is the magnetic diffusivity and ∇ represents the gradient operator. The velocity of the fluid u shears, stretches, and twists the existing magnetic field lines, a process which drives currents ($\mathbf{J}_{\text{ind}}$) that act to amplify or reorganize the magnetic field. Currents induced by fluid motion ($\mathbf{J}_{\text{ind}}$) are the source of field generation and amplification. They are described by the term $\nabla \times (\mathbf{u} \times \mathbf{B})$. The dissipation of

the total field-producing currents (**J**) leads to the decay of the field. This is described by the term $\eta\nabla^2\mathbf{B}$.

The fluid motion creates a self-sustaining dynamo through which kinetic energy transforms into magnetic energy as a result of magnetic field and fluid motion interactions. The feedback mechanism sustains the geomagnetic field across geological periods (Glatzmaiers & Roberts, 1995).

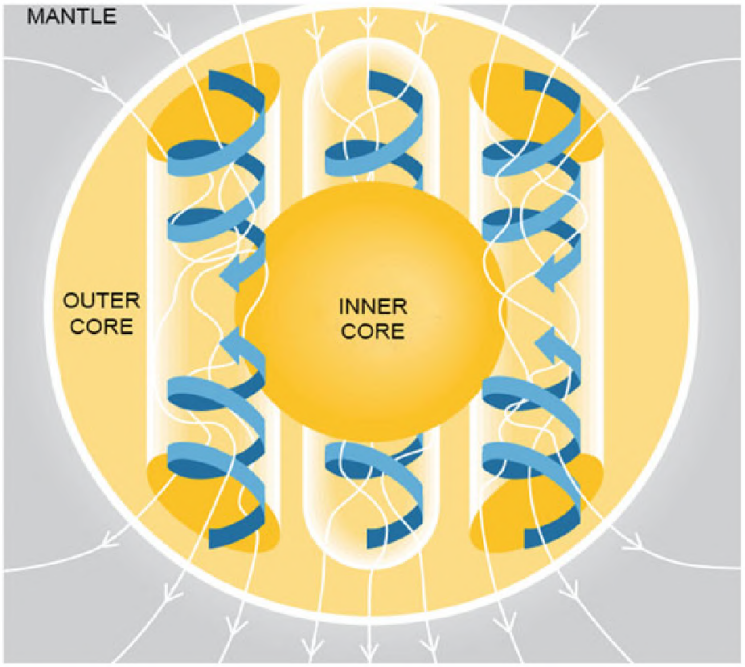

Figure 2.9: The internal sources of the Earth's dynamo. Image source: Gvishiani and Soloviev (2020).

The inherent non-linearity of the dynamo system produces chaotic behavior, which leads to both geomagnetic secular variations and periodic polarity reversals studied by researchers through paleomagnetic analysis of geological records. Numerical simulations of the geodynamo as done by Glatzmaiers and Roberts (1995) have generated important findings regarding the complex nature and extended durability of the field.

2.7.3 Magnetosphere

First explained by Gold (1959), the magnetosphere is the region of influence of the Earth's magnetic field above the ionosphere. It holds the motion of charged gas particles. The magnetosphere is an integral part of Earth's space environment, playing a crucial role in the dynamics of geomagnetic field parameters under both quiet-time Sq currents and geomagnetic storms. The magnetosphere is defined as the region around Earth where the planet's magnetic

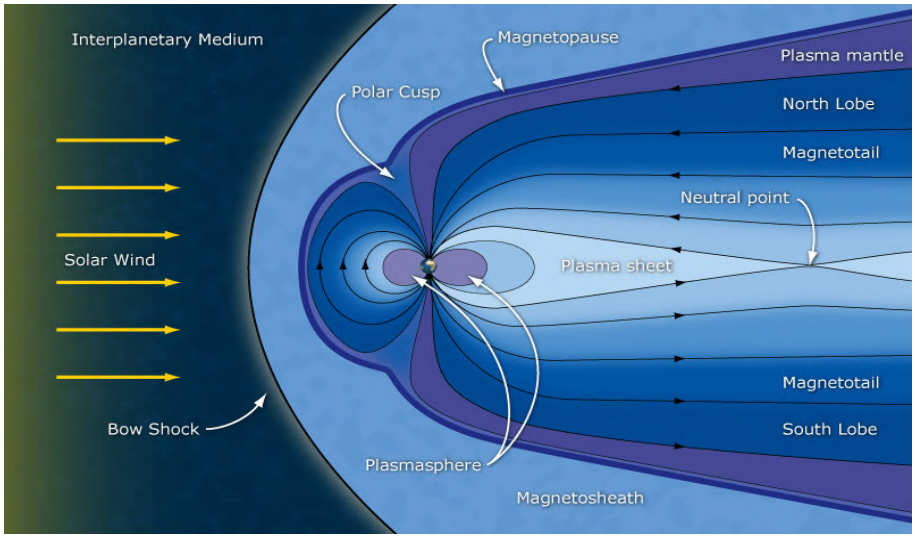

Figure 2.10: An illustration of the Earth's magnetosphere-the region of space dominated by the Earth's magnetic field but constrained by the impinging solar wind and IMF. Image Source: Case (2014)/ESA (C. T. Russell).

field dominates over the solar wind's influence. This area is characterized by various current systems, including field-aligned currents that connect the ionosphere to the magnetosphere. These currents are particularly significant in near-pole regions, where they exhibit distinct patterns based on solar activity and IMF conditions (Feldstein & Levitin, 1986). Figure 2.10 shows the Earth's magnetosphere and its components.

The solar wind induces reconnection events that occur at the dayside magnetopause when the IMF links with Earth's magnetic field. The IMF connection becomes stronger during southward orientations because it facilitates magnetic flux movement to the magnetotail (Russell, 2002). The magnetotail stores transferred magnetic flux before releasing it through reconnection events. The energy released from this process maintains the magnetospheric structure while producing substorm events according to Sinha et al. (2010) and Bengtson (2017). The reconnection process generates FACs to transfer magnetospheric energy into the ionosphere. The magnetic field orientation and speed of solar wind determine the formation of these current systems, which control Dungey cycle flux circulation within the magnetosphere (Fleetham et al., 2023). The stability of geomagnetic fields depends on the ring current and magnetotail currents that develop from reconnection. Solar wind-driven variations affect the magnetosphere's external response and its current system operation (Lühr & Maus, 2010). The energy distribution pattern due to magnetic reconnection supports geomagnetic field sustainability in the magnetosphere and ionosphere. Dorelli (2019), along with Lühr and Maus (2010), agree that this equilibrium prevents large-scale geomagnetic disruptions.

The outer magnetosphere is a region characterized by complex interactions between the solar wind and the Earth's magnetic field. These interactions lead to various phenomena that

significantly influence geomagnetic field parameters and quiet-time Sq currents. The structure and dynamics of the outer magnetosphere are essential for understanding the overall behavior of the magnetosphere and plasmasphere. The convectional circulations within the magnetosphere, as described by Axford and Hines (1961), play a crucial role in interpreting the physical results obtained from observations. This circulation is driven by the solar wind and can be modeled in order to understand the distribution of electric fields and currents in this region (e.g., Feldstein & Zaitzev, 1968).

Field-aligned currents at high latitudes are controlled by parameters such as velocity, density, and temperature of the solar wind. These currents exhibit distinct distributions based on these controlling factors (Levitin et al., 1982). The interaction between solar wind and Earth's magnetic field at the magnetopause results in complex variations that are crucial for understanding geomagnetic disturbances.

2.8 Identification of Normal and Abnormal Quiet Days in Geomagnetic Observatory Data

Earlier studies contribute to the understanding of the definitions of normal and abnormal quiet days and their limitations. The ideal Sq schema and the different normal and abnormal Sq variations on quiet days (QDs) are explained with examples to show their relative variations due to changing Sq foci positions.

2.8.1 Literature Definitions of Normal and Abnormal Quiet Days

Normal quiet days (NQDs) are the days with regular local time variations in the H or X component of the geomagnetic field variation, where the maximum magnitude is achieved between 10:30-13:30 SLT for low-latitudinal magnetic observatories (Last et al., 1976; Sastri, 1982). If the maximum Sq(H) magnitude is found outside this time interval, then those days are termed as abnormal phase-shifted quiet days (APQDs) (Last et al., 1976; Sastri, 1982). For a mid-latitudinal observatory, if the minimum magnitude of Sq amplitude in nT is achieved within ±2.5 hours centered around 11:30 SLT, then the quiet day is a NQD (Brown, 1974; Butcher & Brown, 1981a). If the minimum SQ amplitude on a quiet day doesn't fall within this criterion, then the day is defined as an APQD.

2.8.2 Observations of NQDs in Magnetograms

Magnetic variation observed at ground observatories on a quiet day in 2009 is shown in Figure 2.11. The figure shows Sq(H) variations as observed in the ground magnetometer data in the Asia-Australian sector along 140° - 180°E longitudes in the Northern Hemisphere (a) and along 100° - 155°E in the Southern Hemisphere (b). The equivalent current vectors (ECVs) were computed by using the X and Y components of observatories in the Northern Hemisphere and Southern Hemisphere and by combining them into vectors, rotating them by 90° and plotting them as currents (Vichare et al., 2017; Soloviev et al., 2019; Gvishiani & Soloviev, 2020). The ECVs confirmed the direction as anti-clockwise in the Northern Hemisphere and clockwise in the Southern Hemisphere, and the calculated Sq focus positions within ±35° magnetic latitude, according to Nopper (1978) and Matsushita (1967) (Figures 2.11 (a) and (c)). The magnetograms clearly showed a peak for observatories in the Northern and Southern Hemispheres lying below the Sq foci within the shaded time slots for low latitudes. Similarly, for observatories in the Northern Hemisphere and Southern Hemisphere lying above the Sq foci positions (mid-latitudinal), a dip was observed (Figure 2.11 (b) & (d)). A phase shift is observed for the low-latitudinal observatory (CTA in blue, Figure 2.11 (d)) in the Southern Hemisphere, whereas the rest of the observatories displayed NQDs.

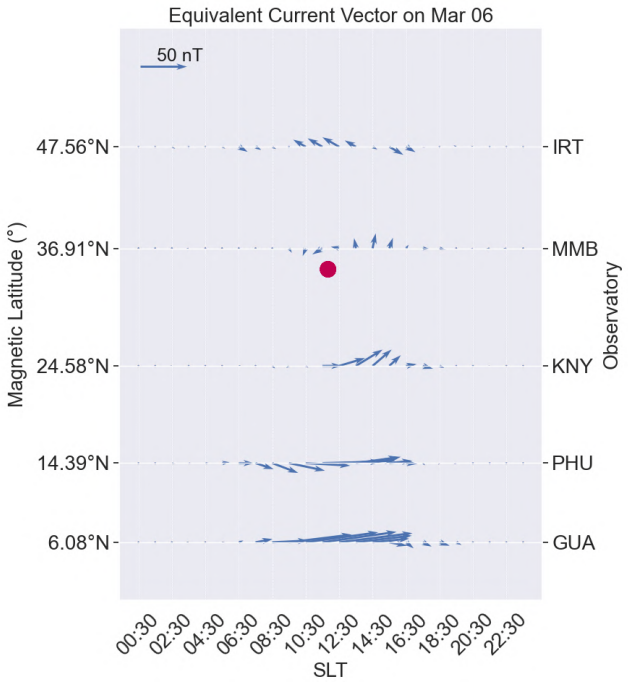

(a) ECVs in NH

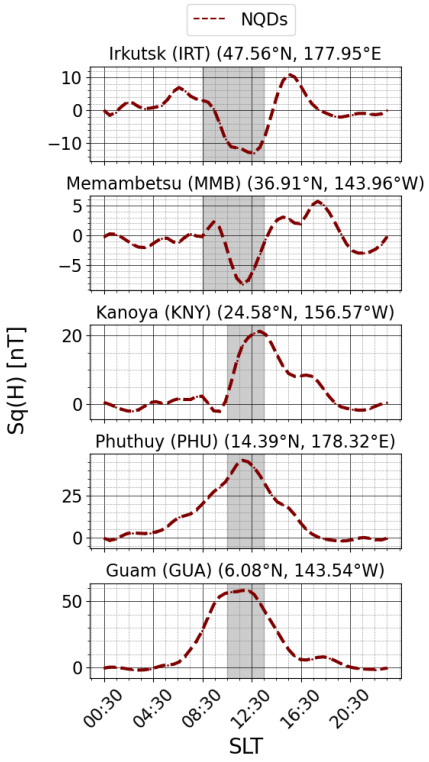

(b) Magnetograms of NH

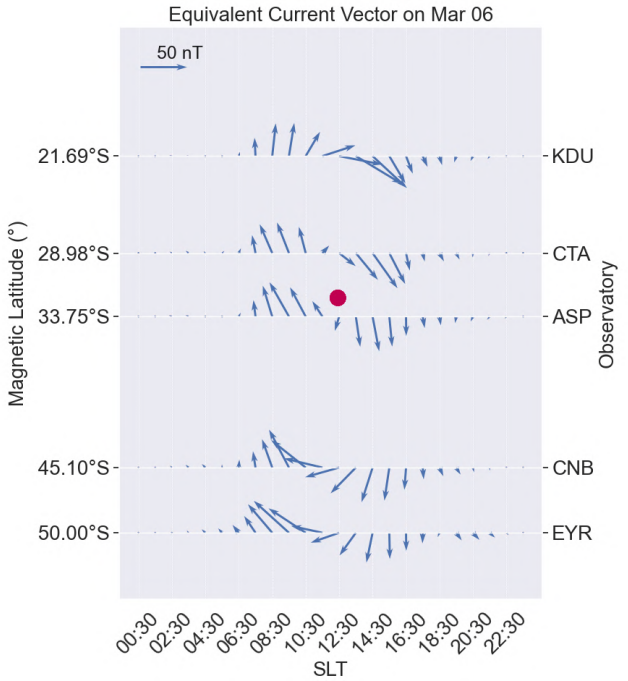

(c) ECVs in SH

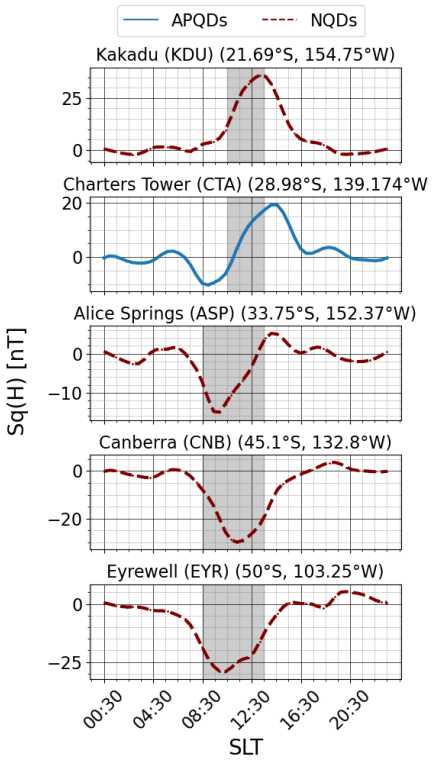

(d) Magnetograms of SH

Figure 2.11: The illustration depicts the NQDs in the Asia-Australian sector on 6 March 2009. The equivalent current system plots for the NH (a) show the Sq foci positions (red dots) found at 35°N and for the SH (c) show the Sq foci positions at 32°S magnetic latitudes. The magnetograms (b) and (d) depict NQDs (dashed lines in maroon) for magnetic observatories in the Asia-Australian sector. The magnetic coordinates are used.

2.8.3 Ideal Sq Schema and its Observational Relation to Sq Focus Position

According to Nopper (1978) and Matsushita (1967), during magnetically quiet times, the Sq current system has two spirals in the day-side hemisphere centered at about ±35° latitude around 11:00 SLT in the Northern Hemisphere, and at around 12:00 SLT in the Southern Hemisphere (Figure 2.12). The centers of these spirals or vortices are referred to as Sq focus positions. Recent studies (e.g. Anad et al., 2016; Soloviev et al., 2019) define an ideal Sq schema as having Sq focus at ±30° magnetic latitude, as depicted in Figure 2.13.

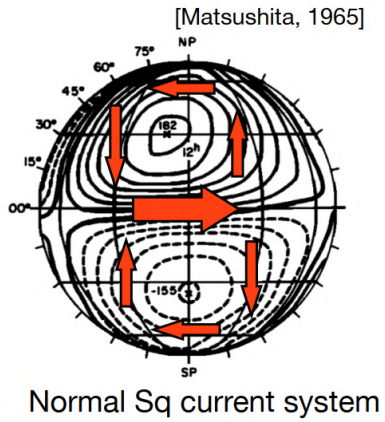

Figure 2.12: Current vortices of a normal Sq current system in the Northern/Southern Hemispheres. Image source: Yamazaki (2015).

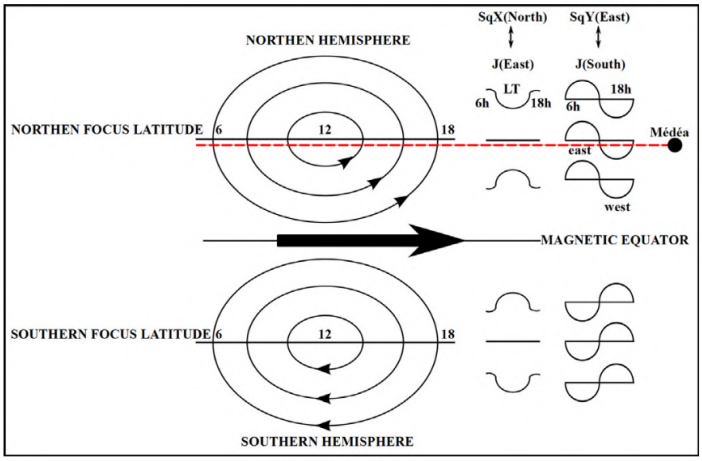

Figure 2.13: An illustration of the ideal Sq foci positions found at ±30° magnetic latitudes. Image source: Anad et al. (2016).

According to the ideal Sq schema, for a low latitude observatory in the Northern Hemisphere and below the Sq focus latitude, the peak is observed in the H or X component of Sq variations within the NQD time range. Similarly, a dip is observed at a mid-latitudinal observatory located higher than the Sq focus latitude within the NQD time range. The same is true for low- and mid-latitudinal observatories in the Southern Hemisphere (Figure 2.13). However, variation has been observed on NQDs where the Sq focus position determines the peak or dip of any low- or mid-latitudinal observatory. An example is shown in Figure 2.14, where for the KNY (24.58°N, mlat) and CNB (45.1°S, mlat) observatories, both peaks and dips are seen for different NQDs (11 November and 8 December 2009). The Sq focus position in the Northern Hemisphere was located at 30°N magnetic latitude and hence, the normal peak was observed at KNY. In the Southern Hemisphere, the Sq focus was found at 37°S magnetic latitude, hence the normal dip was observed at CNB. Similarly, on 8 December 2009, the Sq foci positions in the Northern and Southern Hemispheres were found at 12°N and 53°S magnetic latitudes respectively. Hence, a normal peak and dip can be observed at CNB and KNY, respectively.

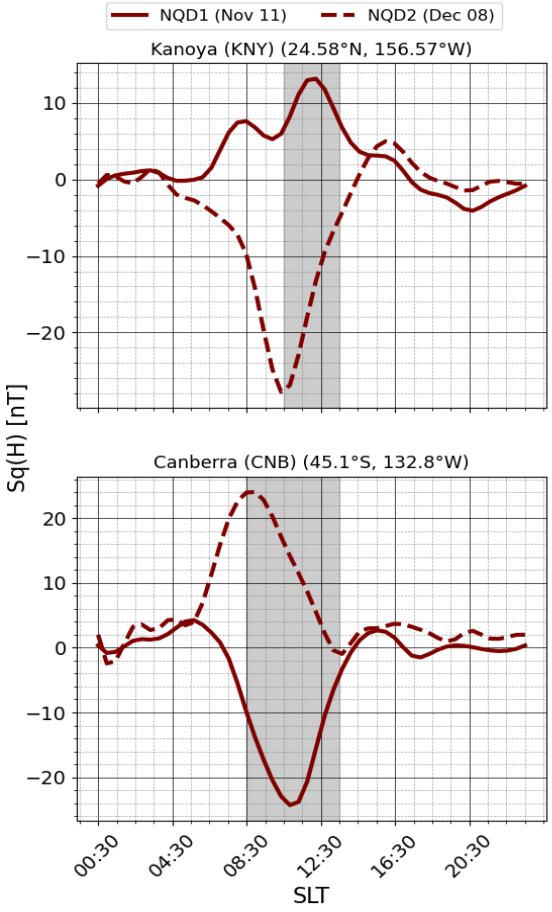

Figure 2.14: NQDs in NH and SH on 11 November 2009 (maroon) and 8 December 2009 (maroon-dashed) in the Asia-Australian Sector. The magnetic coordinates are used.

2.8.4 Irregular Movement of Sq Current Focus positions and Quiet Day Variation

The concept of QD variation of Sq foci latitudes is integral to understanding geomagnetic variations and ionospheric dynamics. The positions and movements of Sq foci, or centers of these current systems, are critical for understanding geomagnetic field behavior. The variability in the latitude of Sq foci can be influenced by negative magnetic perturbations. Determining true focus positions requires analyzing days without such perturbations, emphasizing seasonal variations and its impact on geomagnetic models (Butcher & Brown, 1981b). Both theoretical models and observed values at the mid-latitudinal regions offer steady features that help measure total current flows within Sq foci vortices and thus offer insights into their day-to-day variations, especially on QDs (Forbes & Garrett, 1979).

Accurate estimation of foci latitudes on magnetically quiet days involves considering horizontal intensity values at specific meridians. Comparing these results with historical data

provides insights into long-term trends and variations within the Sq current system (Hasegawa, 1960). The statistical analysis highlights that small-scale southward perturbations modulate the normal diurnal development of Sq and the electrojet current systems around their usual maximum times. This modulation is responsible for phase variability in Sq on NQDs within equatorial electrojet regions (Sastri, 1982).

In summary, understanding the variation of Sq foci on NQDs involves examining normal and abnormal variations in these currents, their models, and influences from magnetospheric currents. The interplay between solar activity, ionospheric dynamics, lunar tides, changes in the Sq focus positions and inter-hemispheric currents is essential for comprehending the behavior of geomagnetic fields during quiet periods (Patil et al., 1983; Hall, 1966; Gupta, 1973; Torta et al., 1997; Brown, 1975).

2.8.5 Observations of APQDs in Magnetograms

Examples of abnormal magnetic variation observed at ground observatories on a QD in 2009 are shown in Figure 2.15. The ECVs were computed by using the X and Y components of closely located magnetic observatories in the Northern Hemisphere and Southern Hemisphere lying within the African-European longitudinal sector. Thus, ECVs confirmed the calculated Sq foci positions beyond $\pm 35^{\circ}$ magnetic latitude that were not the ideal Sq schema in relation to APQDs (Figure 2.15 (a) and (c)).

The magnetograms clearly show unusual peaks for observatories in the Northern and Southern Hemispheres lying below the observed Sq foci positions, where dips would have been expected (Figure 2.15 (b)). Since the Sq focus is at 54°N, the mid-latitudinal observatories of ESK (52.37°N, mlat) and KIV (46.3°N, mlat) show APQDs as positive peaks outside the shaded regions. The double peaks of EBR (34.97°N, mlat) were compared and the one with the highest amplitude is positive, but lying within the normal quiet time period. Observatories in the Southern Hemisphere, HER (42.48°S, mlat) and CZT (53.12°S, mlat), also depict APQDs (Figure 2.15 (d)). Although the Sq focus position is at 45°S, HER shows a peak which is phase-shifted and CZT shows a phase-shifted dip. The magnetograms clearly show peaks for observatories in the Northern and Southern Hemispheres lying below the Sq foci (low-latitudinal region) within the shaded time slots for low-latitudinal regions, indicating NQDs. Such Sq foci positions observed at the upper mid-latitudinal regions during the December solstice have been reported by, among others, Archana and Arora (2022).

Figure 2.16 shows APQDs overlaid on NQDs for the DOU and HER observatories in the Africa-European Sector in 2009. For NQDs (25 September 2009), the Sq foci latitudes were located at 36°N and 46°S magnetic latitudes, which clearly explains the dip and peak observed

at DOU and HER, respectively. However, there were phase shifts in the dips observed on the APQDs (2 April 2009). The Sq foci positions in the Northern and Southern Hemispheres were at 39°N and 40°S magnetic latitudes, respectively. Hence, dips are phase-shifted at both DOU and HER.

Quiet ionospheric currents exhibit average values that vary monthly and for each station, providing insights into normal and abnormal variation in Sq currents. These variations are smoothed and detrended to identify raw average Sq fluctuations, including sudden phase-shifts (Campbell & Schiffmacher, 1985). Mid-day peaks observed during solstices at low-latitudinal regions suggest significant diurnal influences on Sq variation, potentially leading to abrupt shifts (Rastogi & Crandra, 1996). An examination of spatial distribution by means of magnetograms revealed cases where modulation results in depression rather than in augmentation. Such cases provide clear evidence of sudden shifts in geomagnetic field parameters during quiet days (Onwumechili & Akasofu, 1972).

Solar activity significantly influences geomagnetic field parameters and the behavior of quiet-time Sq currents. The intensity of solar activity, which varies with the solar cycle, impacts the ionospheric conductivity and subsequently affects the Sq current system. According to Takeda (2002), the enhancement of local conductivity due to solar activity leads to a linear increase in the Sq field variation without any significant change in wind or electrostatic fields. This suggests that while ionospheric winds may have some dependence on solar activity, their role in Sq field variation is minimal when considering fixed monthly data. Sunspot cycle variation also contributes to these shifts, with occurrences noted about 1 hour earlier at sunspot minimum compared to sunspot maximum years (Sastri, 1982).

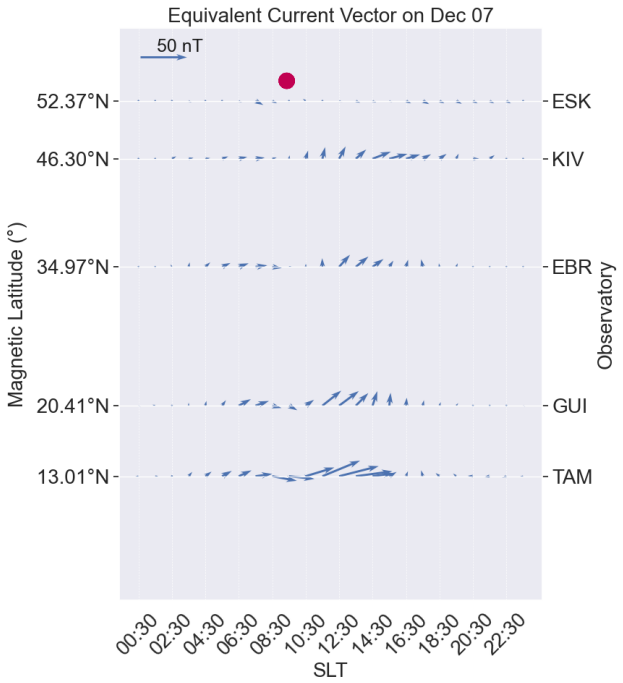

(a) ECVs in NH

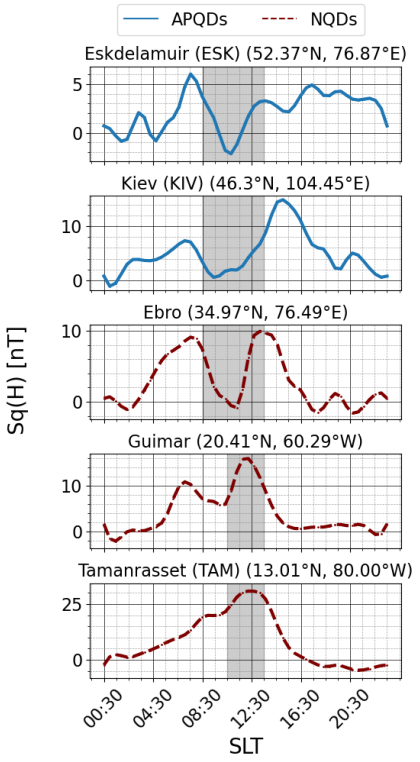

(b) Magnetograms of NH

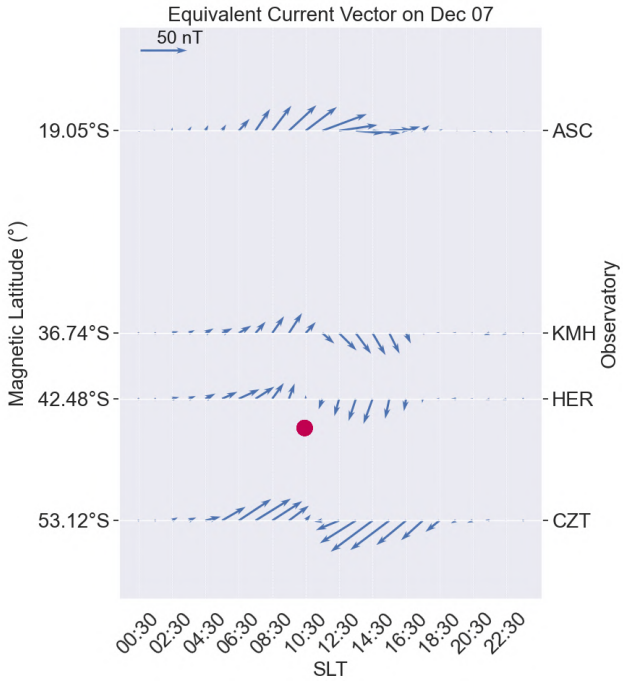

(c) ECVs in SH

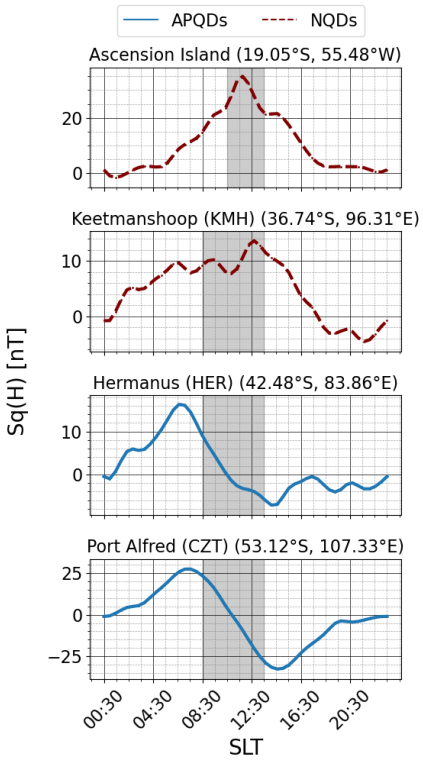

(d) Magnetograms of SH

Figure 2.15: The illustration depicts the APQDs in the Africa-European sector on 7 December 2009. The equivalent current system plot for the NH (a) shows the Sq focus position (red dot) found at 54°N, and for the SH (c) shows the Sq focus position at 45°S magnetic latitudes. The magnetograms (b) and (d) depict APQDs for magnetic observatories in the Africa-European sector (blue lines). The NQDs are represented as dashed lines in maroon. The magnetic coordinates are used.

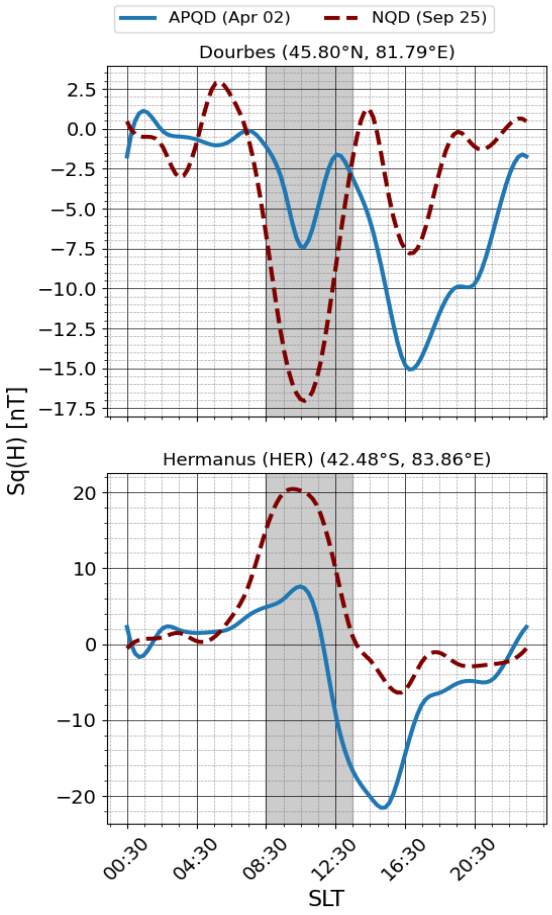

Figure 2.16: NQDs (dashed lines in maroon) are shown overlaid on APQDs (blue) as observed in the NH and SH on 2 April 2009, and 25 September 2009 in the Africa-European sector. The magnetic coordinates are used.

2.9 Types of Tilted or Deformed Sq Current Models

According to de Haro Barbas et al. (2013), deformed or tilted Sq current systems exist under quiet geomagnetic conditions and account for asymmetries and shifts in the Sq current system due to the changes in solar activity and the Earth's magnetic field. The definition and overview of normal and deformed or tilted Sq current models are essential for understanding the geomagnetic field parameters and quiet-time Sq currents, especially at focal latitudes. The variations of the Sq system have been described by different models, each describing how the magnetic field components are influenced under specific conditions. These are manifested in ground-level magnetic effects which are represented by a two-dimensional equivalent current system expanded in a spherical harmonic series (Schieldge et al., 1973). Mayaud and IAGA (1967) and Gupta (1973) provide a brief overview of the models R, T and F, and are summarized in the following subsections.

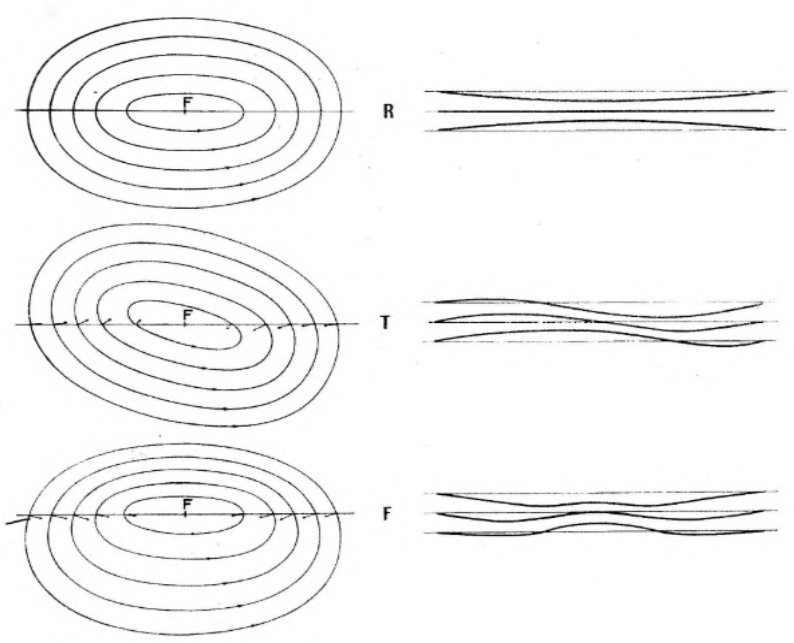

Figure 2.17: The illustration compares the normal Sq current model with the tilted Sq equivalent current models R, T and F. Image source: Mayaud (1965) and Amory-Mazaudier (2005).

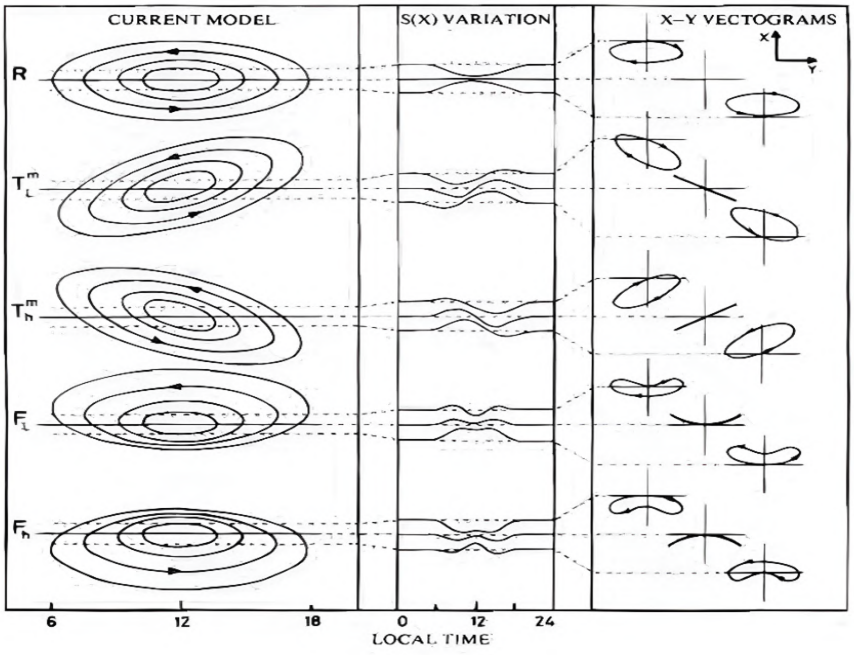

Figure 2.18: The illustration shows the variations of the deformed or tilted Sq equivalent current models R, T and F. Image source: Scheepers (1978).

2.9.1 Model R

Model R serves as a baseline for understanding the daily variations of the magnetic field components. It is characterized by the consistent shape of the H or X component variation,

which remains stable across different latitudes. This indicates that NQDs have the ideal Sq schema (Figure 2.13), such as model R, which ensures that the NQD conditions are fulfilled with little to no variation at the latitude of the Sq focus. The H or X component variation retains the same shape as the ideal Sq schema for model R, indicating that it does not significantly change with latitude. This consistency is crucial for establishing a reference point for analyzing other models.

2.9.2 Model T

The second and third rows of Figure 2.18 show the model T of the two-dimensional equivalent current system. In the Northern Hemisphere, T_h^m has a tilt which depicts magnetic variations shifted towards higher latitudes (h) in the morning (m), while T_l^m depicts a tilt with magnetic variations shifted towards lower latitudes (l) in the morning. The tilt of the opposite variation is valid for the Southern Hemisphere. In model T, the Sq variation in the H or X component exhibits a maximum in the morning and a relatively larger amplitude minimum in the afternoon at the focal latitude in the Northern Hemisphere for model T_h^m, which is the opposite for T_l^m. This means that the magnetic field experiences anomalous peaks and troughs throughout the day, the knowledge of which can be critical for understanding local or global abnormal geomagnetic conditions.

2.9.3 Model F

Model F introduces the concept of a shift in the focus, which can occur in two scenarios: F_h (focus shifted towards higher latitudes) and F_l (focus shifted towards lower latitudes), as seen in the fourth and fifth rows of Figure 2.18, respectively. F_l pattern occurs when current contours are closer together at lower latitudes, resulting in a different pattern of variation. For model F_l, the Sq focus is located at a lower magnetic latitude in the Northern Hemisphere. At observatories below the Sq Focus position, there is a small dip between secondary maxima, noticed by geomagnetic field observations, while above the Sq focus, this model exhibits a pure minimum between two secondary maxima. The opposite is true for the Southern Hemisphere. F_h occurs when current contours are closer together at higher latitudes, leading to a specific pattern of magnetic variation, as depicted in the bottom panel of Figure 2.18. This dual behavior highlights the complexity of magnetic variations and its dependence on latitude.

These models collectively enhance our understanding of the Sq system's behavior and the factors influencing abnormal geomagnetic variations.

2.10 Summary

This chapter provided an overview of solar activity, solar wind conditions, the ionosphere and quiet time regular current systems. The intricate relationship between solar activity and geomagnetic field parameters highlights the importance of understanding the dynamics of the ionosphere and its associated currents during quiet periods. The E-region dynamo plays a crucial role in generating electric currents that significantly influence geomagnetic variation, particularly the quiet-time Sq currents. These currents exhibit both normal and abnormal variations as observed in geomagnetic observatory data. Earth's magnetic field and its sources, as well as the identification of NQDs and APQDs were explained. ECV computation was depicted in vector form to confirm the calculated Sq foci latitudes for both NQDs and APQDs examples. The relationship between irregular Sq foci latitudes and APQDs observed at observatory data near the Sq foci latitudes highlighted their occurrences in both hemispheres. Models of Sq current systems were used to confirm the Sq foci latitudes and assess their influence in the occurrence of APQDs under quiet conditions.

Chapter 3

Data Sources and Methodology

This chapter explains, in sequential order, the method by which the correct times and amplitudes of APQDs were extracted from geomagnetic field data. It provides an overview of the geomagnetic field components, observation instruments, the International Network of Magnetic Observatories (INTERMAGNET), magnetic field measuring instruments, geomagnetic indices, and in particular, the derivation of the Symmetric H (SYM-H) index that was used to extract QDs for processing Sq(H) variations for selected longitudinal sectors in different phases of solar cycle 24.

3.1 Components of the Geomagnetic Field

The geomagnetic field is defined by three perpendicular vector components, i.e. X, Y, and Z. From these three components, other parameters, such as declination (D), inclination (I), horizontal component (H), and total intensity (F), can be computed. Figure 3.1 illustrates the parameters of the geomagnetic field, which are described in detail below:

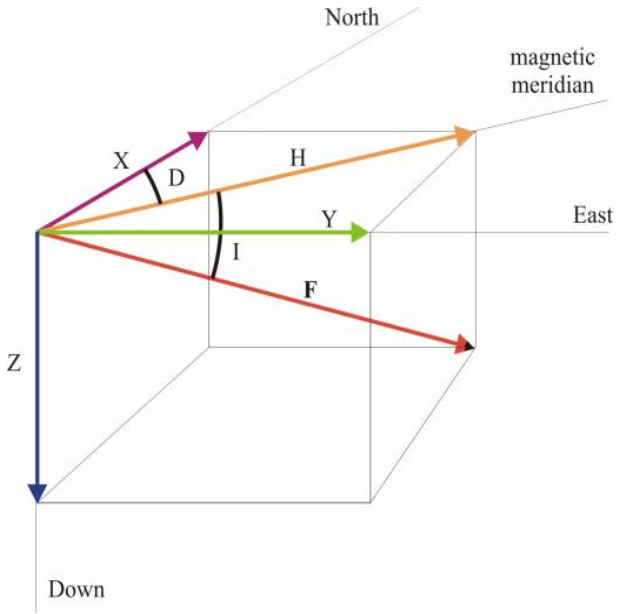

Figure 3.1: Parameters of the geomagnetic field (Arinze et al., 2016).

X (northward component) describes the magnetic field strength that points to the geographic north.

Y (eastward component) represents the magnetic field strength of geographic east-west.

Z (vertical component) points downward toward the Earth when its value is positive and upward when it is negative.

H is the horizontal component of the field, derived from the X and Y components:

$$H = \sqrt{X^2 + Y^2}. \tag{3.1}$$

F is the total magnetic field intensity derived from X, Y, and Z as:

$$F = \sqrt{X^2 + Y^2 + Z^2}. \tag{3.2}$$

D is declination, which is the angle between true north and magnetic north. It is positive when magnetic north is east of true north, and defined as:

$$D = \tan^{-1}\left(\frac{Y}{X}\right). \tag{3.3}$$

I is inclination and is defined as the angle between the magnetic field vector and the horizontal plane. Positive inclination, with respect to the local horizon, means the field points downward into the Earth (Northern Hemisphere), and when the inclination is negative, the field points upward (Southern Hemisphere). Inclination is defined by:

$$I = \tan^{-1}\left(\frac{Z}{H}\right). \tag{3.4}$$

The X and Y components can be defined in terms of H and D as:

$$X = H\cos(D). \tag{3.5}$$

$$Y = H\sin(D). \tag{3.6}$$

These parameters provide a complete characterization of the local geomagnetic field and are crucial for interpreting magnetic field measurements. The components and angles change according to location and time due to secular variation, magnetic storms, and diurnal changes due to solar radiation (Campbell, 2003).

3.2 Geomagnetic Observation Techniques and Instruments

Geomagnetic field study requires different instruments and techniques to measure and monitor the geomagnetic field. These instruments and techniques range from early compasses to modern digital magnetometers on the ground and in space-based satellites. The earliest known research into magnetism can be traced back to ancient civilizations, with the Chinese demonstrating an understanding of the magnetic phenomenon and its directional properties, leading to the invention of the compass, which served as the foundational instrument for navigation and preliminary geomagnetic studies (Smit, 2007). The development of the compass marked a crucial first step toward understanding and utilizing the Earth's magnetic field, and paved the way for more advanced geomagnetic instruments and measuring techniques (Campbell, 2003). Later, significant contributions were made by figures like William Gilbert, whose work "De Magnete", proposed that the Earth itself was a giant magnet, which attracted compass needles and influenced magnetic phenomena (Mandea et al., 2019). The establishment of geomagnetic observatories, such as the Greenwich Magnetic Observatory, marked a significant leap forward in the systematic study of the Earth's magnetic field (Campbell, 2003). These observatories were equipped with instruments designed to continuously monitor the magnetic field's variations over time. Early geomagnetic measurements relied on mechanical magnetometers, such as declinometers, which measured the direction of the magnetic field, and variometers, which recorded its temporal variations (Curto, 2019). These instruments, while groundbreaking for their time, were limited in resolution and accuracy, often requiring manual readings and photographic recordings (Curto, 2019). The process of collecting and analyzing geomagnetic data was labor-intensive and prone to errors, hindering the ability to capture the full complexity of the Earth's magnetic field dynamics. Despite these limitations, the data collected by these early observatories provided invaluable insights into geomagnetic phenomena, including diurnal variations, magnetic storms, and long-term secular changes (Onovughe, 2015). Over time, scientists noticed the slow drift of the compass direction in locations like London, which led to the discovery of the secular variation of declination (Mandea et al., 2019).

3.2.1 Ground-based Magnetic Field Observation Instruments

The transition from analog to digital geomagnetic measurements involved the development of new sensor technologies, data acquisition systems, and signal processing techniques. Flux-

gate magnetometers, for instance, emerged as a dominant technology for measuring magnetic fields with high sensitivity and stability. These vector magnetometers measure the field along one or more axes using the ferromagnetic properties of some materials (Gvishiani & Soloviev, 2020). Other instruments, such as induction coil magnetometers, were developed to record field variations at higher temporal frequencies, and cryogenic superconducting quantum interference device (SQUID) magnetometers found specialized use in paleomagnetism (Mandea et al., 2019). Digital data loggers and computer-controlled systems automated the recording process, thus eliminating manual errors and enabling the continuous monitoring of the magnetic field. Absolute measurements are essential for observatory operations, with world magnetic observatories comprising a substantial portion of the stationary geomagnetic field monitoring sites (Gvishiani & Soloviev, 2020).

Modern magnetic observatories employ at least three magnetometers, due to the large electromagnetic fields (EMF) induction values and the necessity to measure variation with great accuracy (Gvishiani & Soloviev, 2020). Sophisticated algorithms and software packages were developed to process and analyze the vast amount of geomagnetic data, thus enabling researchers to extract meaningful information about the Earth's magnetic field and its interaction with the solar wind and magnetosphere (Gvishiani & Soloviev, 2020). Today, modern instruments fall into two broad categories: fluxgate magnetometers and scalar magnetometers (Mandea et al., 2019). The former often serve as the primary instrumentation in INTERMAGNET observatories as they maintain reliability during extended monitoring periods (Ripka, 2021). In Figure 3.2, the photograph on the left shows a fluxgate magnetometer which measures vector magnetic field components (X, Y, Z) by means of the non-linear magnetization of ferromagnetic cores, while the photograph on the right shows a theodolite and scalar proton magnetometer which is used for absolute measurements.

The proton precession magnetometer (scalar instrument) measures the total magnetic field strength. The instrument generates a precession frequency from protons in hydrogen-rich fluids that exposes them to external magnetic fields, and this frequency directly relates to the external magnetic field strength. Figure 3.2 (right) shows the Overhauser magnetometer, which is an improved version of proton magnetometry, because it delivers continuous field measurements with improved sensitivity while requiring less power.

The Declination and Inclination fluxgate (DI-flux) theodolite, in conjunction with a proton magnetometer, provides absolute measurements of the field (D and I) in SI units. The measurements are crucial for both observational data accuracy verification and network calibration operations (Jankowski & Sucksdorff, 1996). Figure 3.3 shows the DI-flux theodolite at the Abdus Salam Geomagnetic Observatory, Sonmiani, Pakistan.

The continuous recording instruments, like fluxgate magnetometers, generate relative mea-

surements that identify field changes, but not absolute field values. These instruments serve to detect geomagnetic storms and diurnal variation by monitoring temporal field changes.

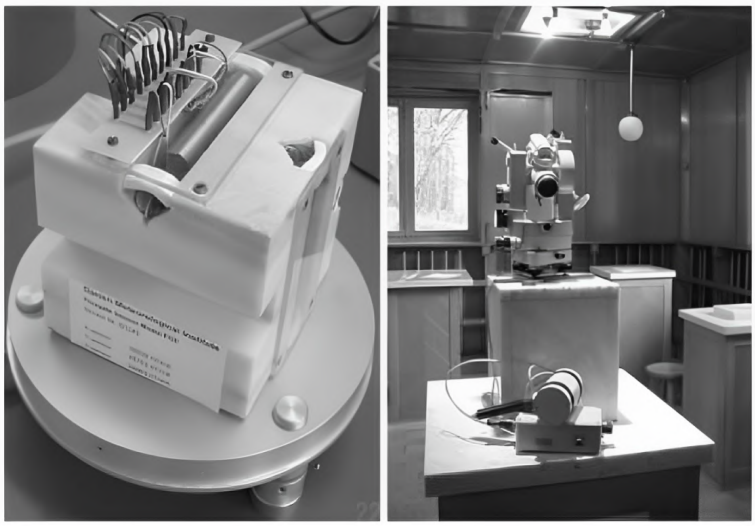

Figure 3.2: Examples of tri-axial fluxgate magnetometer (left), and Overhauser proton magnetometer, which is a scalar magnetometer (right). Source: Rasson (2007).

3.2.2 Applications of Geomagnetic Field Data

Magnetic instruments provide precise measurements and serve both geophysical surveys and observatory monitoring purposes (Telford et al., 1990). The H and D components serve as fundamental elements for navigation and orientation needs, offering an alternative to GPS, especially in environments where GPS signals are unreliable, such as underwater or in polar regions. This method is particularly valuable for autonomous vehicles and military applications (Zhang & Zhao, 2008). The Z and I components are primarily used in mineral exploration and geophysical surveying (Lanza & Meloni, 2006). Scientific and practical applications depend on this data, because it aids in the lithospheric field mapping of the Earth, in core dynamic monitoring and in the assessment of the impact of space weather. (Friis-Christensen et al., 2006). Geomagnetic data is crucial in forecasting geomagnetically induced currents (GICs) and assessing their impact on infrastructure (Gvishiani & Soloviev, 2020). In the oil and gas industry, geomagnetic data is used for high-precision navigation in directional drilling, which is essential for efficient resource extraction (Gvishiani & Soloviev, 2020). Long-term changes in the geomagnetic field are studied by means of paleomagnetic records. These help in understanding the Earth's magnetic history and the role of the geomagnetic field in shielding life on Earth against cosmic radiation (Panovska, 2024).

Figure 3.3: MINGEO Zeiss 010 DI-flux non-magnetic theodolite, Abdus Salam Geomagnetic Observatory, Sonmiani. Image credit: Pakistan Space Weather Centre (PSWC).

3.3 INTERMAGNET: The International Network of Magnetic Observatories

The International Real-time Magnetic Observatory Network, called INTERMAGNET, functions as a global partnership between magnetic observatories that deliver standardized real-time geomagnetic data. INTERMAGNET had been functioning as an integrated consortium for data collection, exchange, and dissemination since 1987, but was commissioned in 1991 through national geophysical institute partnerships to lead global magnetic observatory coordination and data standardization efforts. The main purpose of INTERMAGNET is to create a worldwide network of cooperating observatories that deliver high-quality geomagnetic data through standardized methods for research and operational applications.

Approximately 150 observatories have been actively contributing data to the consortium. The correct calibration of instruments is a fundamental requirement. Observatories follow strict protocols, and networks like INTERMAGNET enforce quality standards, which require observatories to conduct regular absolute measurements and cross-calibrate instruments (Love, 2008). Figure 3.4 shows the geomagnetic observatories that contribute data to INTERMAGNET. The data in various formats is freely available for scientific purposes, which allows timely data access for research and space weather forecasting purposes. The INTERMAGNET observatory network data is used to update global geomagnetic field models such as IGRF (International Geomagnetic Reference Field), which serves as a standard for mapping Earth's magnetic field

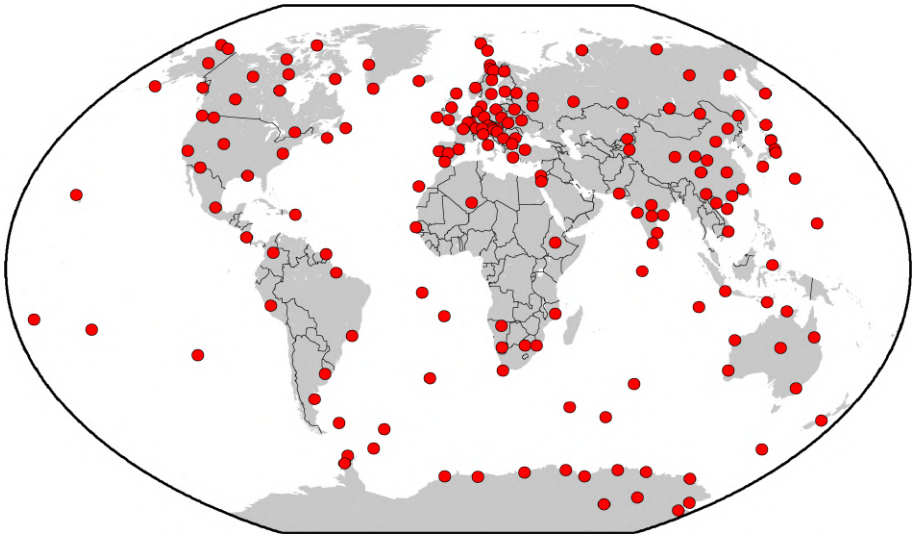

Figure 3.4: The map shows magnetic observatories that contribute data to INTERMAGNET; Source: BGS-Geomagnetism (https://geomag.bgs.ac.uk/education/earthmag.html).

with five-year model updates (Thébault et al., 2015). Real-time monitoring of geomagnetic storms and disturbances by means of geomagnetic indices relies on the high-resolution data from INTERMAGNET stations.

3.4 Geomagnetic Indices

The calculation of magnetic indices is based on the measurement of geomagnetic activity at various timescales and across different geographical areas and then standardized. Scientific studies and operational space weather services, along with geomagnetically quiet day identification, rely on these essential tools. The planetary K-index (Kp) was one of the first indices used in the 1950s. It is derived from 13 observatories at mid-latitudes, specifically between 44 and 60 degrees magnetic latitude, and is still crucial for space weather near real-time monitoring and forecasting. Other indices include the disturbance storm time (Dst) index, which depicts the ring current behaviour. The auroral electrojet (AE) index measures the electrojet intensity at the polar latitudes. The am and aa are both derived from the K-index scalings, but the aa index uses antipodal stations Hartland (HAD) and Canberra (CNB) to produce a long magnetic index series (Olsen & Kotsiaros, 2010). The am index is derived from the longitudinal sector groups of observatories close to 50° magnetic latitudes. There are 5 such groups in the Northern Hemisphere, and 4 in the Southern Hemisphere with a total of 24 observatories (Mayaud et al., 2023; Menvielle & Berthelier, 1991). The identification of geomagnetically quiet or disturbed days with minimal magnetic field disturbances serves as a fundamental requirement for ionospheric and magnetospheric research baseline studies. The selection of international quiet days (IQDs) and international disturbed days (IDDs) occurs monthly by assessment of global magnetic indices, including Kp and the equivalent daily amplitude index (Ap), and has

been widely used in past research studies of Sq variation (Menvielle et al., 2010).

This study focuses on the statistical analysis of APQDs and makes use of the Symmetric-H (SYM-H) index, which is derived from high-resolution and high-quality geomagnetic field data for enhanced understanding of the ring current and field-aligned currents during both quiet periods and geomagnetic storm conditions.

3.5 Symmetric-H (SYM-H) Index

The SYM-H index provides one-minute resolution geomagnetic data, which displays the worldwide average horizontal magnetic field component measurements near the magnetic equatorial region. The index provides better temporal resolution than the Dst index (Sugiura & Poros, 1971). The World Data Center for Geomagnetism in Kyoto handles the processing and distribution of the indices obtained from the data of observatories which form part of the world data services (WDS) (Imajo et al., 2022).

The derivation of these indices comprises three steps: removing background disturbances, creating a unified data structure, and determining the mean (symmetric) component and its deviations (asymmetric) from this average. Researchers use this standardized approach to track and compare time-dependent magnetic field deviations across various locations for studying geomagnetic activity and space weather phenomena. The Dst and SYM-H indices are critical tools for studying operational forecasting of satellite anomalies, radiation belt dynamics, ionospheric disturbances, and scientific modeling of magnetospheric dynamics and current systems (Ahmad & Widyanto, 2023; Zou et al., 2024).

3.5.1 Contributing Magnetic Observatories

The SYM-H index is derived from the horizontal component of the Earth's magnetic field as measured by a network of low- and mid-latitudinal ground magnetic observatories. The observatories that form this network are shown in Figure 3.5. The SYM-H derivation requires observatories that are situated near the geomagnetic equator and span across different longitudes at conjugate points to maintain an accurate global representation. The observatories are selected for their low noise levels, stable operations, and their long-term stability (Iyemori, 1990).

3.5.2 Derivation of the SYM-H and ASY-H Indices

This section briefly describes the derivation of SYM-H and asymmetric-H (ASYM-H) as presented by Iyemori (1990). The first step involves extracting the "disturbance" components

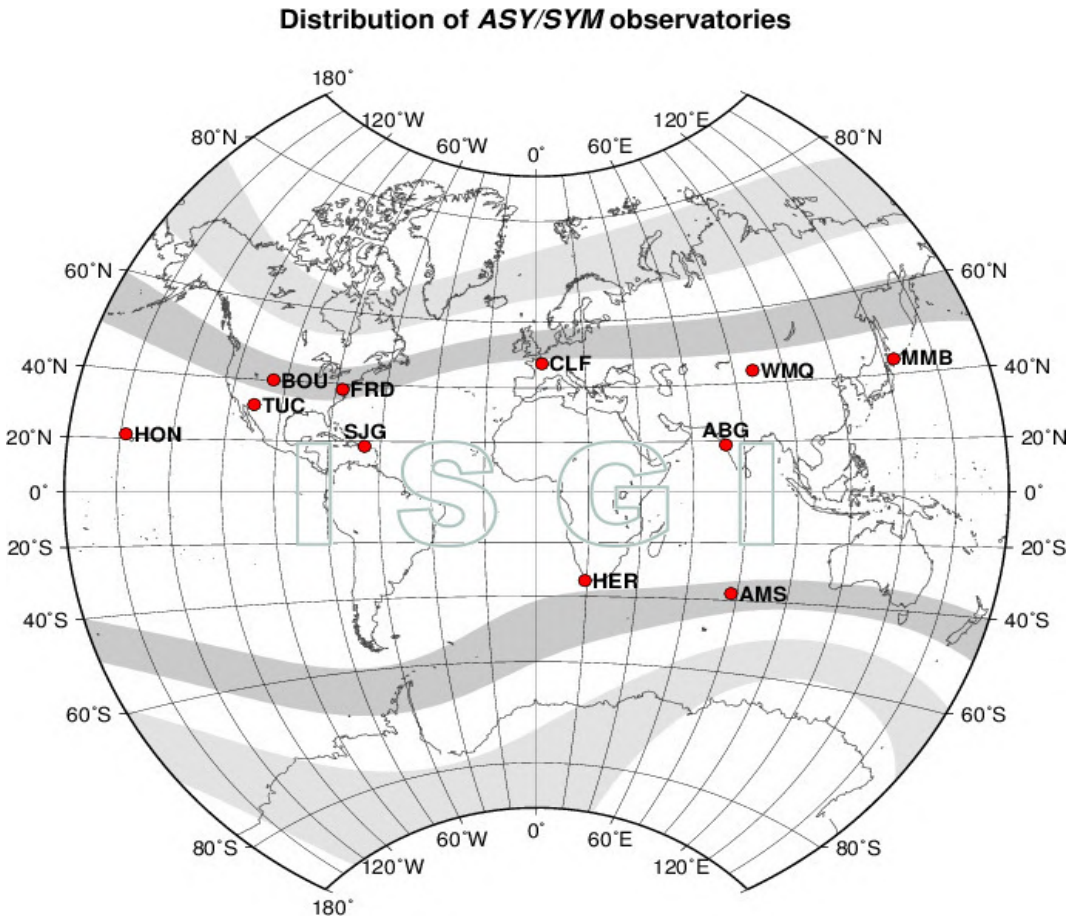

Figure 3.5: Locations of the magnetic observatories are depicted, the data of which is used for the generation of the SYM-H Index. Source: International Service of Geomagnetic Indices (ISGI) (https://isgi.unistra.fr/indices_asy.php).

from the magnetic field variations. The Sq currents, which generate daily variation along with the main geomagnetic field, are removed through this process. To calculate the Sq variation, B-spline functions are used to fit the 1-minute averaged data of designated "quiet days" (5 or 10 international quiet days) per month. This results in a base value that contains both the main field and the Sq field. This background data is subtracted from the original data to get the disturbance component. The latitudinal dependence correction is performed on the disturbance data from different observatories to achieve equal amplitude of magnetic variations.

The symmetric index is computed after the correction of the disturbance fields. Data from six observatories are combined through minute-by-minute averaging. The H-component receives its latitudinal correction by division by the average dipole latitude cosine of the stations.

The asymmetric indices track variations that differ from the symmetric average values. The symmetric component is computed from the disturbance field at each station by subtraction of background base values from the original data to obtain the asymmetric variation. A further round of latitudinal correction is applied to the H component by an empirically determined

normalization coefficient. The ASY-H obtains its final values by calculating the difference between maximum and minimum deviations across all stations in the set. The range measures how much the disturbance field deviates from uniformity.

3.6 Selection of Magnetic Observatory Data and Distribution of Longitudinal Sectors

The Sq variations of the H, X and Y components were derived from 1-minute resolution data supplied by 46 INTERMAGNET geomagnetic observatories. These stations are located between the $\pm 60^{\circ}$ magnetic latitudes. The quasi-dipole magnetic coordinates were calculated by using (https://geomag.bgs.ac.uk/data_service/models_compass/coord_calc.html). The observatories were grouped into three longitudinal sectors as suggested by Price and Wilkins (1963), namely the American (180°W to 30°W), Africa-European (20°W to 60°E), and Asia-Australian (65°E to 180°E) sectors.

Figure 3.6 shows the locations of the geomagnetic observatories as grouped in three sectors. The geographic and geomagnetic coordinates of all these INTERMAGNET observatories are shown in Appendix A. The data for the years (2008-2019) was downloaded from the INTERMAGNET website at (https://imag-data.bgs.ac.uk/GIN_V1/GINForms2) in IAGA-2002 format (http://www.ngdc.noaa.gov/IAGA/vdat/iagaformat.html). The data of the SON observatory for the years 2009-2019, was provided by the Pakistan Space Weather Centre (PSWC), Pakistan Space and Upper Atmosphere Research Commission (SUPARCO).

3.7 Selection Criteria for Solar Cycle Phases and Quiet Days

The phases of solar cycle 24 were characterized by Gyébré et al. (2018) with respect to benchmarking the relative sunspot number introduced by Rudolph Wolf (Wolf, 1859):

$$\mathrm{R_Z} = \mathrm{k} \times (10 \times \mathrm{G} + \mathrm{N}) \tag{3.7}$$

where R_Z represents the sunspot numbers, G represents the number of sunspot groups, N is the total number of observed individual spots in all the groups, and k is the correction factor. The annual mean sunspot numbers (SN) were extracted from the Sunspot Index and Long-term Solar Observations (SILSO), (https://sidc.be/silso/) Royal Observatory of Belgium (Clette & Lefèvre, 2015).

Based on the standard number of sunspots, the four phases of solar cycle 24 were classified as follows (Gyébré et al., 2018):

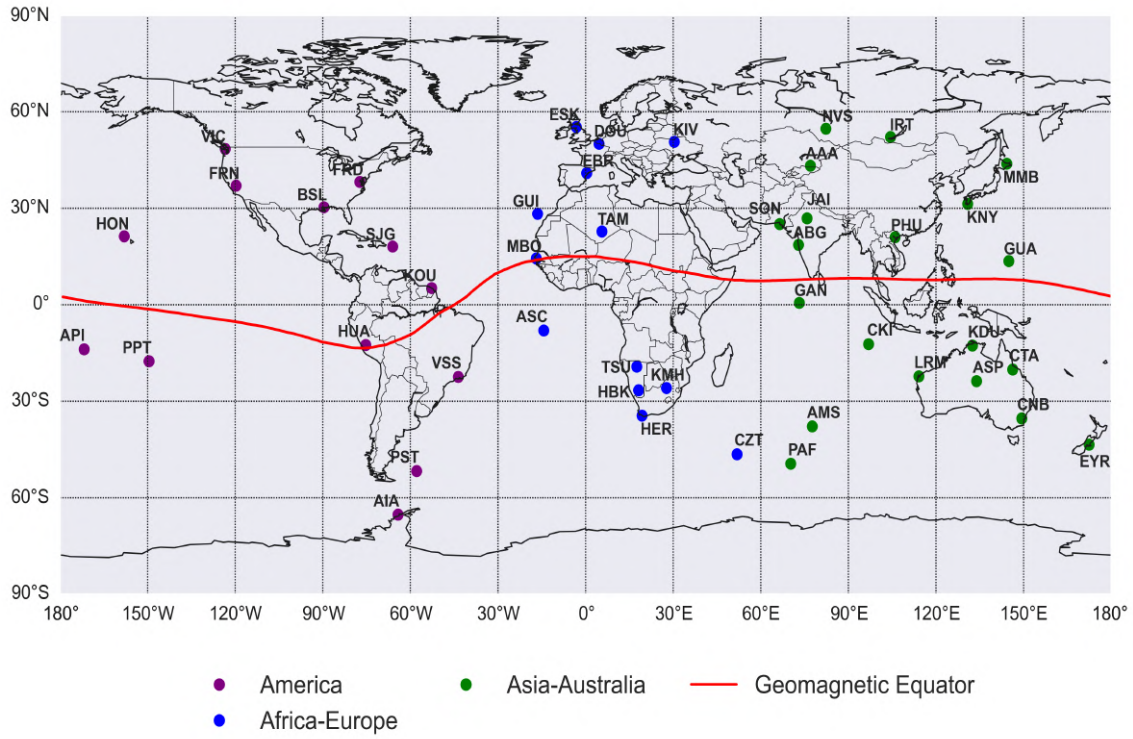

Figure 3.6: The magnetic observatories that formed part of this study.

(a) Solar Minimum ($R_Z < 20$);

(b) Increasing or Ascending Phase ($20 \leq R_Z \leq 100$);

(c) Solar Maximum ($R_Z > 100$). In the case in which the maximum value is less than 100, the maximum phase is defined by ($R_Z > 0.8 \times R_{Z_{max}}$);

(d) Decreasing or Descending Phase ($100 \geq R_Z \geq 20$).

Using the selection criteria for solar cycle phases as suggested by Gyébré et al. (2018), the duration of the solar cycle phases of 2024 were delineated as follows:

(a) Solar Minimum (2008-2009; 2018-2019);

(b) Ascending Phase (2010-2011);

(c) Solar Maximum (2012-2014);

(d) Descending Phase (2015-2017).

Although the year 2012 should have been included in the ascending phase according to the selection criteria, for our analysis, it was placed in the maximum phase. Solar cycle 24 was double-peaked, as are most solar cycles (Kane, 2007). The double peaks are known as the Gnevyshev peaks, (Gnevyshev, 1967). It has been suggested by many researchers, most notably

by Georgieva (2011), that the maximum phase begins soon after the first peak. For this reason, 2012 was included in the maximum phase. Figure 3.7 shows the phases of the solar cycle 24.

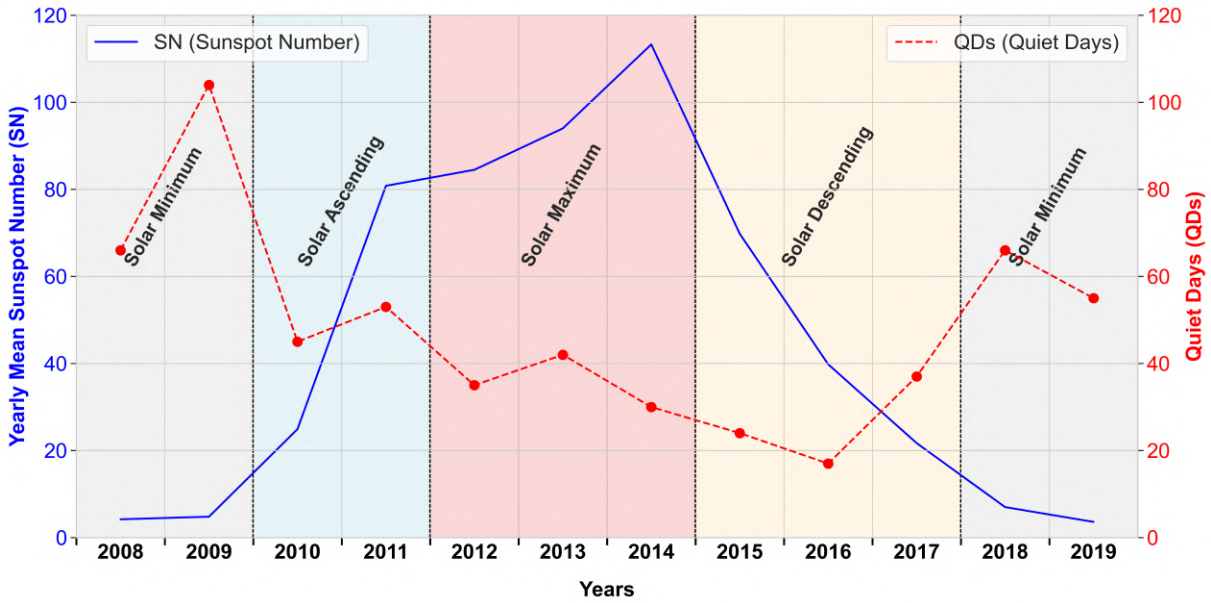

Figure 3.7: Annual mean sunspot numbers (SN) plotted with quiet days (QDs) and segmented according to the 4 phases of solar cycle 24 (2008-19).

3.7.1 Selection of Quiet Days based on SYM-H Index

Joselyn (1989) conducted a survey across the scientific community of magnetic, ionospheric and magnetospheric researchers to interrogate techniques for assessing quietest geomagnetic conditions based on ground observatory data and other indices that were used back then. The study concluded that:

(a) geomagnetic disturbances are localized in spite of the fact that most of the data indicated quietest day conditions;

(b) geomagnetic indices, although convenient, may have uncertainties based on threshold values for a 24-hour UT day;

(c) a range of factors possibly influencing the ionosphere or the magnetosphere, may not be appropriately indicated by the geomagnetic activity level indicator.

In Jocelyn's study, many indices, such as Kp, Ap, equivalent daily amplitude of averaged northern and southern Kp (Am), AE, etc., were evaluated for their authencity and shortcomings, but when it came to the Dst index, the conclusion was that the Dst index values for some geomagnetic quiet conditions on an hourly basis were greater than -10 nT. Therefore, a further check on timescales more precise than 1 hour was required to ensure that a quiet period had been correctly identified.

The 1-minute resolution of SYM-H index plays a crucial role in determining quiet periods in geomagnetic activity, offering a high-resolution alternative to other indices like Dst. Its ability to capture minute-by-minute variations makes it particularly useful for identifying and analyzing quiet intervals, which are essential for understanding the baseline state of the magnetosphere. The SYM-H index's high temporal resolution and sensitivity to solar wind parameters make it a valuable tool for distinguishing between quiet and active geomagnetic conditions. This high resolution allows for more precise monitoring of geomagnetic activity, making it easier to identify quiet periods and small-scale variations that might be missed by lower-resolution indices (Wanliss & Showalter, 2006). A comparative study of the Kp and SYM-H indices by Wanliss (2005) compared the statistical results of the quiet periods and geomagnetic storm events. It was found that quiet periods had a Kp $\leq$ 1 and SYM-H > -30 nT. The finding led to the conclusion that a much lower threshold of |SYM-H| $\leq$ 10 nT throughout 24 hours was necessary for determining QDs in every year of solar cycle 24. The high-resolution 1-minute SYM-H index was obtained from the GSFC/SPDF OMNIWeb interface at (http://omniweb.gsfc.nasa.gov/form/omni_min.html).

Figure 3.7 shows the number of QDs per year. The deep solar minimum year 2009 had the most QDs per year, namely 104, with the month of December having the most quiet days, namely 16. The least number of QDs were during 2016 which is in the descending phase of the solar cycle. This is not unusual as Singh and Patel (2021) and Gerontidou et al. (2018) have reported greater numbers of ICMEs and high-speed solar wind streams (HSSWS) during the declining phase of the solar cycle. Gerontidou et al. (2018) reported that 46 and 41 storms were catalogued during 2015 and 2016, respectively. During 2015 and 2016, the highest number of storms due to ICMEs and HSSWS reported were 34 and 17, respectively.

3.8 Processing Sq Variation

In order to evaluate APQDs, the H component was utilized in processing Sq variations. $Sq(H)$ variations were calculated by means of a consolidated method by Rabiu et al. (2007), Adhikari et al. (2017), and Bello et al. (2014). It can be described as follows:

1. The minute data of the horizontal component of the magnetic field was first converted from UT into SLT using:
$$\text{SLT} = \text{UT} + \frac{\text{Longitude}}{15}. \tag{3.8}$$
2. The H component was calculated by means of the following equation:
$$\text{H} = \sqrt{\text{X}^2 + \text{Y}^2}. \tag{3.9}$$

3. The QDs were selected according to the 1-minute SYM-H Index, based on the threshold |SYM-H| $\leq$ 10 nT.

4. The baseline was calculated by taking the averaged data of 120 minutes flanking around midnight between 00:00 and 01:59. In the case of missing data, the values between 22:00 and 23:59 were considered for the same day. The baseline is expressed as follows:

$$\mathrm{BL_H} = \frac{\mathrm{H_{00:00} + H_{01:59}}}{120}. \tag{3.10}$$

or

$$\mathrm{BL_H} = \frac{\mathrm{H_{22:00} + H_{23:59}}}{120}. \tag{3.11}$$

This BL_H was corrected to the nearest whole number in nT.

5. Hourly mean values of Sq, i.e., H_t were calculated by taking the average of 60 minutes for every hour t_i, represented by i = 00,...,23 and minutes by m = 00,...,59, as given in the following equation:

$$\mathrm{H_t} = \frac{1}{60}\sum_{\mathrm{m=00}}^{59}\mathrm{H_{t_{i,m}}}. \tag{3.12}$$

Here, H_t is defined as the hourly mean value centered at each hour from 00:30 to 23:30 in SLT.

6. For hourly $Sq(H)_t$ was obtained when the BL_H value of the given day was subtracted from the hourly value of the same day.

$$\mathrm{Sq(H)_t} = \mathrm{H_t} - \mathrm{BL_H}. \tag{3.13}$$

7. $Sq(H)_t$ is corrected for non-cyclic variation such that the value at 23:30 is the same as the value at 00:30 of the considered day. This correction is done by making a linear adjustment on the daily hourly values, so that the $Sq(H)_t$ values at 00:30, 01:30, 02:30 ,...., 23:30 SLT taken into consideration:

$$\Delta\mathrm{K} = \frac{\mathrm{Sq(H)_{23:30} - Sq(H)_{00:30}}}{23}. \tag{3.14}$$

The linearly adjusted hours were defined as follows:

$$\mathrm{Sq(H)_t} = \mathrm{Sq(H)_t} - (\mathrm{t}+1) \times \Delta\mathrm{K}. \tag{3.15}$$

These corrected hourly values for the whole day represents the Sq variation of the H-component. A similar procedure was applied to $Sq(X)$ and $Sq(Y)$.

3.9 Identification of Accurate Time for the Maximum or Minimum value in Sq Variation Data

An algorithm was formulated to calculate the time durations of QDs for NQDs, as well as the one-hour time-shifted APQDs lying outside the NQD interval, by using the processed Sq variations. The times of the peaks or dips in normal and abnormal Sq amplitude variations using the ideal Sq schema in the low- and mid-latitudes by means of the ideal Sq schema, were calculated as follows:

(a) Low-latitudinal regions (between 0° and $\pm 30^{\circ}$): peak or dip of $\mathrm{Sq(H)}_t$ amplitude lying one hour shifted outside the interval of 10:30 to 13:30 SLT (Last et al., 1976; Sastri, 1982)

(b) Mid-latitudinal regions (between $\pm 31^{\circ}$ and $\pm 60^{\circ}$): peak or dip of $\mathrm{Sq(H)}_t$ amplitude lying one hour shifted outside the interval of 08:30 to 13:30 SLT (Brown, 1974; Butcher & Brown, 1981a)

Procedures like the B-splines, piece-wise polynomial, spline smoothing, and 15- and 30-minute moving averages on processed data were analyzed for consideration of the near-accurate time of phase-shifts. 5-, 15-, 20-, 30- and 60-minute rolling means for the mentioned time windows were assessed for raw 1-minute data. The code, based on the tested algorithm, was adapted to automatically identify the accurate time of NQDs, using processed Sq variations and time shifts in amplitude peaks or dips of APQDs in the low- and mid-latitudinal regions for each longitudinal sector. The accuracy of the identified times for APQDs was further confirmed by visual inspection of a few suspicious days in the low- and mid-latitudinal regions near the Sq foci positions. If the plots depicted the exact time of the peaks or dips in the Sq variation data of APQDs in SLT in low- and mid-latitudinal regions of both hemispheres, the algorithm of the code was considered authenticated. Upon comparison and evaluation, it was observed that the cubic spline smoothing on processed Sq variations was able to derive the calculated time of phase shifts (both peaks and dips of QDs for both NQDs and APQDs) from the codes on plots. Thus, the times and amplitudes of NQDs and phase-shifts on APQDs in the low- and mid-latitudinal regions for all sectors were obtained for all years of solar cycle 24.

3.9.1 Calculation of Sq Foci Positions and Verification with Equivalent Current Systems

There were cases in which there was uncertainty as to the identification of the APQDs by means of the criteria (a) and (b) (as mentioned in Section 3.9), especially for observatories

near the Sq foci latitudes. These observatories produced fluctuating variations in Sq, with significantly low amplitudes, usually between ±5 to ±10 nT. The presence of a peak and a dip at the same time in the Sq variation data needed verification, for which deviation from the Sq zero baseline was considered, in order to determine whether a QD is an APQD or an NQD. This ambiguity was dealt with by calculating the square foci positions. The Sq foci positions of two years, namely 2009 and 2014, were calculated in order to differentiate between NQDs and APQDs and to compare the solar minimum with the maximum phase.

There are practical methods with which to calculate the Sq foci positions before resorting to the techniques of spherical harmonics, which produce greater accuracy. The technique suggested by Tarpley (1973) involves locating the position of the Sq foci near observatories with $\Delta H = 0$ between 11:30-12:30 SLT.

In an evaluation of methods for determining the location of Sq foci, Stening et al. (2005) suggested that the latitude of the focus of the Sq current system should be determined by using at least 3-4 magnetic observatories having at least 95% available data. Moreover, for a more accurate determination of the Sq foci latitude, a longitudinal chain, in which the local time difference should not be more than 2 hours (30°) in each hemisphere, must be selected. The time of the zero axis crossing of the $Sq(Y)$ component is used to estimate the Sq value at that particular time. The observatory at Sq foci position will have almost no variation in the H-component. The magnetic observatories are then aligned according to the ascending magnetic latitudes and a linear regression fit (>95%) is used to correctly locate the Sq foci positions. To confirm the maximum or minimum phase shift already calculated, the $Sq(H)$ for the considered longitudinal sector is plotted in panels starting from the Northern Hemisphere to the Southern Hemisphere. Then the calculated Sq foci position is confirmed by comparing the calculations with the plots and the equivalent current vectors. Using this procedure, the Sq foci positions for 2 April 2014 were calculated by using the mentioned method for the Asia-Australian sector on 02 April 2014 and were verified with Archana and Arora (2024). A slight difference of 2° in the Northern and 1° in the Southern Hemisphere was found in the Sq foci latitudes in both hemispheres (Figure 3.8).

In cases where there seemed to be ambiguity with respect to APQDs and Sq foci positions, the equivalent current vectors were calculated by using the orthogonal components of the magnetic field, namely X and Y. The data from the same observatories used to determine the Sq variations were utilized to process $Sq(X)$ and $Sq(Y)$. Data of the observatories that were used to determine the latitude of the Sq foci in each longitudinal sector were selected with a time difference of no more than 2 hours (longitudinal difference under |30|°) to ensure accuracy of the calculated Sq foci positions and times in SLT. The $Sq(X)$ and $Sq(Y)$ of observatories that had more than 95% available data were combined in the form of vectors and rotated by 90° to

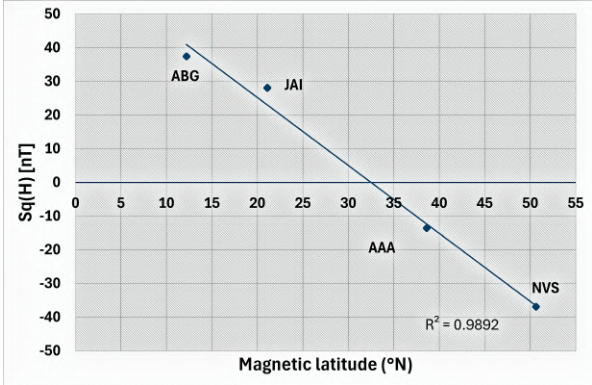

(a) The calculated Sq focus at 33°N magnetic latitude

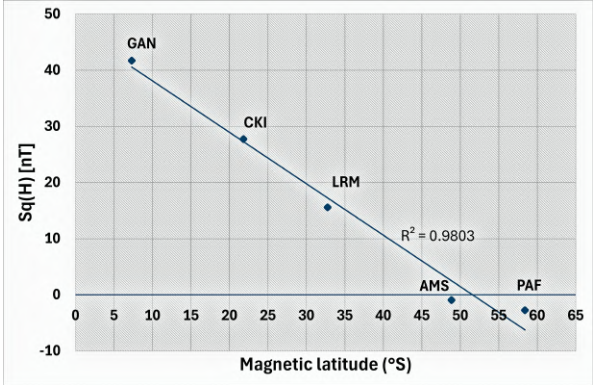

(b) The calculated Sq focus at 52°S magnetic latitude

Figure 3.8: Plots of calculated Sq foci latitudes in magnetic latitudes for 2 April 2014, in the Asia-Australian sector.

create the equivalent current vectors in order to match the calculated positions and associated times of the Sq foci latitudes. The process was repeated for every year of the solar cycle, in order to establish the times of dips and peaks of NQDs and APQDs which seemed ambiguous. Certain cases of deformed, tilted or distorted Sq current vortices in which the number of APQDs seemed unusually high, were analyzed to determine the existence of APQDs in both the low- and mid-latitudinal regions, by using the equivalent current vectors.

3.9.2 Statistical Analysis of APQDs

Statistical analysis by sector, latitude and hemisphere during every phase of the solar cycle was done, incorporating Lloyd's seasons Lloyd (1874). This has been widely used by many studies, more recently in Zhao et al. (2022). Statistical analysis of data was done for stations with data availability of 85% for each solar cycle phase. The categories are: November-February belong to the December solstice (D), March, April, September, October belong to the equinoxes (E) and May-August belong to the June solstice (J).

The occurrence rates of Sq foci positions offset from the ideal Sq schema in the years 2009 and 2014 were calculated. The Sq foci offsets included Sq foci latitudes beyond the magnetic latitude of the ideal Sq schema (30° N or S) in either the low- or mid-latitudinal regions of either hemisphere.

$$\%\text{ideal Sq schema} = \frac{\text{ideal Sq schema counts}}{\text{QDs}} \times 100. \tag{3.16}$$

$$\%\text{Sq foci offsets} = \frac{\text{counts of offsets}}{\text{QDs}} \times 100. \tag{3.17}$$

The rates of occurrence of APQDs were calculated for an equal number of low- and mid-latitudinal observatories in each hemisphere with respect to magnetic latitude and geographic longitude as:

$$\%\text{APQDs} = \frac{\text{APQDs}}{\text{QDs}} \times 100. \tag{3.18}$$

where QDs = NQDs + APQDs. The annual averages were then calculated for each solar cycle phase to determine consolidated results.

Statistical variations of APQDs according to sectors and hemispheres were calculated separately for the low- and mid-latitudinal regions. An equal number of observatories per hemisphere (at least 3 or more in each hemisphere), situated at magnetically conjugate latitudes in each longitudinal sector, was included. The following equation was applied:

$$\%\text{APQDs}_{\text{NH}} = \left(\frac{\text{APQDs}_{\text{NH}}}{\text{APQDs}_{\text{NH}} + \text{APQDs}_{\text{SH}}} \right) \times 100. \tag{3.19}$$

where APQDs represents the total sum of APQDs available for the considered longitudinal sector for each year. The same equation was applied to APQDs_{SH}. The seasonal annual averages were then calculated for each solar cycle phase to determine consolidated results by sector and hemisphere in each phase.

The distribution of APQDs was statistically analyzed using magnetic observatories in the same longitude sector for conjugate latitudinal regions. This was undertaken to illustrate an unusually higher number of APQDs in each hemisphere for both low- and mid-latitude to upper mid-latitudinal regions. This analysis was undertaken to understand the symmetric or asymmetric occurrence distribution of APQDs for such pairs of observatories and to understand whether variation of the Sq foci positions and IHFACs play a role.

The occurrence times for the hourly distribution of the NQDs and APQDs were tabulated according to Lloyd's seasons for each observatory pair for every year of the solar cycle. The occurrence rate of hourly distribution (HD) of NQDs and APQDs, evaluated between 03:30 and 21:30, was calculated using the formula below:

$$\%\text{HD} = \frac{\text{HC}}{\text{QDs}} \times 100. \tag{3.20}$$

where HC represents hourly occurrence counts of both NQDs and APQDs during the mentioned time span for each considered observatory pair: QDs = NQDs + APQDs.

3.10 Flowchart of the Methodology

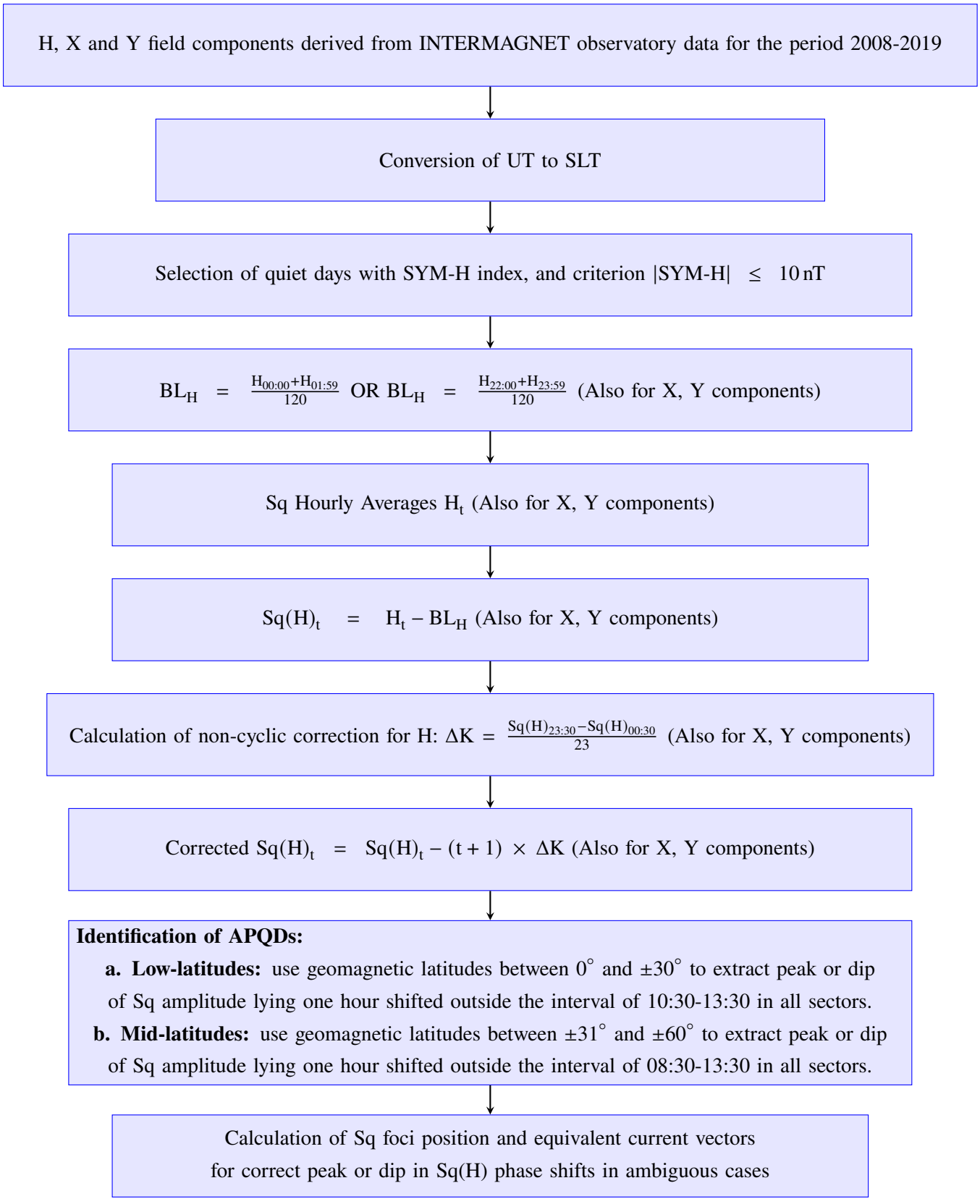

3.11 Summary

In this chapter, the method used to extract the APQDs was discussed. The solar cycle 24 phases were defined by means of the time distribution of annual mean sunspots over 11 years. These phases identified the years that each phase, namely minimum, ascending, maximum, and descending, spanned. The geomagnetic field data was downloaded from the INTERMAGNET database and consolidated into 3 longitudinal sectors. The quietest days were selected by means of the SYM-H index for every year. In order to process Sq variation for the quietest days, geomagnetic data was converted from universal time (UT) to SLT, and the baselines and non-cyclic corrections were taken into account. This process led to correctly identifying the exact time of the maximum/minimum amplitude of Sq (peaks/dips) relative to the expected phase shift for each observatory at magnetic latitudes in low- and mid-latitudes. Moreover, temporal analysis techniques were tested, which required the best fit on hourly processed and 1-minute raw data for checking the accuracy of APQD times. The calculation of the Sq foci positions and the use of the equivalent current vectors provided useful insight into the assessment of the calculated correct times of the APQDs in order to rectify ambiguous cases.

Once the rigorous assessments had been verified and inferred, APQDs were identified in the low- or mid-latitudes. Statistical variation was analyzed, and the rate of APQD occurrence by season and hemisphere in all longitudinal sectors were calculated. The hourly distributions of NQDs and APQDs for using conjugate observatory pairs in different phases were also carried out for all phases of solar cycle 24.

Chapter 4

Results

The investigation into APQDs during solar cycle 24, segmented into phases across various sectors, provides a comprehensive framework for understanding ionospheric variability as manifested in ground magnetic field data. This chapter examines the global, local, and regional occurrences of APQDs, spanning the period 2008 to 2019, with a focus on latitudinal and hemispheric statistics to detect patterns in APQD occurrences relative to magnetic latitudes and geographic longitudes. The examination of the hourly distribution of NQDs and APQDs for magnetically conjugate observatory pairs, which were selected based on the highest percentage of APQD occurrence within each sector, revealed asymmetries in the low- and mid-latitudes of the Northern and Southern Hemispheres. A comparative analysis of 2009 and 2014 facilitated the identification of key differences in APQD characteristics between the solar minimum and maximum phases, while a detailed examination of Sq foci position variations across all sectors shed light on the dynamic behavior of ionospheric currents. Additionally, the research quantified the percentage occurrence of the Sq foci at $\pm 30^{\circ}$ and beyond, by comparing these occurrences across all three sectors to gauge the extent of Sq foci latitude displacement.

To understand the variation in the Sq foci positions on the quietest days and their impact on APQDs, a detailed statistical analysis was undertaken, using Lloyd's seasons as a framework (Lloyd, 1874). These seasons encompass the June (J) and December (D) solstices and the equinoxes (E) for each longitudinal sector, (i.e. June (J) and December (D) Solstices, and Equinoxes (E)) for each longitude sector, solar cycle phases, each hemispheres, and low-latitudinal (between 0° and $\pm 30^{\circ}$) and mid-latitudinal (between $\pm 31^{\circ}$ and $\pm 60^{\circ}$) regions. The results of the statistical analysis were combined for different phases of solar cycle 24, making use of the categories suggested by Gyébré et al. (2018) and Ouattara and Amory-Mazaudier (2012):

(a) Solar Minimum (2008-2009; 2018-2019);

(b) Ascending Phase (2010-2011);

(c) Solar Maximum (2012-2014);

(d) Descending Phase (2015-2017).

4.1 Statistical Results of the Investigation of Regional and Global APQDs Occurrence for Different Phases of Solar Cycle 24

This section presents the statistical results of the investigation of regional (in longitudinal and hemispheric regions) and global APQD occurrence rates for different phases of solar cycle 24. An equal number of low- and mid-latitudinal observatories in each hemisphere (minimum 2) was chosen for the plotting of the statistical distribution of regional and global APQDs for each solar cycle phase. However, due to an insufficient number of low-latitudinal observatories and low data availability in the Africa-European sector, the low-latitudinal statistics will not be presented for this region.

Figure 4.1 presents global (a) and regional (b) occurrence rates of APQDs during solar minimum. These results indicate that the occurrence rate, both globally and regionally, of APQDs during the E seasons decreased. In general, the seasonal sequence for the global as well as regional APQDs was observed to be D, J and E seasons in the descending percentage order. However, the Asia-Australian sector deviated from the general seasonal sequence to depict the D, E and J seasons sequence in the mid-latitudes. In the mid-latitudes, the Africa-European and Asia-Australian sectors had the highest APQD occurrence during the D season, while the American sector had the highest occurrence in the J season. During the E-season, the APQDs occurrence rate was the highest in the Africa-European sector, and lowest in the American sector. Furthermore, the occurrence rate of APQDs was dominant in the Southern Hemisphere compared to the Northern Hemisphere, except in the D and E seasons in the American sector, where this trend was reversed. In low latitudes, the American and the Asia-Australian sector had the highest APQD occurrences during the D and J seasons. The fewest APQDs were observed in the E season in the American sector compared to the Asia-Australian sector. Moreover, the occurrence of APQDs was dominant in the Northern Hemisphere compared to the Southern Hemisphere.

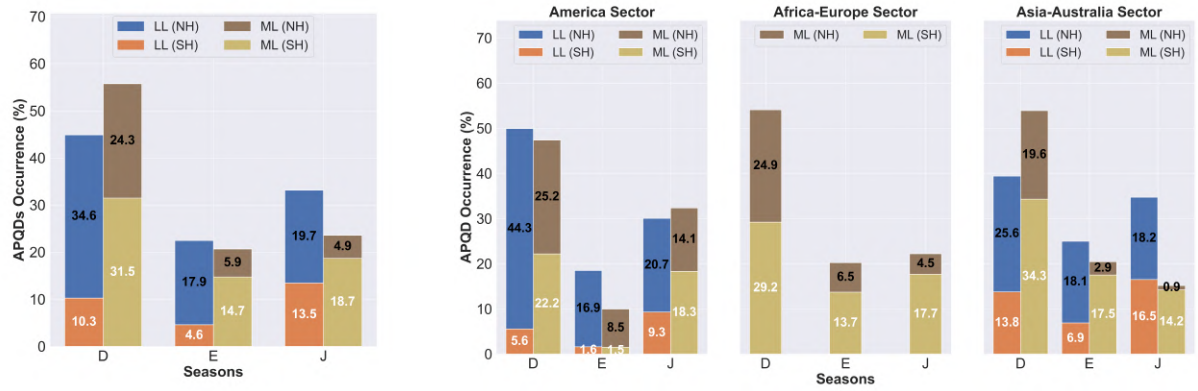

(a) (b)

Figure 4.1: Global (a) and regional (for the America, Africa-Europe and Asia-Australia sectors) (b) APQDs occurrence rates for solar minimum phase. The seasons of June (May, June, July and August) and December (November, December, January and February) solstice, and equinoxes (March, April, September and October) are abbreviated as D, J and E respectively. The low-latitudes (LL) are depicted by blue and orange bars for the northern hemisphere (NH) and the southern hemisphere (SH), respectively. Similarly, the mid-latitudes (ML) are depicted by brown and beige bars for the northern hemisphere (NH) and the southern hemisphere (SH), respectively.

Figure 4.2 shows similar statistics as Figure 4.1, but for the ascending phase of solar cycle 24. Figure 4.2 (a) and (b) indicates that for the low latitudes, the seasonal occurrence rate of APQDs decreased in the order of D, J, and E, both globally and regionally. While the same seasonal order was observed in the American mid-latitudes, the order changed to D, E, and J in the African-European and Asia-Australian mid-latitudes. The American sector displayed unique patterns, with APQDs being absent in the Southern Hemisphere during the E season for both low- and mid-latitudes. The Southern Hemisphere depicted increased APQDs at mid-latitudes compared to the Northern Hemisphere, with the exception of the American sector during the E and J seasons. However, this trend was in reverse order in the low-latitudes, where the APQD occurrence in the Northern Hemisphere was greater than in the Southern Hemisphere. The highest rates of occurrence of APQDs were observed in the American sector for the D season in both the low- and mid-latitudes.

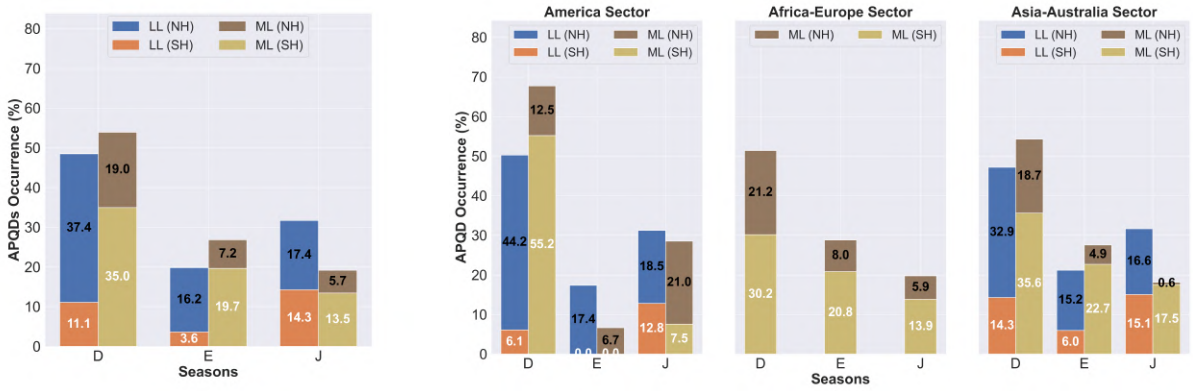

(a) (b)

Figure 4.2: Same as Figure 4.1 for the solar ascending phase.

Figure 4.3 presents the same statistics as in Figure 4.1, but for the solar maximum phase. The seasonal global and regional APQD occurrence trend was similar to that of the solar minimum phase, when the highest and lowest occurrences were observed for the D and E seasons, respectively. As in the ascending phase, no APQDs were observed in the American sector in the Southern Hemisphere during the E season for both low- and mid-latitudes. The occurrence of regional APQDs was consistently higher in the Southern Hemisphere in the mid-latitudes for all seasons, except for the E season in the American sector. However, regional APQD occurrence rates were consistently higher in the Northern Hemisphere in the low-latitudes for all seasons, except globally and for the Asia-Australian sector in the J season. For low-latitude observatories, the American sector dominated in APQD occurrences, particularly during D and J seasons.

Figure 4.4 gives the same information as Figure 4.1, but for the descending phase of solar cycle 24. The seasonal sequence globally for APQDs was D, J and E for the low-latitudes and D, E and J for the mid-latitudes. A similar seasonal sequence was observed for the regional APQDs in both low- and mid-latitudes, except for the American mid-latitude sector, where the highest and lowest occurrence rates were observed during the D and E seasons, respectively. The Africa-European sector exhibited the highest APQD occurrences in mid-latitudes during the D season, followed by the Asia-Australian and American sectors. In the low-latitudes, the Asia-Australian sector observed the most APQDs during the D season than the other sectors. APQDs occurrence rates were dominant in the Northern Hemisphere at low-latitudes. However, this trend was reversed for mid-latitudes, except for the E season in the American sector, as no APQDs were observed in the mid-latitudes of the Southern Hemisphere during this season.

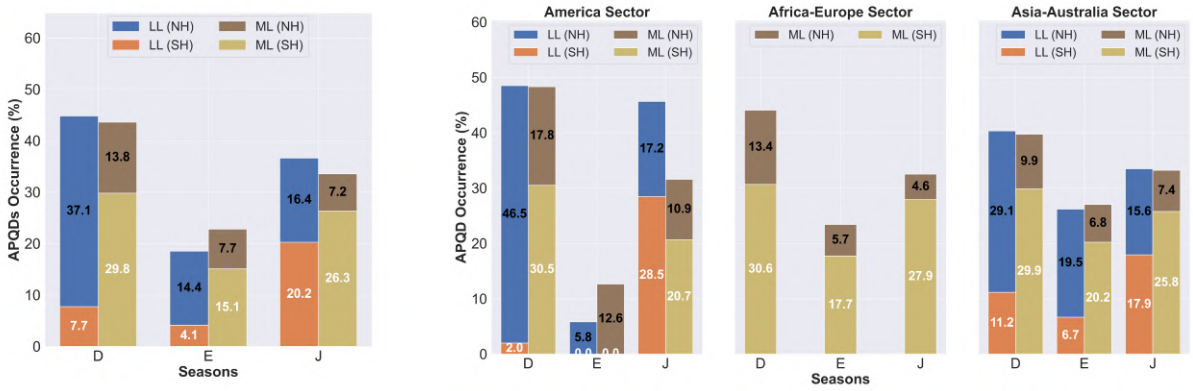

(a) (b)

Figure 4.3: Same as Figure 4.1 for the solar maximum phase.

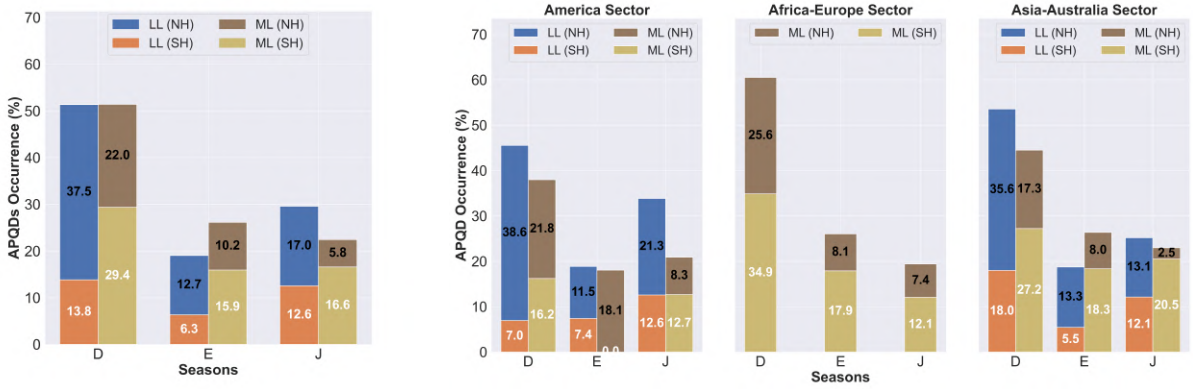

(a) (b)

Figure 4.4: Same as Figure 4.1 for the solar descending phase.

A noteworthy outcome from global APQDs in each solar cycle phase is depicted in Table 4.1.

Table 4.1: APQDs occurrence rates observed in individual hemispheres for each solar cycle phase

Phase / **Hemisphere**	Minimum (%)	Ascending (%)	Maximum (%)	Descending (%)
(NH)	37	27	32.3	35
(SH)	31.2	33	35	31.4

4.2 APQD Occurrence Rate Distribution by Hemisphere and Magnetic Latitude

An investigation of the APQD occurrence rates, based on the data from an equal number of observatories in each hemisphere with respect to magnetic latitude and geographic longitude, facilitates a balanced assessment of hemispheric contributions to APQD generation and its mechanism. Making use of the same number of observatories in each hemisphere minimizes potential bias arising from uneven spatial distribution and ensures a more robust comparison of APQD occurrence rates. The use of magnetic latitude as a reference coordinate accounts for the interaction of the geomagnetic field with the dynamics of ionospheric plasma, offering a more accurate representation of APQD distribution. Some observatories in conjugate latitudinal regions (mostly selected from 14 and 17 observatories in each hemisphere) were not included in some of the phases of solar cycle 24 due to the absence of APQDs or missing data of up to 15%. Some recorded NQDs only; hence, they were replaced with only observatories that depicted APQDs.

Figure 4.5 (a) presents APQD occurrence rates for the solar minimum phase. These results were based on the data from 17 observatories in each hemisphere. The analysis of APQD occurrence rates revealed notable hemispheric asymmetries and regional variations. In the Africa-European (20°W to 60°E) sector, mid-latitudinal observatories TSU, HER, and CZT in the Southern Hemisphere showed significantly higher APQD occurrences than observatories in the conjugate latitudinal region. The Asia-Australian (65°E to 180°E) sector exhibited a similar trend as depicted by the southern mid-latitudinal observatories PAF, AMS, and CTA. In addition, in the low latitudes, the Northern Hemisphere had higher APQD occurrence, as seen in KNY, compared to the Southern Hemisphere. Low-latitude observatories in the American (180°W to 30°W) sector demonstrated a marked variation in the occurrence rates of APQD, with SJG and HON showing considerably higher rates than the observatories in the conjugate regions.

Figure 4.5 (b), (c) and (d) represent APQD occurrence rates for 14 observatories in each hemisphere in the solar ascending, maximum and descending phases, respectively. The analysis revealed a consistent pattern of higher APQD occurrence rates in the Southern Hemisphere for mid-latitudes, except for the American sector where both hemispheres had similar occurrence rate. Similarly, in the Northern Hemisphere for low-latitudes, a consistent pattern of higher APQD occurrence rates was observed, except for the Africa-European sector which had similar occurrence rates in both hemispheres.

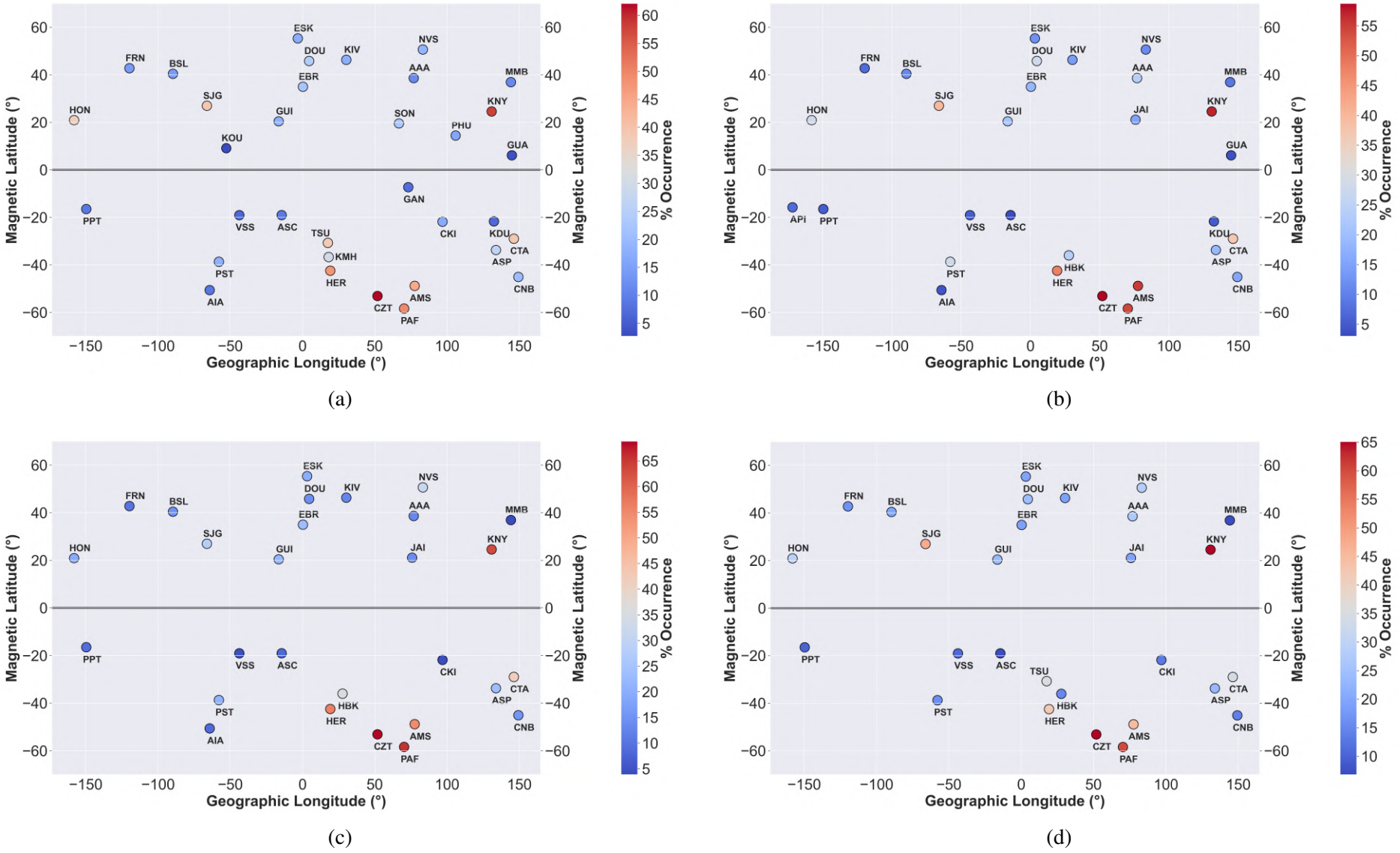

Figure 4.5: APQD occurrence rates for minimum (a), ascending (b), maximum (c), and descending (d) phases of solar cycle 24 as consolidated for equal number of observatories in each hemisphere (17, 15, 14, 14) in each phase, respectively.

This hemispheric asymmetry was particularly pronounced in the Africa-European sector, where the observatory, CZT (69%) in the Southern Hemisphere, exhibited a nearly five-fold higher occurrence rate than its northern counterpart, ESK (20%), in the maximum (b) phase. Similar trends were observed in the Asia-Australian sector, when the Southern Hemisphere observatories generally exhibited higher APQD occurrence rates at PAF-NVS (65% vs. 32%) and AMS-AAA (55% vs. 13%) than the conjugate latitudinal regions for all phases. The low-latitudinal observatory, KNY, exhibited 63% in contrast to the conjugate observatory CTA which exhibited a 42% APQDs occurrence rate for the solar maximum phase. Furthermore, the American sector exhibited lower occurrence rates than the conjugate latitudes, but maintained an asymmetric pattern at SJG and HON. Such trends prevailed in the ascending (a) and descending (c) phases.

4.3 Hourly Distribution (HD) of AQPD Occurrence at Magnetically Conjugate Observatory Pairs

The conjugate observatory pairs for both the low- and mid-latitudes with highest APQDs occurrence rates in every longitudinal sector, were presented in this section. The closest conjugate pairs were found in the Africa-European sector, whereas the conjugate pairs in other sectors were selected due to the availability of complete data for solar cycle 24 and these were separated by less than 10°. The hourly distributions of APQDs alongside the NQDs for each conjugate pair were presented in Figures 4.6 - 4.9 for every phase of solar cycle 24. These results highlight the latitudinal as well as temporal asymmetry between the morning and afternoon hours for each observatory pair in all phases of solar cycle 24. However, in the Africa-European sector, the low-latitudinal observatory data, being insufficient, was not considered for HD plots, and two pairs of mid-latitude stations were used instead.

The magnetic latitudes of the observatories that were used in this subsection were shown in Table 4.2. The IAGA codes and observatory names of all these INTERMAGNET observatories can be found in Appendix A. In each sector, at least 2 conjugate observatory pairs in the mid- and low-latitudes were selected and were represented in blue (NH) and brown (SH) in Figures 4.6 - 4.9. For the sake of comparison, conjugate observatory pairs for each sector were plotted together to depict similarities and differences in the occurrence times of NQD (hatched bars) and APQDs (solid bars).

Table 4.2: NH and SH conjugate observatory pairs by sector

Sector	OBS Pair 1	Geom Lat(°)	OBS Pair 2	Geom Lat(°)
American	BSL (ML)	40.82	SJG (LL)	26.98
	PST (ML)	-38.73	VSS (LL)	-19.07
Africa–Europe	ESK (ML)	52.37	DOU (ML)	45.80
	CZT (ML)	-53.12	HER (ML)	-42.48
Asia–Australia	NVS (ML)	50.62	KNY (LL)	24.58
	PAF (ML)	-58.76	CTA (LL)	-28.98

During solar minimum, for the mid-latitude pair, BSL-PST (Figure 4.6(a)) and the low-latitude pairs SJG-VSS (Figure 4.6 (d)) in the American sector, greater occurrence of APQDs was observed during the morning hours (07:30-08:30 SLT) than during the afternoon for all seasons, with higher percentages during the D season. No APQDs were observed for VSS for the E season, while they were observed at its conjugate observatory (SJG). Furthermore, there were more APQDs at SGJ than at VSS during all seasons, while this occurrence trend was not clear at the mid-latitudinal pair (BSL and PST). In the Africa-European sector, CZT recorded higher APQDs during the afternoon (04:30 SLT) during all seasons, while ESK recorded APQDs during both the morning (03:30-07:30) and afternoon (14:30-21:30) hours (Figure 4.6(b)). A similar trend was observed for DOU and HER, where HER observed higher APQDs during the morning (06:30-07:30 SLT), while DOU observed APQDs in both the morning (03:30-07:30 SLT) and afternoon (14:30-21:30 SLT) hours (Figure 4.6(e)). CZT and HER had a higher occurrence of APQDs than their conjugate observatories. In the Asia-Australian sector (Figure 4.6(c) & (f)), NVS and PAF showed a significant occurrence of APQDs during the afternoons of the D and E seasons (14:30-15:30 SLT). However, APQDs occurred mostly during the morning (07:30 SLT) at PAF and no APQDs were observed at NVS during the J season. KNY and CTA depicted APQDs throughout the day in all seasons, with higher APQDs in the morning hours (07:30-09:30 SLT) and relatively less APQDs during the afternoon hours (14:30-16:30 SLT).

During the ascending phase in the American sector, the mid-latitude pair, PST-BSL (Figure 4.7(a)) and the low-latitudinal pairs SJG-VSS (Figure 4.7(d)), both showed a higher occurrence of APQDs in the morning hours (06:30-07:30 SLT) during all seasons, with the highest percentages during the D season. No APQDs were observed at VSS during the E season, with sparse occurrence during the afternoon hour (16:30 SLT) of the D and J seasons. On the other hand, APQDs were observed during all three seasons at SJG, but with sparse occurrence during the E and J seasons. In the Africa-European sector (Figure 4.7(b) & (e)), CZT recorded APQDs during the afternoon (14:30 SLT), while ESK recorded them during both the mornings (06:30-

07:30 SLT) and afternoons (14:30-19:30 SLT). There were more APQDs at CZT than at ESK for all seasons, with higher APQD occurrence for the D season. On the other hand, HER and DOU both observed APQD occurrence rates during the morning as well as during the afternoon for the D season, but primarily during the afternoon (14:30-15:30 SLT) for E and J seasons. In the Asia-Australian sector (Figure 4.7(c) & (f)), PAF showed significant occurrence of APQDs during the D season afternoons (14:30-20:30 SLT) in all seasons, while NVS also had higher APQD occurrence during the afternoon during the D season. APQDs were scarce during the E and J seasons. KNY and CTA observed APQDs throughout the day in all seasons. An increased APQDs occurrence rate was observed during the morning hours (07:30-09:30 SLT) of D season, but during the afternoon hours (15:30-17:30 SLT) in the E and J seasons for KNY. However, for CTA, a higher occurrence rate was observed in the morning hours (06:30-09:30 SLT) for three seasons. At CTA, relatively lower APQDs were observed than for KNY during all the seasons.

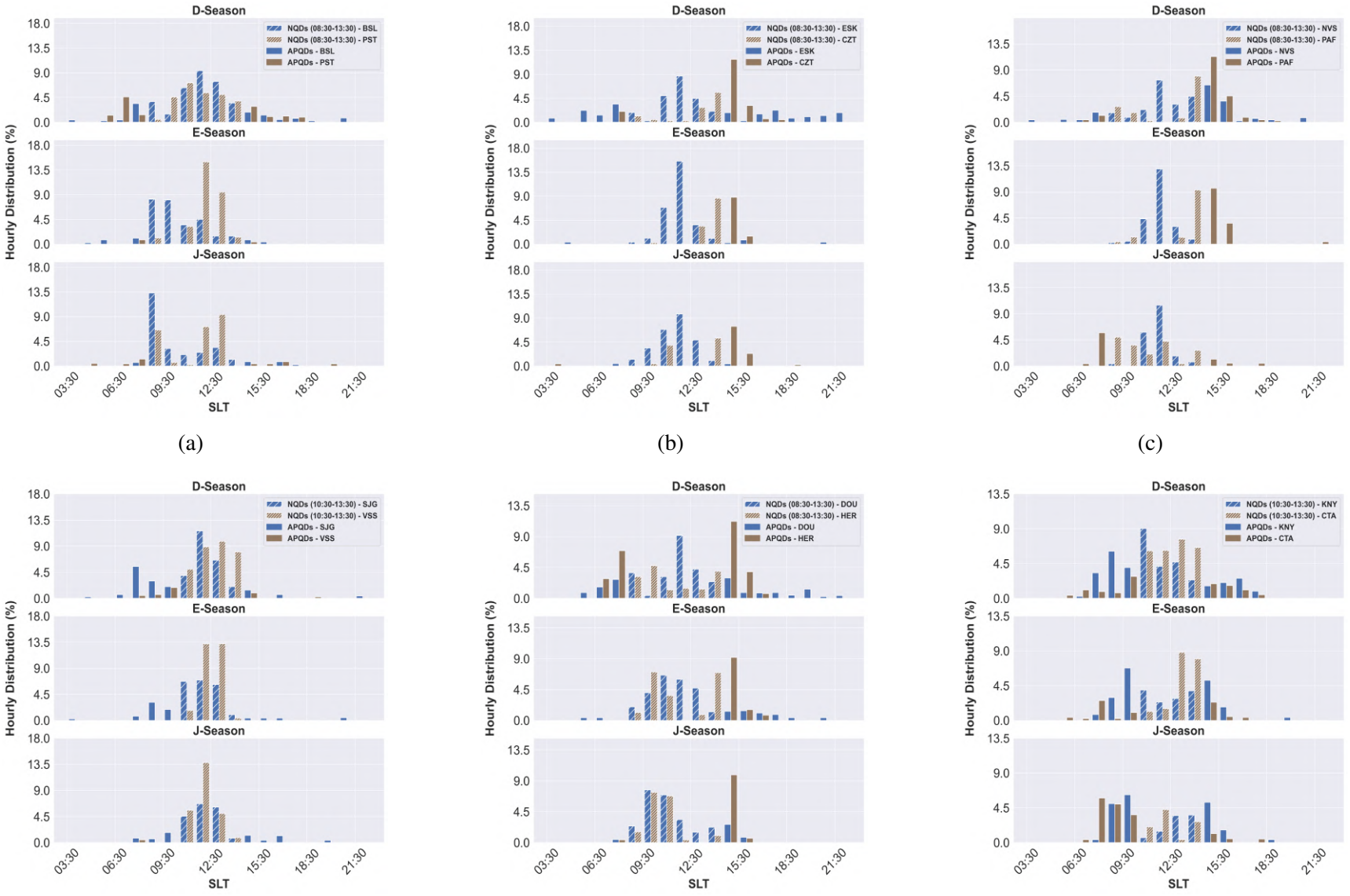

Figure 4.6: HD bar graphs of conjugate observatory pairs for the period 03:30 to 21:30 SLT in the American sector (a) & (d), the Africa-European sector (b) & (e) and the Asia-Australian sector (c) & (f) for the solar minimum phase. The hemisphere for the low- and mid-latitude observatories were represented by blue (NH) and brown (SH), respectively.

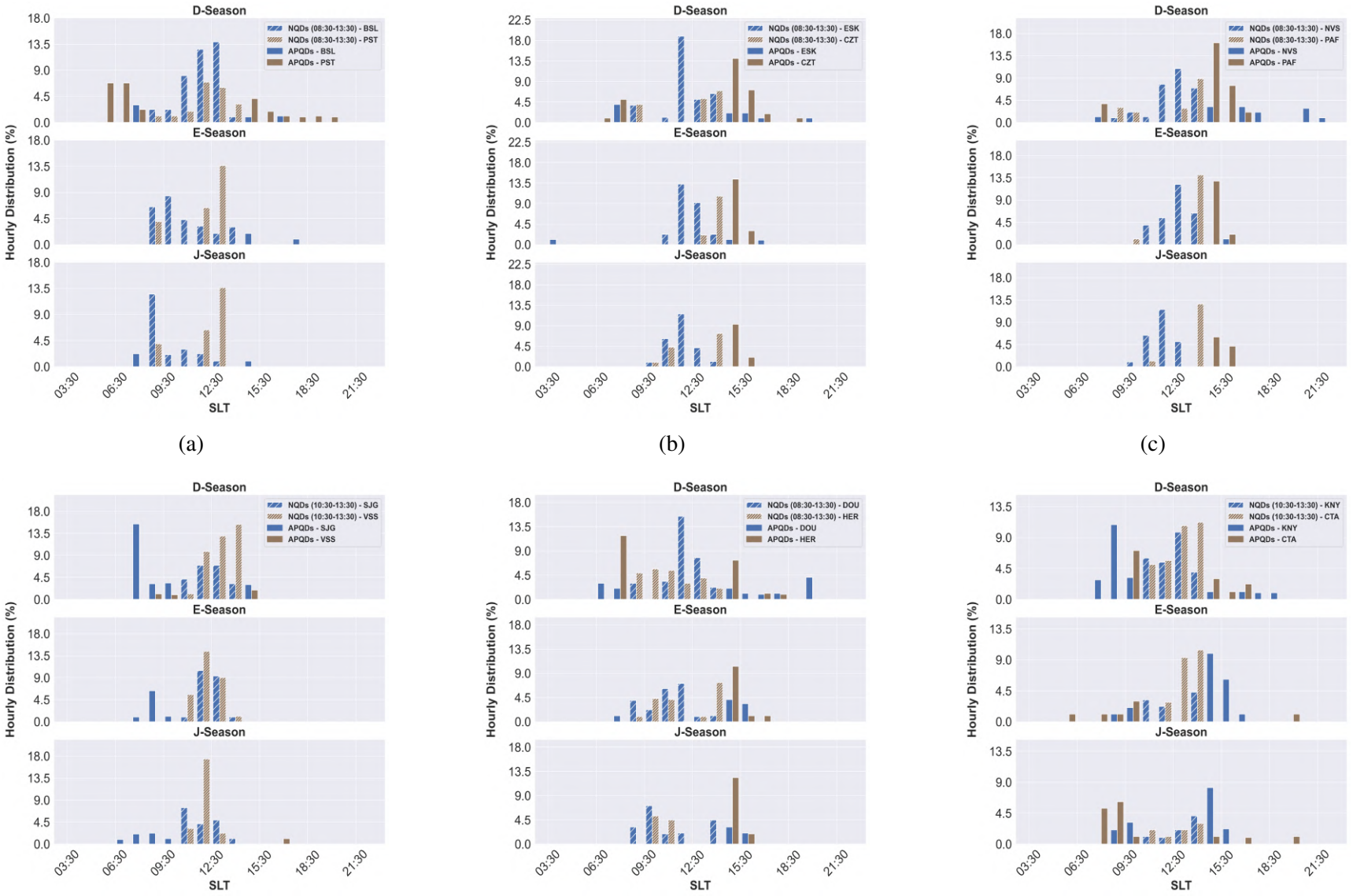

(a) (b) (c)

(d) (e) (f)

Figure 4.7: Same as Figure 4.6 for the solar ascending phase.

During solar maximum of the American sector (Figure 4.8(a) & (d)), APQDs were observed more during the morning (05:30-07:30 SLT) for the conjugate pairs of BSL-PST during 05:30-07:30 SLT in the D season, while afternoon APQDs were generally less than 1% (14:30-19:30 SLT) during the other seasons. For the conjugate pairs of SJG-VSS, mostly morning (06:30-09:30 SLT) APQDs were observed during all the seasons, with significantly higher rates during the D season. However, no APQDs were observed at VSS during the E season, while at SJG they were sparse during the E and J seasons. In the Africa-European sector (Figure 4.8(b) & (e)), afternoon APQDs dominated at 14:30 SLT at ESK and CZT during all seasons, and occurrences were higher in CZT than at ESK during all seasons. DOU and HER observed higher APQDs during the morning (03:30, 06:30-07:30 SLT) during the D season and during the afternoon (15:30-16:30, 21:30 SLT) during the E and J seasons. HER recorded more APQDs than DOU during all seasons. The Asia-Australian sector (Figure 4.8(c)) exhibited mostly afternoon APQDs at PAF and morning APQDs at NVS, with higher occurrences at PAF than at NVS. Most APQDs were observed during the morning hours (07:30-09:30 SLT) during the D season and afternoon hours (14:30-16:30 SLT) during the E and J seasons for KNY, but in the afternoon (14:30-16:30 SLT) during the D season and mornings (07:30-09:30 SLT) during the J season at CTA (Figure4.8(f)). APQD occurrences were more dominant at KNY than at CTA.

The American sector (Figure 4.9(a) & (d)) displayed complex APQD distributions at PST and BSL during the descending phase. In Figure 4.9(a), PST (brown) observed APQDs during the morning and afternoon hours during the D season, but only morning APQDs during the J season. BSL, on the other hand, observed more APQDs in the morning hours during the D season, and only afternoon APQDs during the J season. No APQDs were observed for PST during the E season, as was the case during the ascending and maximum solar cycle phases, but APQDs were seen during both the morning and afternoon hours at BSL during the same season. The SJG-VSS pair displayed higher APQDs occurrence rates during the morning hours (06:30-09:30 SLT) during all seasons. In the Africa-European sector (Figure 4.9(b) & (e)), CZT and HER showed notable occurrence of APQDs during the afternoon hours (14:30-15:30 SLT) for all the seasons, with an increase during the D and J seasons, respectively, as compared to their conjugate observatory pair. HER also observed a significant occurrence of APQDs during the D season during 06:30-07:30 SLT, while APQDs at DOU mostly occurred in the afternoon. No APQDs were observed at ESK during the J season, while CZT observed only afternoon APQDs in this season. In the Asia-Australian sector (Figure 4.9(c), PAF observed greater APQDs in the afternoon (14:30 SLT) during all seasons, with greater occurrence during the D and E seasons. However, APQD occurrence was greater in the afternoon during the D season at NVS and scarce or absent during the E and J seasons (Figure 4.9(f)).

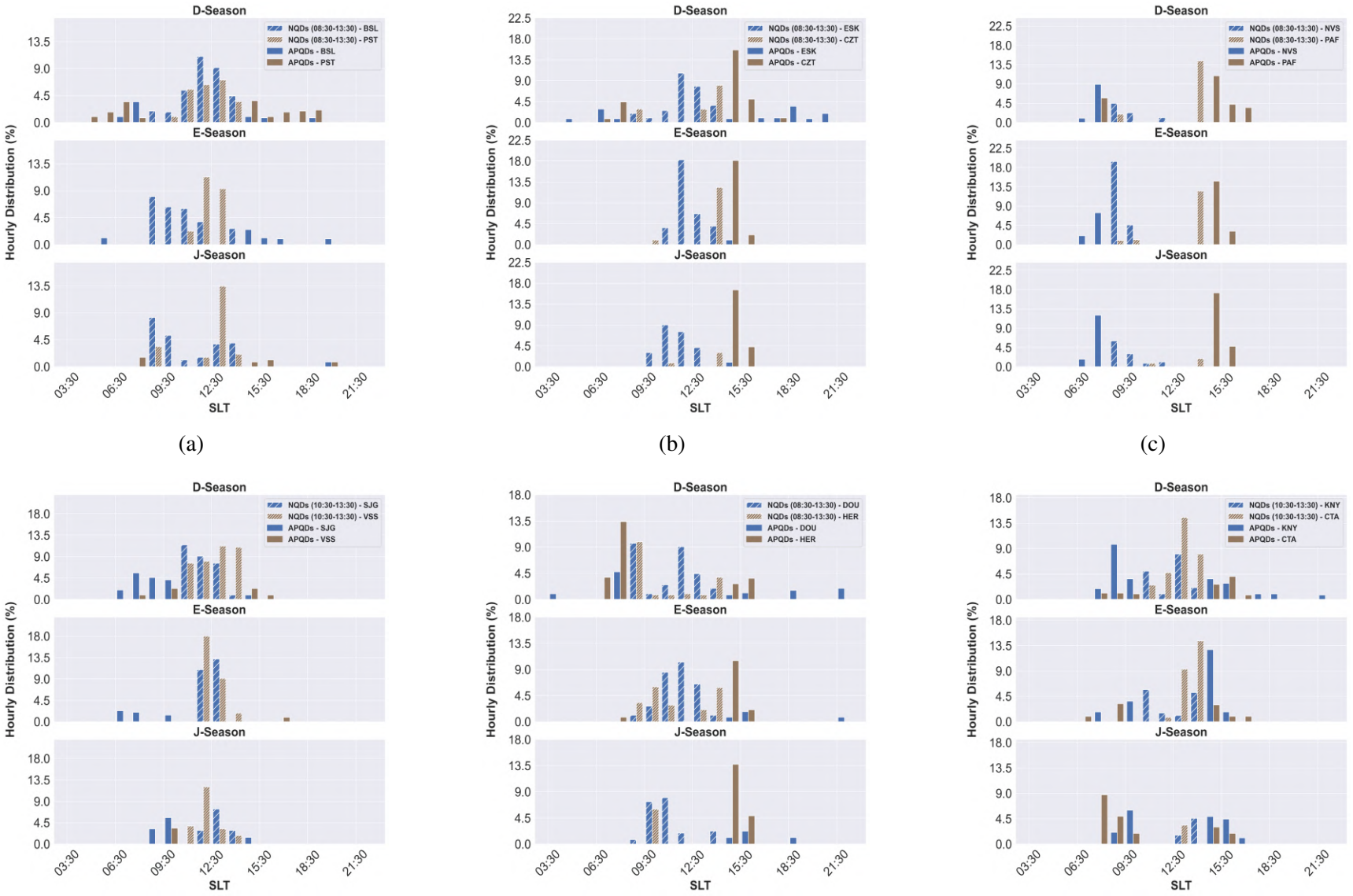

Figure 4.8: Same as Figure 4.6 for the solar maximum phase.

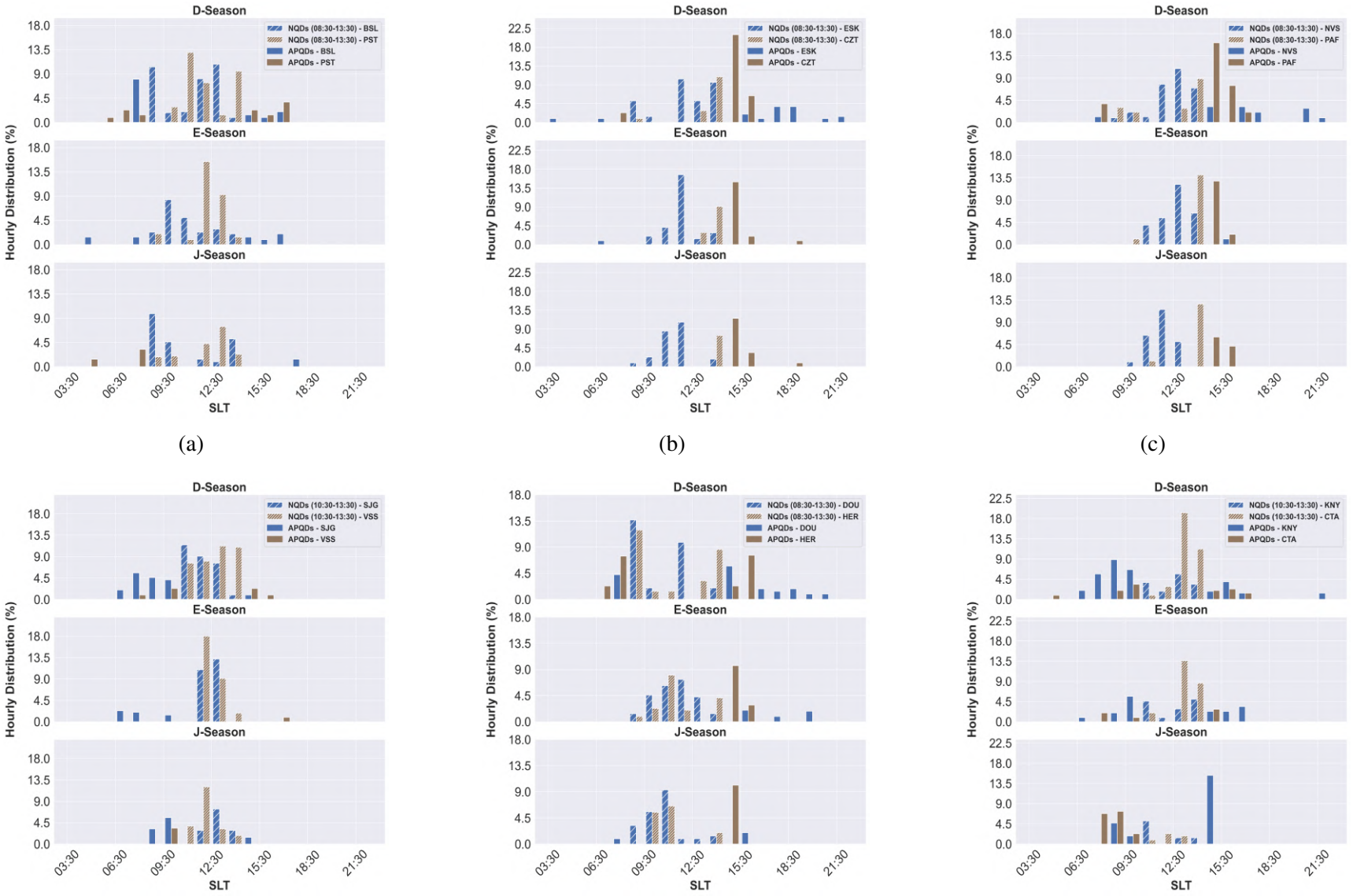

Figure 4.9: Same as Figure4.6 for the solar descending phase.

In the low latitudes, KNY observed higher APQD occurrences during the morning (08:30-09:30 SLT) during the D and E seasons, and during the afternoon (14:30 SLT) during the J season. However, CTA observed a greater occurrence of APQDs in the morning (08:30-09:30, 07:30-09:30 SLT) during D and J seasons, but in both morning hours (08:30-09:30 SLT) and afternoon hours (14:30 SLT) during the E season.

4.4 Spatial Distribution of APQDs Occurrence Rates and Relation with Sq Foci Positions: Comparison of Solar Minimum and Maximum Phases

In this section, a comparison of the characteristics of APQDs during solar minimum (2009) and solar maximum (2014) with regard to the Sq foci positions was presented. Furthermore, the variation of Sq foci latitudes by seasons and the deviation of Sq foci latitudes from the ideal Sq schema were compared. The occurrence rates of APQDs at the ideal Sq schema was also presented.

4.4.1 Comparison of the Variation of Sq Foci Position During the Minimum and Maximum Phases

A comparison of the seasonal distribution of the Sq foci latitude positions during 2009 and 2014 has been made in Figure 4.10 (a) and (b), respectively. The number of QDs in 2009 was 104, and in 2014 it was 30. The plots show the Sq foci positions in magnetic latitudes in both hemispheres for the D, E and J seasons. During solar minimum, the largest variation in the Sq foci positions were found in the J season (Figure 4.10 (a)) in the Southern Hemisphere in all three sectors, where poleward drifts were observed. Furthermore, large poleward migrations of the Sq foci latitudes were also observed in the D season for both hemispheres of the Africa-European, the Southern Hemisphere of the Asia-Australian sector, and the Northern Hemisphere of the American sector. Large excursions of the Sq foci positions towards the magnetic equator were observed mostly in the E seasons in the American sector, and mostly in the E and D seasons in the Northern Hemisphere of the Africa-European and Asia-Australian sectors. Similar excursions were observed in the D season of all sectors. In the Southern Hemisphere of the American sector, most of the Sq foci positions were observed near the ideal Sq schema for 2009.

During solar maximum, the most deviations of the Sq foci latitudes from the ideal Sq schema, particularly excursions towards the poles, were also found in the J season of 2014 (Figure 4.10(b)), as most QDs were observed in this season. However, sparsely similar deviations were also observed in the D and E seasons of the Africa-European sector. Most excursions of the Sq

foci latitudes towards the magnetic equator were observed in the J season of the Asia-Australian sector in the Northern Hemisphere.

(a)

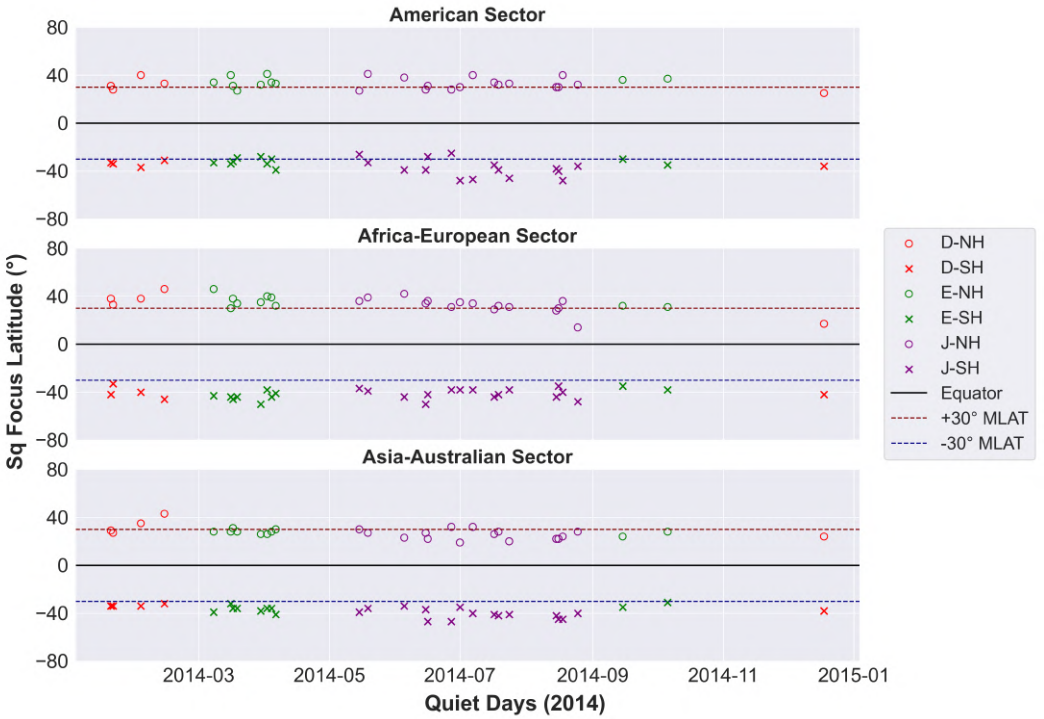

(b)

Figure 4.10: Seasonal distribution of Sq foci latitudes in NH and SH of all three longitude sectors in 2009 (a) and 2014 (b).

4.4.2 Statistical Analysis of Sq Foci Positions at both Ideal Sq Schema and Beyond

The occurrence rates of Sq foci positions in magnetic latitudes of the ideal Sq schema ($\pm 30^{\circ}$) in both hemispheres were depicted in Figures 4.11 (a) and (b) for 2009 and 2014, respectively. Mostly, under 5% of the Sq foci latitudes were observed at the ideal Sq schema, with the exception in the American sector in the E (6.7%) and J (10%) seasons of 2014. In 2009, the highest occurrence of the ideal Sq schema was found in the American sector in the E seasons (3.8%), followed by the D sector in the Southern Hemisphere (2.9%). However, the occurrence rates of the Sq foci latitudes found beyond the ideal Sq schema varied across seasons as well as longitudinal sectors. For example, Figure 4.11 (a) shows that in the American sector, the largest occurrence of Sq foci lying beyond the ideal Sq schema was during the D season, while the lowest was during the J season for both hemispheres. A similar trend was observed in the Southern Hemisphere in the African-European and the Asia-Australian sectors. The seasonal sequence of these two sectors in the Northern Hemisphere was E, D, and J, as per descending occurrence rates. Generally, for both hemispheres, the seasonal occurrence rates of Sq foci latitudes beyond the ideal Sq schema were in the descending order of D, E, and J seasons. In the Asia-Australian sector, for both hemispheres, there was the exception of equal rates of occurrence beyond the ideal Sq schema during the E season, while no occurrences were found at the ideal Sq schema.

Figure 4.11 (b), which shows the results for 2014, indicates that in the American sector, the largest occurrence of Sq foci lying beyond the ideal Sq schema was during the J season, while the lowest was during the D season for both hemispheres. However, in the Northern Hemisphere, the seasonal sequence of the occurrence rate of the ideal Sq schema in descending order was J, E, and D for all sectors. Equal occurrence of the ideal Sq schema was observed in E and J seasons of the Northern Hemisphere of the Africa-European and Asia-Australian sectors (3.3%), while no occurrence was recorded in the same hemisphere for the D season in all three sectors. In addition, the ideal Sq schema was not observed in the Southern Hemisphere for all seasons and sectors, except for the E seasons of the American sector, which was 6.7%.

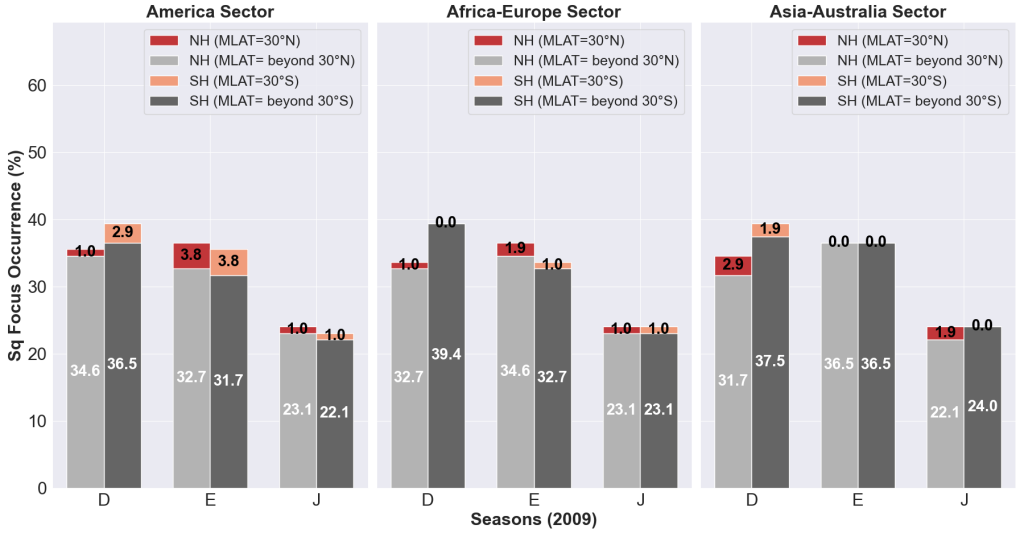

(a)

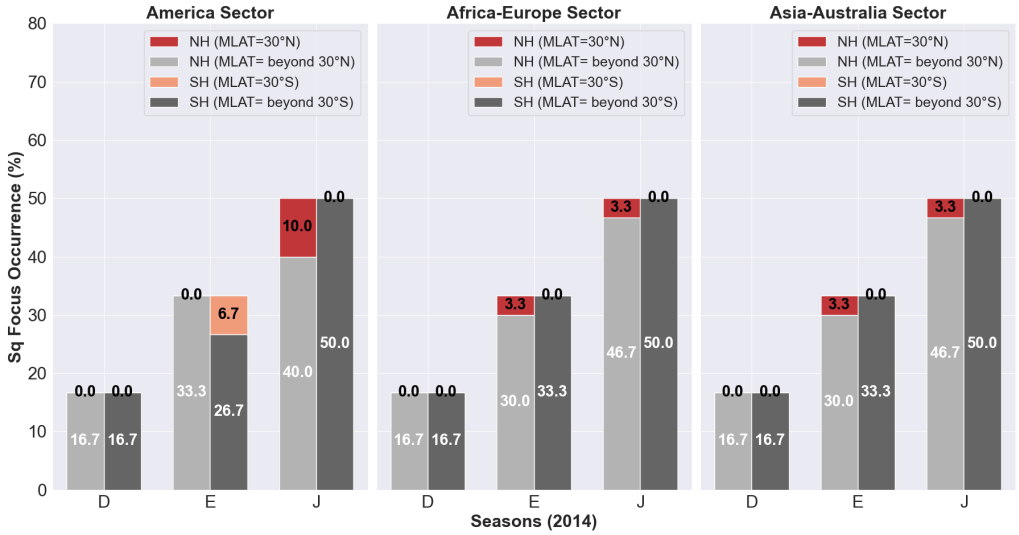

(b)

Figure 4.11: Bar graphs of occurrence rates of Sq foci at ±30° and outside for LL and ML in both hemispheres for QDs in 2009 (a) and 2014 (b).

4.4.3 APQDs Observed During Ideal Sq Schema in 2009 and 2014

The analysis of specific cases in 2009 and 2014, with particular scrutiny of the most elevated Sq foci positions and their corresponding APQDs within specific sectors, elucidates the most pronounced instances of ionospheric current system displacement as observed during these solar cycle phases. Investigating the characteristics of APQDs occurring under normal Sq foci positions provides a baseline for comparison, enabling the identification of unique features

associated with APQDs that occur under extreme Sq foci variations. On the other hand, APQDs have also been observed at normal foci positions in 2009 and 2014, and were tabulated in Table 4.3.

Table 4.3: APQDs occurrence rate as observed at normal Sq foci latitudes

Years	2009 (%)	2014 (%)
NH	8.6	3.8
SH	4.8	1

As depicted in the Table 4.3, the Northern Hemisphere had higher occurrence rates of APQD during the ideal Sq schema in both 2009 and 2014.

Research indicates that the ionospheric response depends on the sector structure of the IMF, because sector boundary crossings may influence the ionosphere during periods of geomagnetic quiet conditions (Butcher & Brown, 1980). The ionosphere shows variation in electron temperature and density, as well as electric field conductivity during quiet periods, and modifies the ion-neutral coupling, which indirectly affects the Sq foci latitudes (Richmond, 2011). The modulation of ionospheric parameters and the Sq foci latitudes shows variations without major geomagnetic activity due to solar radiation, tidal winds, and electrodynamic processes in the coupled thermosphere-ionosphere system (Liu et al., 2013).

4.5 Cases of Localized APQDs in 2009 and 2014 and Relationship with Sq Foci Positions

The geomagnetic field configuration influences the distribution of ionospheric currents, the flow of FACs between hemispheres, and the coupling between the ionosphere and magnetosphere from a localized perspective. Key features of the geomagnetic field influences for localized phenomena include the following:

1. The Earth's magnetic field exists as a dipole, but its structure includes major non-dipolar elements. The non-dipolar components of the geomagnetic field produce asymmetries which affect the distribution of ionospheric currents and FACs (Le Sager & Huang, 2002; Gasda & Richmond, 1998).

2. The geomagnetic field shows variations that extend across both longitude and latitude, which modify the ionospheric current system. The equatorial and polar regions show the

most significant variations in these geomagnetic field characteristics (Le Sager & Huang, 2002; Gasda & Richmond, 1998).

3. The geomagnetic field links the ionosphere to the magnetosphere through FACs and ionospheric currents. The Earth maintains its global electrical circuit through this essential coupling process (Le Sager & Huang, 2002; Tsunomura, 1999).

In order to visually depict and comprehend the influence of IHFACs on localized APQDs occurring in a certain longitudinal sector, a comparative analysis of APQD characteristics for the years 2009 and 2014, representing contrasting phases of solar cycle 24, was presented in this section. Valuable insights were documented based on the analysis of the dependence of the phenomena on the solar cycle.

Narrowing the research down to specific cases in 2009 and 2014, the research identifies instances of the most elevated Sq foci latitudes, as well as foci positions near to ideal Sq schema and associated localized APQDs in particular sectors. The APQDs occurring under normal Sq foci positions have been considered and reported on, thereby establishing a comprehensive overview of the range of APQD phenomena during minimum and maximum phases of solar cycle 24.

Three cases have been discussed using noteworthy examples to demonstrate the influence of IHFACs on APQDs:

1. Sq foci positions found beyond 35° magnetic latitudes in both hemispheres
2. One of the Sq focus positions is identified between 30° and 35° magnetic latitudes in one hemisphere, and the other position beyond 35° magnetic latitudes in the other hemisphere
3. APQDs at magnetic latitudes between 30° & 35° in both hemispheres

4.5.1 Cases of Localized APQDs in 2009 & 2014, and the Relationship with Sq Foci Positions

As mentioned in Section 4.5, this subsection elaborates on the three cases individually and presents the contour plots of Sq(H) and Sq(Y) alongside the magnetograms to depict localized APQD occurrence in specific longitudinal sectors for 2009 and 2014 (Figures 4.12-4.17). The contours were plotted using Sq(H) and Sq(Y). IHFACs can be observed in Sq(Y) contours as the Y and D components in nT were most susceptible to such current systems.

4.5.1.1 Sq Foci Beyond the Ideal Sq Schema

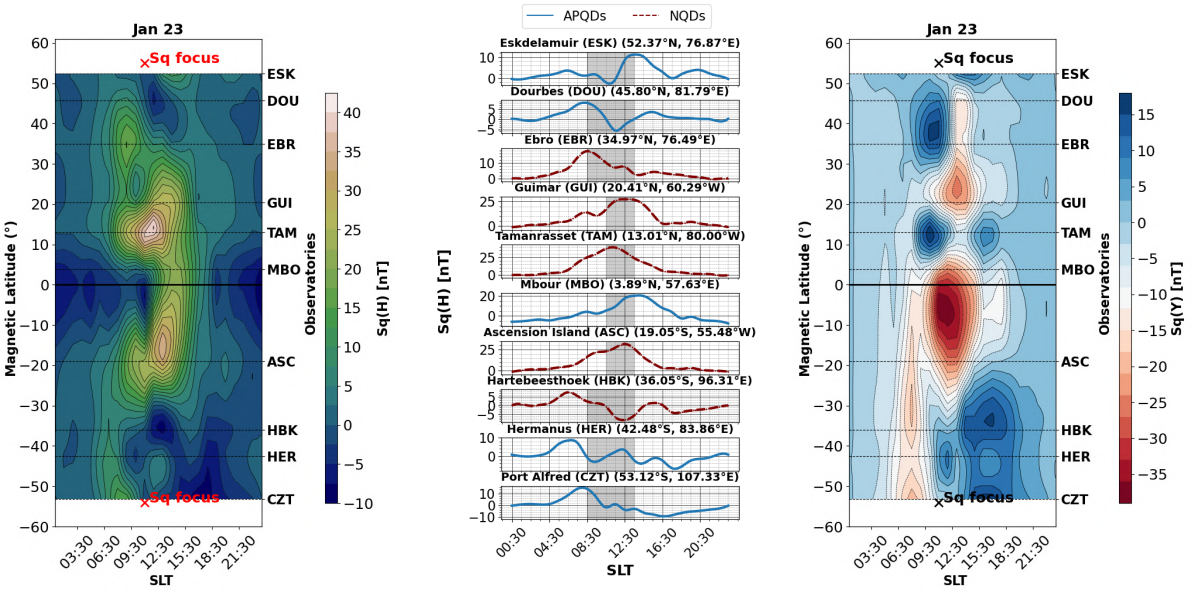

(a) (b) (c)

Figure 4.12: A comparison of contour plots of Sq(H) in (a) and Sq(Y) in (c) overlaid with calculated Sq foci latitudes. The magnetograms (b) for the Africa-European sector were depicted with NQDs (in maroon) and localized APQDs (in blue) for 23 January 2009.

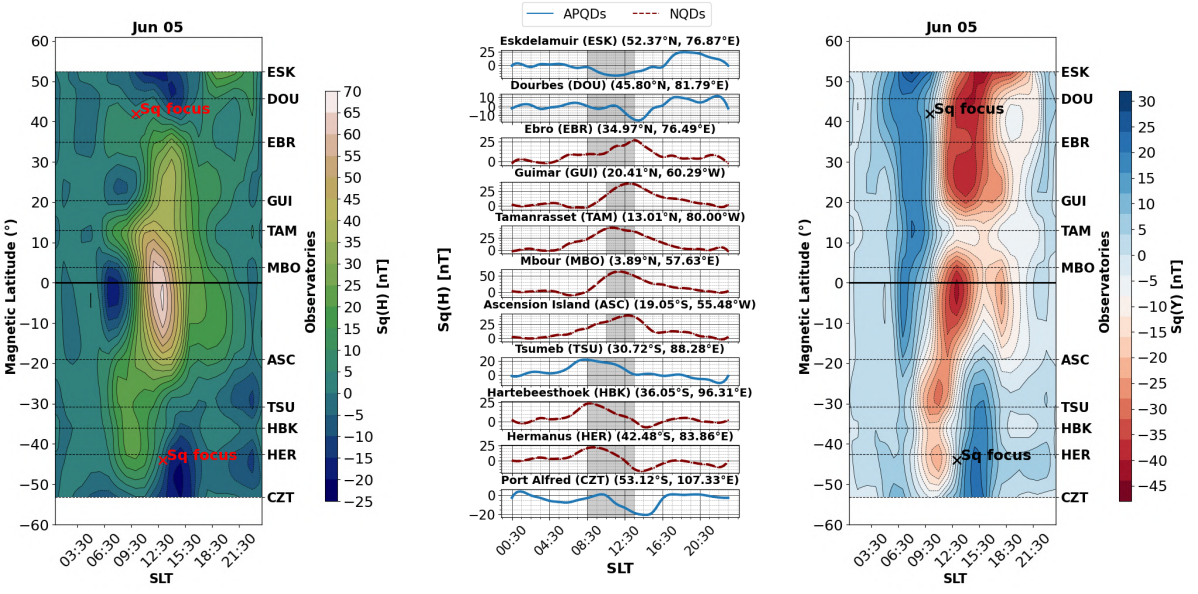

(a) (b) (c)

Figure 4.13: Same as Figure 4.12 for the Africa-European sector on 5 June 2014.

On 23 January 2009, during the sudden stratospheric warming (SSW) event, APQDs were observed in the Africa-European sector. The foci positions in each hemisphere were located at

55°N and 54°S (Figure 4.12 (a) and (c)) magnetic latitudes. At the observatories of ESK and DOU in the Northern Hemisphere, and HER and CZT in the Southern Hemisphere, as well as at MBO in the equatorial region (Figure 4.12 (b)), the peaks as APQDs were observed as the Sq foci latitudes were situated closer to high latitudes in both hemispheres.

On 5 June 2014, the foci positions in each hemisphere were located at 42°N and 44°S magnetic latitudes (Figures 4.13(a) & (c)). APQD dips were recorded at ESK and CZT, in the Northern and Southern Hemispheres, respectively. However, morning and afternoon peaks were observed at TSU and ESK in the Southern and Northern Hemispheres, respectively, as depicted in Figure 4.13(b).

4.5.1.2 Sq Focus between 30° and 35° in One Hemisphere

On 17 June 2009, in the Asia-Australian sector, the Sq focus in the Southern Hemisphere was located at 71° and at 32° in the Northern hemisphere (Figure 4.14 (a) and (c)). APQDs in the form of peaks were phase-shifted in the afternoon for KNY and in the morning for PHU in the Northern Hemisphere, and for CTA and ASP in the Southern Hemisphere (Figure 4.14(b)). As the Sq focus position was situated at higher latitudes in the Southern Hemisphere, normal peaks were observed for CNB and EYR, where a normal dip was expected.

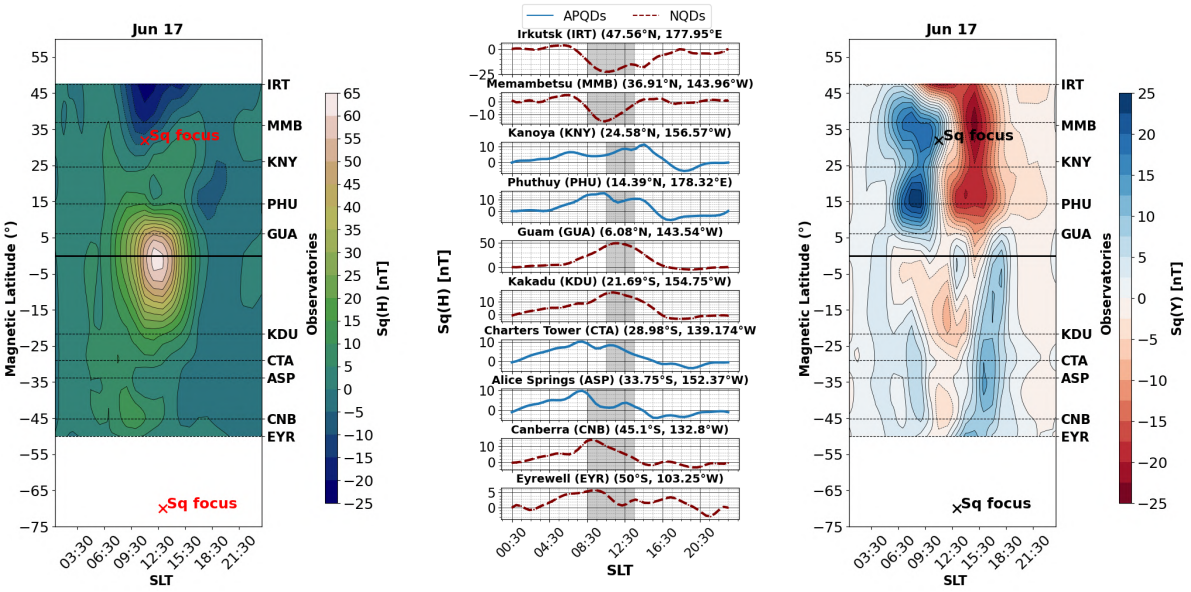

(a) (b) (c)

Figure 4.14: Same as Figure 4.12 for the Asia-Australian sector on 17 June 2009.

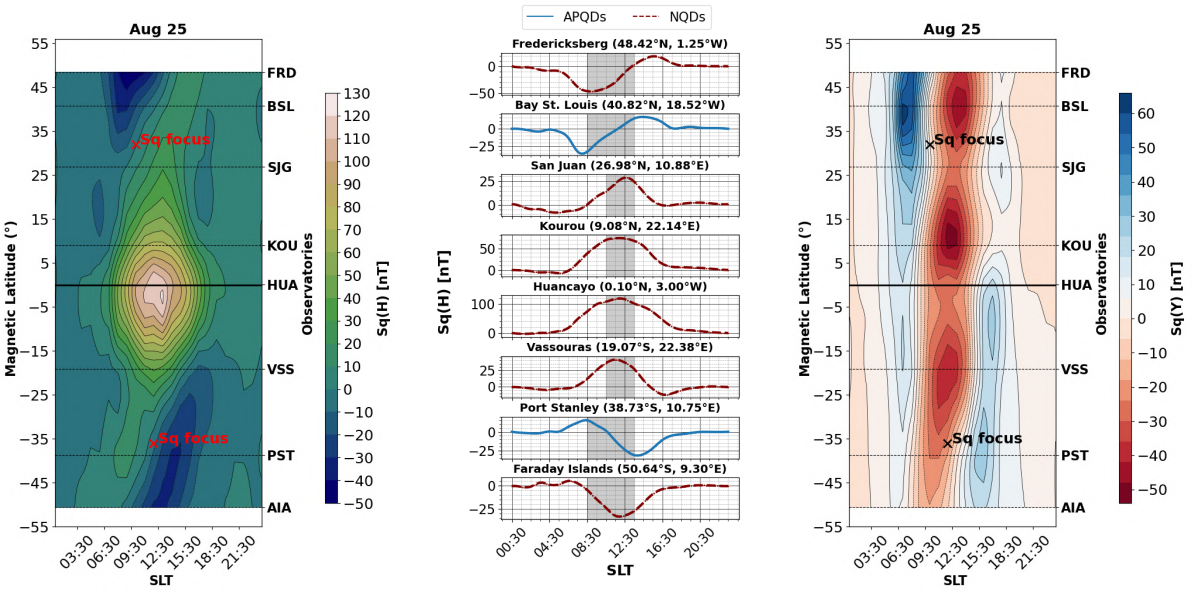

(a) (b) (c)

Figure 4.15: Same as Figure 4.12 for the American sector on 25 August 2014.

Localized APQDs were observed in the American sector on 25 August 2014 when the Sq foci latitudes were situated at 32°N and 36°S magnetic latitudes as depicted in Figures 4.15 (a) & (c). Phase-shifted dips were observed in the morning at BSL in the Northern Hemisphere and in the afternoon at PST in the Southern Hemisphere (Figure 4.15 (b)).

4.5.1.3 Sq Foci between 30° and 35° in the Northern and Southern Hemispheres

On 8 September 2009, the Sq foci latitudes were situated at 34°N & 31°S (Figures 4.16(a) & (c)). In the Northern Hemisphere, a localized APQD in the form of a phase-shifted dip was observed at BSL as the Sq focus was located between BSL and SJG, hence a normal peak was observed at SJG. In the Southern Hemisphere, the SQ focus was located between VSS and PST; hence, a normal peak and dip were observed, respectively (Figure 4.16(b)). However, a phase-shifted peak in the early morning hours at PST was observed, where a normal dip was expected in the afternoon within the shaded time region, similar to that which was recorded at BSL.

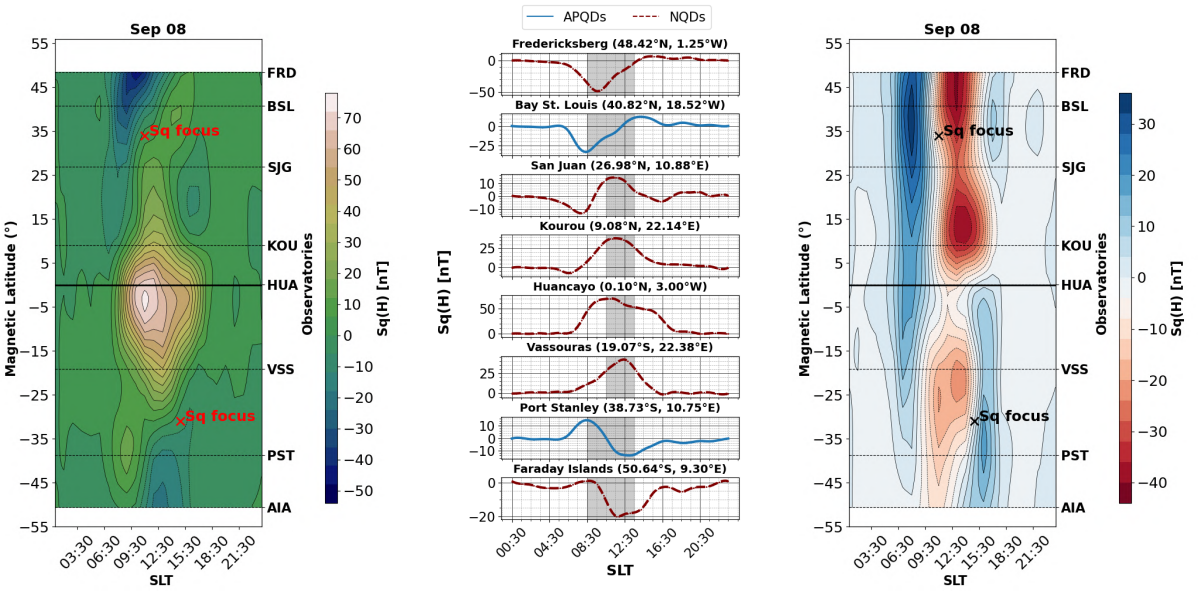

(a) (b) (c)

Figure 4.16: Same as Figure 4.12 for the American sector on 8 September 2009.

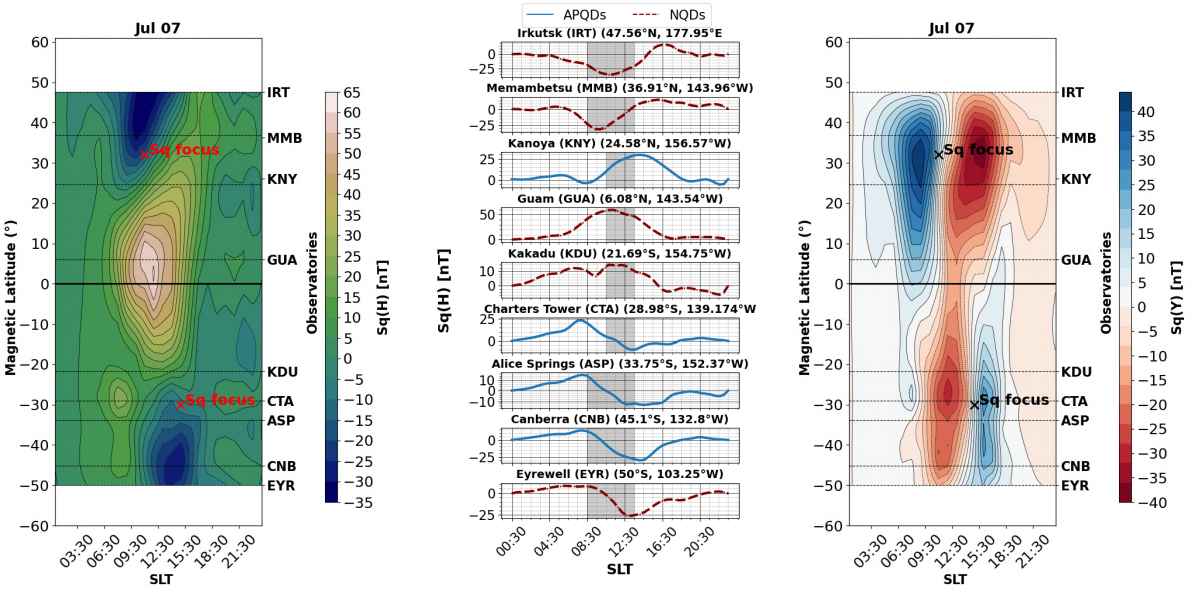

(a) (b) (c)

Figure 4.17: Same as Figure 4.12 for the Asia-Australian sector on 7 July 2014.

Localized APQDs were observed in the Asia-Australian sector on 7 July 2014. The Sq foci positions were located at 32°N and 30°S (Figures 4.17 (a) & (c)). Afternoon and morning phase-shifted peaks were observed at KNY in the Northern Hemisphere as well as at CTA and ASP in the Southern Hemisphere, respectively (Figure 4.17 (b)). Additionally, a phase-shifted dip was observed at CNB.

4.6 Summary

This section presents the results of the study and concludes that all the objectives were met. The statistical analysis of APQDs in the low- and mid-latitudes for selected conjugate magnetic observatory pairs in both hemispheres provided insights into the asymmetric nature of the geomagnetic field over seasons and during the solar cycle phases. The main results from all sections are summarized in the paragraphs.

Generally, it was observed from Section 4.1 that both regionally and globally, APQDs occurred at a high rate in the Northern Hemisphere's low-latitudes and in the Southern Hemisphere's mid-latitudes. Furthermore, the highest rate of occurrence was observed for the D season in the low- and mid-latitudes, while the lowest occurrence was observed for the E season in the low-latitudes, but in the E and J seasons in mid-latitudes during all phases of solar cycle 24. However, the sector with the dominant APQD occurrence rates changed with latitude and solar cycle phase. The most APQDs were observed in the NH of the solar minimum phase (37%) and SH of the solar maximum phase (35%). The least APQDs were observed in the NH of the solar ascending phase (27%) and the SH of the solar minimum phase (31.2%).

In general, it was observed in Section 4.2 that the occurrence rates of APQDs were higher in the low latitude observatories of the Northern Hemisphere, while the occurrence rates were higher in the mid-latitudes of the Southern Hemisphere. Also, the low-latitudinal observatory, KNY, in the Asia-Australian sector of the Northern Hemisphere and the mid-latitudinal observatory, CZT, in the Africa-European sector of the Southern Hemisphere exhibited higher occurrence rates of APQDs in all phases of solar cycle 24. The observed patterns suggest that APQD generation mechanisms may vary across different latitudes and geographic regions. The magnitude of this hemispheric difference varied across sectors, suggesting potential regional influences on APQD generation mechanisms.

Generally, from results of Section 4.3, it was observed that most of the NQDs occurred during 08:30-13:30 SLT and 10:30-13:30 SLT for the low- and mid-latitudinal observatory pairs in the Northern and Southern Hemispheres, respectively. Irrespective of the hemispheres, a higher APQDs occurrence rate generally occurred during the morning hours of the low-latitudes, especially during the D season, and during the afternoon hours for the mid-latitudes during all the seasons.

The stark differences between the solar minimum (2009) and solar maximum (2014) highlighted the complexity of ionospheric dynamics in the quietest periods. In general, the results from Section 4.4 depict that equatorward drifts of the Sq foci latitudes were observed in the northern hemisphere of the E and D seasons of all sectors in 2009 while it was observed only

in the J season of the Asia-Australian sector in 2014. Moreover, the most poleward drifts were observed in the J season of the Asia-Australian sector in 2009 but were observed in the American sector in 2014. Moreover, most APQDs observed at normal Sq foci latitudes were in 2009 in the NH (8.6%). During QDs, most of the Sq foci latitudes were observed beyond 30° for both 2009 and 2014. However, normal Sq foci latitudes for the America sector, 3.8% in both hemispheres of the E season, and 10% in NH of the J season were observed in 2009 and 2014, respectively.

As manifested in ground magnetic observatory data, the results demonstrate a close connection between APQDs and Sq foci latitudes. These were elucidated by case studies of the characteristics of the localized APQDs in 2009 and 2014. Generally, as depicted in Section 4.5 localized APQDs were observed near the Sq foci latitudes during the ideal Sq schema. Variations in Sq foci latitudes in the Southern Hemisphere were recorded and it caused APQDs at observatories located close to the Sq foci latitudes during the June solstice of 2009. However, APQDs were observed at the mid-latitudes beyond the Sq foci latitudes on the June solstice of 2014.

The scientific insights are discussed in more detail in Chapter 5.

Chapter 5

Discussions and Conclusion

This section presents discussions on significant findings made in this research project. The aim of this study was to formulate the methodology for the identification and characterization of APQDs using ground magnetic observatory data. The H component was processed to calculate Sq variations for QDs in every phase of solar cycle 24 using a selection criterion of sunspot number as mentioned in Chapter 4. SYM-H index was used to evaluate QDs in all solar cycle phases by applying a threshold of |SYM-H| $\leq$ 10 nT for QDs. The correct times of the peaks and dips for NQDs and APQDs were assessed according to the criteria defined in Chapter 3, Section 3.9. The statistical analysis in terms of local, regional and global occurrences of APQDs has been carried out according to the methodology mentioned in Section 3.9.2. The seasonal statistical analysis, along with notable discrepancies, is highlighted and discussed. Regional and global seasonal statistics of APQDs and for conjugate latitude regions have been reported in all phases of solar cycle 24. The occurrence rates of APQDs and hourly distribution plots of conjugate magnetic observatories with the highest APQDs report the asymmetries of the hemispheres. The X and Y components of the geomagnetic field were formed into vectors and rotated to form equivalent current vectors. These vectors were also used to assess the Sq foci latitudes that were calculated for 2009 and 2014. These latitudes were also used to compare the occurrence rates of the ideal Sq schema and the extent of influence on APQDs. The localized influence on APQDs occurrences has been assessed for 2009 and 2014 in case studies for Sq foci latitudes in all the sectors. The chapter culminates with conclusions reached based on the results of this research project as well as suggestions on possible future work.

5.1 Discussions

The examination of global, local, and regional APQDs throughout 2008-2019 reveals a complex interplay of factors influencing their occurrence, most of which have been discussed in the following paragraphs. The analysis of APQDs on a global scale provides a broad perspective on the overall ionospheric dynamics during solar cycle 24, showing how variability in the solar cycle can induce abnormal phase shifts. APQDs are identified according to phase-shift occurrence with respect to local time and maximum amplitude of peaks and dips. During

APQDs there is both enhanced amplitude of Sq(H) and phase-shift of both peaks or dips, but only the discussion on the statistical results of occurrence rates of the phase-shifted peaks and dips is presented here.

5.1.1 Hemispheric and Latitudinal Asymmetry

Statistical analysis of latitudinal and hemispheric APQD occurrence, incorporating data from an equal number of observatories in the Northern and Southern Hemispheres with respect to magnetic latitude and geographic longitude, highlights the hemispheric asymmetries and latitudinal dependencies in different longitude sectors. Analysis of hemispheric asymmetries reveals differences in APQD occurrence rates and characteristics between the Northern and Southern Hemispheres. The asymmetries can arise due to differences in the geomagnetic field configuration, land-sea distribution, and atmospheric circulation patterns between the two hemispheres (Liu & Lu, 2010). From Figures 4.1 - 4.4, the global and regional APQDs occurrence rates of low- and mid-latitudes were the highest in the D season in all phases of solar cycle 24. Particularly, global APQD occurrences were the highest (56%) in the mid-latitudes of the solar minimum phase, and the regional occurrences were the highest in the American mid-latitudes (68%) in the solar ascending phase in the D season. It is suggested that seasonal and longitudinal atmospheric tides (migrating and non-migrating), the Sq vortex migration, and regional anomalies (for example, over the SAA) modulate conductivity and current geometry and so shift Sq phase on quiet days (Koch & Kuvshinov, 2015). It is well established that changes in Sq(H) results from changes in ionospheric dynamo region which depend on latitude, season, local time and solar activity (Butcher & Brown, 1981a). E-region dynamo control modulates the Sq and phase variations. Quiet-day models and observations show that conductivity (hence phase variability) responds to solar EUV, daylength and local neutral wind structure (Campbell et al., 1989; Campbell, 2003). From Figures 4.1 - 4.4, subplots a and b, it is evident from observations that E season has recorded the lowest APQDs for low-latitudes in all phases of solar cycle 24. Reduced EUV, in the local winter or due to low solar flux, lowers E-region conductivity and can delay or advance the Sq phase relative to the E season (Campbell et al., 1989; Liu et al., 2024). Variations of thermospheric neutral winds, tides and vortex dynamics displace the Sq current vortex and change the phase of local Sq(H) (Morozova et al., 2020; Wu et al., 2021). It is also highly likely that sudden D-region enhancements (e.g., solar crochets) or persistent EEJ/CEJ anomalies can alter current height and phase even when SYM-H is quiet (Koch & Kuvshinov, 2015; Annadurai et al., 2018). However, Yamazaki and Maute (2017) stated that EEJ is associated with the eastward electric field resulting from the ionospheric dynamo at low-latitudes, and the variations in the EEJ current system are due to atmospheric tidal modes, resulting in phase-shifts observed in low-latitude observatories close to the magnetic equator (Figure 4.5, subplot a) during solar minimum phase. A slowly

varying non-storm component (magnetopause and displaced ring/tail currents) contributes to the Dst/SYM-H seasonal baseline and thus to quiet-time H offsets that change seasonally and with sunspot phase (Cliver et al., 2001). The Sq vortex location and shape vary seasonally and with atmospheric tidal forcing, producing the equinoctial/solstice asymmetries and the D-season phase offsets of Sq(H) (Wu et al., 2021; Annadurai et al., 2018). The Sq current vortex is affected by non-migrating thermospheric tides, which can shift and deform the vortex, particularly over the Asia-Australian sector (Zhang et al., 2024). These tides cause the Sq current to form a tilted ellipse as it moves northwestward, deviating from the geomagnetic equator (Zhang et al., 2024). In Figure 4.1, the American sector had higher APQDs in the D and E seasons in low latitudes compared to the Asia-Australian sector. This could be due to non-migrating tidal components producing longitudinal differences in Sq foci latitudes and phase leading to systematic scattering of the Sq foci latitudes and local phase offsets in the D season which are not captured by global indices, particularly in the American sector (Koch & Kuvshinov, 2015; Wu et al., 2021). Moreover, during equinoctial and summer seasons, there is a significant exchange of currents across the equator, which is not observed during the winter season. This exchange contributes to the westward shift of the Sq focus over the Pacific Ocean region (Chandrasekhar & Fontes, 2004). This may explain the higher occurrences of APQDs in the E and J seasons of the Asia-Australian sector (Figures 4.1 - 4.4). Talha et al. (2021) stated that the magnitude of the Sq current depends on ionospheric conductivity, while phase variability depends on winds and electric field. Variations in the electric field are caused by FACs. These currents enter before noon-time and leave at post noon-time at high-latitudes. These currents at mid-latitudes result in west-east currents during daytime, which may build up the super-posed northward field (SPNF) to cause abnormal phase-shifts at the mid-latitudes, (Takeda, 1982; Takeda & Maeda, 1980).

5.1.2 Drivers of APQDs at Low-Latitude Observatories

The Northern Hemisphere observatories of SJG and KNY in the low-latitudes observed higher APQD occurrences throughout solar cycle 24 as depicted in Figures 4.5, subplots a-d. The ionospheric dynamo variations at the equatorial region and low-latitudes induce minor yet distinct southward H perturbations, altering the phase of the Sq(H) diurnal maximum. These perturbations, closely linked to counter-electrojet (CEJ) conditions, significantly contribute to the phase variability observed on geomagnetically quiet days (Sastri, 1982). The CEJ induces a daytime depression in the H-component, shifting the timing of the Sq(H) peak. Although smaller than storm signals, these perturbations can shift the apparent diurnal maximum by several hours on quiet days, likely influencing the phase shifts observed at KNY and SJG. Studies suggest that a slowly varying imposed field, associated with IMF B_y or transported IMF, modulates Sq(H) amplitude and phase shifts on quiet days, consistent with a build-up and decay over multiple

days before and after the APQD interval (Brown, 1986). Moreover, magnetospheric electric fields and resulting ionospheric currents are invoked to explain the low-latitude imposed fields during quiet times. Even during northward IMF B_z, the H-component at low latitudes responds to short-timescale solar-wind dynamic pressure variations, producing minute-to-minute Sq(H) excursions that can perturb phase timing around local noon and midnight (Francia et al., 1999). Quiet-time transient compressions and magnetospheric impulse events (MIEs) driven by solar-wind dynamic pressure can produce low-latitude Sq(H) deflections, altering phase estimates on quiet days. The low-latitude Sq(H) response to pressure changes varies with local time, making phase shifts more likely to be recorded in narrow local-time sectors (Francia et al., 1999; Konik et al., 1995).

5.1.3 Seismic and Telluric Effects at KNY

The high APQD occurrence at KNY thoughout the solar cycle may be explained by tectonic movements (see Figure 4.5, subplots a-d). As an earthquake-prone site, seismic and telluric currents are likely to cause APQDs at KNY. Telluric currents, induced by ionospheric and magnetospheric currents, contribute to geomagnetic variations measured by ground magnetometers (Viljanen et al., 2020). Abnormal magnetic field variations are attributed to telluric current deflections, revealing crustal structure (Le Mouel & Menvielle, 1982). Telluric currents may influence macrofracturing in Earth's crust, potentially triggering earthquakes (Trenkin, 2015). Furthermore, ULF/ELF emissions cause magnetic signatures when lithospheric bursts and atmospheric radiation occur before major earthquakes, perturbing ionospheric currents that affect ground Sq variations (Sharma et al., 2021; Marchetti et al., 2024). Lower ionosphere conductivity changes alter the ionospheric dynamo, modifying Sq current magnitudes and phases regionally (Li et al., 2019; Hayakawa et al., 2021). Atmospheric gravity waves can displace ionospheric plasma, changing dynamo forcing and Sq patterns (Hayakawa et al., 2021; D'Angelo et al., 2022). Conjugate coupling spreads ionospheric perturbations along field lines (Li et al., 2019) as the magnetic conjugate station of KNY, CTA, depicted APQDs in all phases, albeit almost reduced in half, quantitatively (Figure 4.5, subplots a-d). Reduced H or Z amplitudes with phase anomalies indicate Sq alterations during seismic events (Li et al., 2019). External ionospheric currents affect magnetotelluric measurements, with models showing Sq foci latitude variations with season and solar activity (Yamazaki et al., 2011b; Liu et al., 2024). These effects can amplify subsurface anomalies, requiring assessment of ionospheric conditions. At KNY, ocean-induced currents and their phase effects were evaluated in the North Pacific and found not to account for the anomalous responses at Kakioka (KAK) or Kanoya (KNY), so ocean induction is not the primary quiet-time cause at those Japanese stations (Takeda, 1993). Moreover, local magnetization anomalies and spatial gradients have been documented and can explain some quiet-time abnormal phase behavior, with crustal/backfill magnetization and spa-

tially heterogeneous geomagnetic components being important local contributors (Yamazaki et al., 2011a; Sato et al., 2020; Takeda, 1993)

5.1.4 Mid-latitude APQDs and Magnetospheric Coupling

The Southern Hemisphere observatories of CZT (69%), HER (56%), AMS (55%), and PAF (66%) in the mid-latitudes have consistently greater APQD occurrences as depicted in Figures 4.5, subplots a-d, particularly in the solar maximum phase. Ionospheric drivers play a central role in producing large day-to-day phase variability and abnormal phase shifts observed at mid-latitude stations. These drivers involve changes in the ionospheric current system, including the solar-quiet (Sq) variation and superposed anomalous currents. On APQDs, the normal Sq(H) timing and amplitude are altered by an imposed ionospheric current system, reducing the normal H variation and shifting its maximum outside the usual local time window (Butcher, 1989). The formation of abnormal phase-shifts is characterized by a persistent superposed northward field and associated west-east ionospheric currents that build up over several days, modifying Sq amplitude and phase (Brown, 1986). The strength and sense of this imposed ionospheric field correlate with IMF B_y polarity, explaining repeated phase-shifts and poleward movement of the Sq foci latitudes on quiet days having abnormal phase-shifts, particulry for the mid-latitude observatories of the Northern or Southern Hemisphere (Butcher, 1986; Brown, 1986). Day-to-day variability of quiet-time baselines includes Sq fluctuations embedded in derived quiet baselines, contributing to ionospheric timing anomalies even on the "quietest" days (Haberle et al., 2022). Magnetospheric coupling processes play a significant role in creating short-time minima in H records, often reflecting magnetosphere-to-ionosphere forcing on APQDs. Even small substorms can form daily H minima on quiet days, while current vortices link anomalies at separated mid-latitude stations (Schlapp et al., 1988). Magnetospheric substorms are particularly important in producing H minima that define APQDs at mid-latitudes, making magnetospheric dynamics crucial even under low indices (Schlapp et al., 1988). Short-period variations at mid-latitudes are influenced by current systems, including partial ring currents and FACs, which alter H phase and timing (Vieira et al., 2003). Additionally, low-latitude ULF pulsations, such as Pi2 and Pc3, exhibit distinct phase characteristics that can affect phase relationships across latitudes (Li et al., 1998). Field-line resonances (FLRs) are a significant mechanism for generating ULF pulsations, and their presence at mid-latitudes is well-documented (Menk et al., 2000). The variation in resonant frequency with latitude can introduce phase shifts, potentially causing timing anomalies between stations in the mid-latitude region (Menk et al., 2000).

5.1.5 Regional and Longitudinal Factors of Anomalous Sq(H) Variations

Regional and longitudinal factors also contribute to variations in Sq(H). Longitude and season affect how ionospheric dynamo and magnetosphere-ionosphere currents project into Sq(H), causing regional phase variations. Longitudinal variations in the main field modify the ionospheric E-region dynamo's EMF and FACs, resulting in observatories close to Sq foci latitudes in the mid-latitudes observing different Sq phases (Le Sager & Huang, 2002). The main field structure alters dynamo forcing and FAC closure, creating sectoral differences in Sq timing (Le Sager & Huang, 2002). Furthermore, data processing methods, particularly baseline derivation, can cause Sq variability while isolating disturbances (Haberle et al., 2022). In addition, the tilt angle of the geomagnetic field is globally distributed and affects the annual and semiannual variations of the Sq currents (Tian et al., 2022). At mid-latitudes, the annual mean and semiannual amplitudes of the Sq currents are negatively correlated with the magnetic field strength, particularly in geomagnetic anomaly areas (Liu et al., 2024). This correlation is more pronounced in the Southern Hemisphere, where the tilt angle has a stronger influence on the ionospheric currents (Le Sager & Huang, 2002). This can elucidate the large APQDs of mid-latitude observatories of Africa-European and Asia-Australian sectors such as CZT, HER and PAF in all phases of the solar cycle (Figures 4.5 (a-d)). However, the ionospheric dynamo processes in the American sector are less susceptible to disturbances that could lead to abnormal phase shifts. This is because the day-to-day variability in the Sq(H) component is more often due to unrecognized disturbance field variations rather than inherent ionospheric current variability (Hibberd, 1981). According to Le Sager and Huang (2002), the American sector's geomagnetic field configuration is such that it supports a stable Sq current system, reducing the likelihood of phase shifts due to vortex tilting. This stability is attributed to the specific geomagnetic latitude and the main field's modulation of the ionospheric dynamo EMF, which helps maintain current continuity across hemispheres, especially in the Southern Hemisphere (Le Sager & Huang, 2002).

5.1.6 Seasonal Effects in Low-Latitude APQDs

At low-latitudes, global and regional APQDs occurrence rates obtained in the E season are much lower as compared to J and D seasons (Figures 4.1 - 4.4), which is similar to the observations from the low-latitude observatories, Addis Ababa (AAE), Trivandrum (TRD), and Alibag (ABG), reported in Last et al. (1976). However, for low-latitude observatories, high occurrence rate of APQDs was observed in all phases of the solar cycle except for solar maximum phase (Figures 4.1 - 4.2, 4.4 subplots a and b). Last et al. (1976) suggested that dominant APQDs at low-latitudes in summer may be related to the afternoon electrojet that causes abnormal phase-shifts in inverse relation with solar activity, i.e., solar minimum phase, which is supported by

the higher occurrence rates J season for low-latitudes in the Northern Hemisphere. Figure 4.5, subplots a-d, depict the APQD occurrences for low-latitude observatories. A low amplitude negative peak in Sq(H) resulting in a possible peaked phase-shift for low-latitude observatories could be a result of CEJ, (Bolaji et al., 2013). Global Sq current flows eastward while EEJ flows either eastward or westward. Bolaji et al. (2013) proposed that if both currents are directed eastward, then the Sq current will be enhanced, but if EEJ is directed westward and greater than the global Sq current, then it results in CEJ, hence, results in phase-shifts as well as depressions in Sq(H) amplitudes. CEJ results from the late reversal of the night-time westward current to the daytime eastward current. Kane (1975) stated that CEJ at equatorial stations results from the disappearance of equatorial E_s occurrence. Bolaji et al. (2013) also explained that westward magnetospheric ring currents from dusk to night-time period also result in negative perturbations in Sq(H) on QDs.

5.1.7 Ionospheric Conductivity and Sq Current Tilting

Ionospheric conductivity is another critical factor in the tilting of the Sq current system. The conductivity varies with solar activity, and this variation influences the dynamo electric fields and the neutral wind velocities (Takeda, 2013) as is evident from the solar maximum phase (Figure 4.3, subplot c). During solar maximum, the conductivity is higher, leading to stronger ionospheric currents and a more pronounced tilt in the T-type system (Takeda, 2013), causing morning as well as afternoon phase-shifts. Such phase-shifts were observed in HER in the morning and afternoon hours, while afternoon phase-shifts were observed mostly in CZT and PAF (Figures 4.6-4.9). However, higher APQDs rates in the morning and afternoon in solar maximum were observed compared to the solar minimum (Figures 4.6-4.9). The conductivity also varies with season, with higher conductivity during the local summer due to increased solar radiation. This seasonal variation in conductivity contributes to the tilting of the Sq current system, particularly in the Southern Hemisphere (Le Sager & Huang, 2002; Stening, 2008). Solar activity is a significant driver of the tilting in the Sq current system. The solar radiation modulates the ionospheric conductivity and the neutral wind velocities, which in turn affect the ionospheric currents (Takeda, 2013). Solar activity also influences the seasonal variation of the Sq currents. The annual and semiannual components of the Sq currents are more pronounced during solar maximum, particularly in the Southern Hemisphere (Liu et al., 2024; Le Sager & Huang, 2002).

The effective integrated conductivity within different ionospheric regions also plays a significant role in linking various regions electrically. Baker and Martyn (1953) emphasized that regions with high conductivity may shunt others with appreciable conductivity, thereby reducing the overall effective value across the ionosphere's thickness. This electrical linkage is vital for interpreting how different regions interact and influence each other. The tilting of the Sq

current system has significant implications for the ionospheric and geomagnetic field dynamics. The T-type system is associated with inter-hemispheric field-aligned currents (IHFACs), which connect the Sq current systems in the two hemispheres (Tian et al., 2022). These currents play a crucial role in the coupling of the ionospheres in the Northern and Southern Hemispheres (Lühr et al., 2015). The tilting also affects the longitudinal variations of the Sq currents. Tian et al. (2022) suggested that the Southern Hemisphere exhibits stronger longitudinal variations in the annual component (Sq1), particularly in the Eurasia and Australia anomaly zones, as is evident from the localized phase-shifts in the Asia-Australia sector in Figure 4.17, subplots a, b, c. These variations are attributed to the non-dipole components of the geomagnetic field and the ionospheric conductivity (Tian et al., 2022). Takeda (2002) studied the global geomagnetic Sq field from 1980 to 1990 and revealed that the Sq current system exhibits distinct seasonal patterns, with a "northern summer type" and "northern winter type" but no "equinox type". Stening and Winch (2013) showed that the spherical harmonic analysis showed that the current system's vortices have an annual variation, with maximum amplitudes in summer, and that the tilting of current contours is due to midday IHFACs. Yamazaki and Maute (2017) reviewed various data analysis methods, such as spherical harmonic analysis, to interpret the geomagnetic daily variation and its source ionospheric currents. Hobbs (1981) compared Sq analyses with model calculations, highlighting discrepancies due to the location of magnetic observatories and the influence of oceanic currents.

5.1.8 Atmospheric Dynamics Contributing to Morning and Afternoon APQDs

Higher APQD occurrences were observed in afternoon hours for all seasons of the mid-latitude observatories in the Africa-Europe and Asia-Australia sectors across solar cycle phases (Figures 4.6 - 4.9, subplots b, c, e, f). Bolaji et al. (2013) attributed higher afternoon APQDs to increased phase-shifted Sq(H) amplitude during daytime due to solar heating and maximum prevailing winds around noon. Afternoon APQDs could be caused by tilting of the Sq current system. Brown (1975) proposed that Sq movements about the SLT show asymmetry between hemispheres, with skewness and longitudinal movement varying seasonally. The Sq loop in the Northern Hemisphere rotates clockwise in winter and sunspot minimum due to decrease in E-region conductivity, causing greater APQDs occurrences, while rotating anticlockwise in summer and sunspot maximum (Brown, 1975). The geomagnetic field configuration influences Sq current system tilting when non-dipole components of the geomagnetic field modulate ionospheric currents, forming the T-type system (Liu et al., 2024; Le Sager & Huang, 2002). The T-type Sq current system, observed in the Southern Hemisphere, has a tilted structure due to geomagnetic field asymmetry (Liu et al., 2024; Le Sager & Huang, 2002). The F-type Sq current system, typically observed in the Northern Hemisphere, is more symmetric due to the

dominant dipole component and remains stable during solar quiet days (Le Sager & Huang, 2002; Stening, 2008), which could suggest fewer to no afternoon APQDs in the low- and mid-latitudes of the Northern Hemisphere in the Africa-European and Asia-Australian sectors in Figures 4.6 - 4.9, subplots b, c, e and f.

Higher APQD occurrence rates were observed in the morning seasons for mid-latitude observatories of America and Asia-Australia sectors across solar cycle phases (Figures 4.6 - 4.9 subplots b, c, e, f). Brown (1975) found morning APQDs resulting from decreased stratospheric isobaric height, while afternoon APQDs from increased isobaric height. These changes relate to pressure isopleth oscillations at greater heights (Brown, 1975). Decreased stratospheric isobars cause E-region electron density reduction, with greater effect in the dynamo region, causing ionization compression and higher peak density (Brown, 1975). Shinbori et al. (2014) linked high neutral wind speeds to low isobaric heights, while Talha et al. (2021) connected local wind system variation to Sq(H) phase-shifts in the morning hours, causing phase-shifts, especially for low-latitudes.

5.1.9 Sq Foci Latitudes and Current System Shifts

The Sq foci occurrence rate at $\pm 30^{\circ}$ and beyond in all three sectors reveals how the ionospheric current system shifts from its standard position during NQD and APQD events. The Sq foci usually exist between $\pm 30^{\circ}$ magnetic latitude in both hemispheres under normal circumstances because of the EEJ effects and worldwide ionospheric conductivity patterns (Yamazaki & Maute, 2017). The Sq current function shows longitudinal variations because tidal winds affect the dynamo-generated electric fields and currents, hence affecting the Sq foci latitudes differently in different longitudes (Pedatella et al., 2011).

Stable Sq foci latitudes in the D and E seasons of all sectors (Figure 4.11, subplot b) were observed in 2014, whereas similar stable Sq foci latitudes were observed in the J season (June solstice) for the Northern Hemisphere and D season (December solstice) in the Southern Hemisphere in 2009. The intensity of the Sq current is closely related to solar activity, with stronger currents observed during periods of high solar activity because the increased solar radiation enhances ionospheric conductivity, leading to more robust current systems (Zhao et al., 2014). During solar maximum, the peak current intensity tends to occur near the equinoxes, while during solar minimum, it peaks near the solstices (Zhao et al., 2014). Atmospheric conditions, such as tidal winds and solar UV radiation, play a crucial role in shaping the seasonal patterns of the Sq current system (Pedatella et al., 2011).

The large variations of the Sq foci latitudes were observed in the June and December solstices in 2009 and in 2014 (Figures 4.11, subplots a, b). Additional research using numerical

models and satellite data indicates that specific semidiurnal modes such as the (2,4) and (2,3) components and the interaction of tidal winds with planetary waves further contribute to local time and longitudinal variations in electric fields and currents (Richmond et al., 1976). Planetary wave-tide interaction has been observed to have the strongest effects in local winter at low- and mid-latitudes in the minimum phase of the solar cycle(Liu et al., 2010), which can most likely explain the variation in the Sq foci latitudes as depicted in Figure 4.11, subplot a).

Figure 4.10, subplot a, depicts equatorward foci latitudes in the Northern Hemisphere mostly in the D season of all sectors and the E season of the America and the Asia-Australia sector for 2009. According to Butcher (1987), it is found that the current that produces primary variations in Sq(H) is single current vortex (SCV), which causes abnormal quiet days. SCV flows across the equator either clockwise or anticlockwise and its amplitude reduces if it flows counterclockwise, while it increases if it flows clockwise (Butcher, 1989). The driving source of SCV is the diurnal winds, which are also a source of both phase and amplitude variability of Sq(H) amplitude on APQDs (Butcher, 1989). From further investigations by Butcher et al. (1993), it is found that APQDs in the D-season of the Northern Hemisphere are due to additional fields that result from SCV having foci in a latitude range of $15^{\circ} - 20^{\circ}$N.

5.1.10 Solstitial and Equinoctial Asymmetry in Localized APQDs

Localized APQDs are mostly found in the solstices of both solar minimum and maximum phases, as depicted in Figures 4.12 - 4.17. Equinoctial and solstitial asymmetry in the Sq current system due to conductivity, tides, and neutral winds has been revisited in recent studies (Chen et al., 2024; Liu et al., 2025). This asymmetry influences ionospheric dynamics and geomagnetic phenomena. Chen et al. (2024) focused on solar activity's interaction with ionospheric asymmetries, examining the equivalent ionospheric current system from Sq variations at 124 stations. The study identified migrating tidal components influenced by solar radiation and neutral winds. Liu et al. (2025) investigated north-south asymmetry in Sq variations at geomagnetically conjugate regions using data from five station pairs in which ASYM-X shows higher intensity from May to October with latitudinal variability, while ASYM-Y shows seasonal patterns. Migrating tides significantly influence asymmetric activity, with stronger ASYM during June solstice (Liu et al., 2025) hence, APQDs were observed to occur in the solstices of both solar minimum (2009) and maximum (2014) phases. Moreover, the asymmetry of neutral winds between hemispheres causes the observed Sq variation asymmetry, particularly affecting migrating tides' zonal component (Liu et al., 2025). On the other hand, a central role for the variations in non-migrating tidal winds, especially the diurnal eastward wavenumber-3 (DE3) mode, in driving both longitudinal and seasonal variations in dynamo-generated electric fields and currents (Lühr et al., 2008; Pedatella et al., 2011). The strong seasonal variation has been linked to the DE3 tidal wave mode with the strongest response at equinoxes and June solstice

and negligible effect at the December solstice, especially in solar maximum phase (Lühr et al., 2008).

5.1.11 Sq Foci Migration and Connection with IHFACs

The local APQDs in the June solstice of both 2009 and 2014 depict APQDs near the Sq foci latitudes (Figures 4.14 and 4.13). Magnetograms, which record geomagnetic field variations, show peaks and dips that correspond to the Sq current system's behavior. The latitudinal migration of the Sq focus or changes in current intensity can cause these variations, as observed in the distribution of geomagnetic daily variations along station chains (Wang et al., 2011). The primary mechanism for seasonal shifts in Sq foci latitudes is related to the differences in solar heating during various times of the year. As the Earth orbits the Sun, the angle and intensity of solar radiation change, affecting the ionospheric conditions. The ideal Sq schema involves understanding the geomagnetic Sq field's day-to-day variability, which is influenced by the latitudinal shift of the Sq current system focus latitude. This shift results in positive or negative correlations in the daily range of geomagnetic variations, depending on whether stations are on the same or opposite sides of the Sq foci latitudes (Chen et al., 2007). According to Kane (1974), the strength of the Sq current system is related to its focus latitudes, with larger strengths associated with an equatorward shift of the Sq focus latitude. This is also linked to the strength of the equatorial electrojet, which influences the geomagnetic field's intensity (Kane, 1974). While the ideal Sq schema provides a framework for understanding geomagnetic variations, it is essential to consider other factors that influence these variations. For instance, the non-dipole field and seasonal variations can affect the geomagnetic Sq field, as well as the longitudinal effects and universal time variations, which are attributed to the tilt of the geomagnetic axis and regional anomalies (Tian et al., 2022). This leads to a larger shift of the Southern Hemisphere's foci latitudes northwards during the northern June solstice and southwards during the southern December solstice (Koch & Kuvshinov, 2015). This can be observed in Figure 4.10 (a) except for the Asia-Australian sector. The Sq current vortex tends to appear in earlier hours before local noon in local summer months (May-August, NH) compared to local winter months (November-February, SH) (Abbas et al., 2019). This is clearly depicted for the Northern Hemisphere in Figures 4.12 - 4.17. The variations in ionospheric conductivities due to changes in the geomagnetic field strength can result in different behaviors of the Sq current system. For instance, during periods of weak geomagnetic field strength, the ionospheric currents may exhibit more pronounced shifts and scattering, particularly over regions like the SAA, where the field strength is notably lower (Koch & Kuvshinov, 2015). IHFACs are crucial in connecting the Sq current systems of the Northern and Southern Hemispheres, influencing the geomagnetic field and the position of the current vortex (Owolabi et al., 2018), particularly over the Asia-Australia sector as depicted in Figure 4.14. IHFACs are the FACs that

connect the Sq current systems of opposite hemispheres and serve as a focus-to-focus electrical link of the Sq current system within the magnetosphere-ionosphere circuit. They arise from divergences of horizontal currents (driven by electric fields and conductivity gradients) and from magnetospheric sources mapped along magnetic field lines; the ionosphere acts as a load in the current circuit (Yu et al., 2022; Owolabi et al., 2018). Jadhav et al. (2024) and Owolabi et al. (2018) suggested that middle-atmosphere waves and asymmetric wind-dynamo action can modulate low-latitude IHFACs in lower altitudes, imprinting multi-day oscillations (e.g., 16-day) on the inter-hemispheric current pattern via tidal/wind dynamo changes. Hence, it can be presumed that non-migrating thermospheric tides contribute to the deformation and shifting of the Sq current vortex, particularly over regions like East Asia (Zhang et al., 2024), which may explain the migration of the Sq focus latitude in the Southern Hemisphere to the polar latitude.

5.1.12 SSW Events and IHFAC Modulation

Figure 4.12 (c) shows the dispersion of the IHFACs due to a sudden stratospheric warming (SSW) event that occurred on 23 January 2009, affecting the IHFACs' flow from the Southern Hemisphere to the Northern Hemisphere. SSWs are large, rapid disturbances of the high-latitude winter stratosphere characterized by marked stratospheric temperature rises and reversals or strong weakening of the polar-night westerly jet. SSWs are accompanied by altered propagation of planetary and gravity waves and by large changes in tidal amplitudes that can propagate upward into the mesosphere–thermosphere (Zhang et al., 2023). Dynamic SSWs result from amplified planetary-wave forcing of the stratospheric flow, producing zonal-mean wind and temperature anomalies and strong changes in gravity-wave and tidal momentum deposition in the upper atmosphere (de Wit et al., 2014). Observations and modeling of ionospheric signatures show SSWs modify thermosphere/ionosphere parameters (e.g., TEC, composition, plasma drifts) and can drive inter-hemispheric signals through altered tidal/wave activity and wind-dynamo effects (Zhang et al., 2023; Yamazaki et al., 2012). SSWs are suggested to influence the coupling of the magnetosphere and ionosphere primarily by altering the neutral-wind dynamo, tidal composition, and ionospheric conductivity; these changes in turn perturb FACs, including IHFACs and the Sq system. It is also suggested that the altered tidal content (e.g., semidiurnal and planetary waves) modifies the timing (phase) and amplitude of quiet-day ionospheric currents, producing abnormal phase shifts and excursions in IHFACs. Enhanced or asymmetric planetary/tidal waves during SSWs change E-region dynamo winds and thus the wind-driven electric fields that control Sq and IHFACs, producing multi-day oscillations in IHFAC amplitude and timing (Jadhav et al., 2024; Yamazaki et al., 2012). Observed Sq phase changes at longitude sectors in connection with the magnitudes of the Sq vortex system have been shown to change during SSWs (decrease in one hemisphere, increase in the other) with a reduction of longitudinal separation between Sq vortices, and this trend is consistent with

phase-shift anomalies on geomagnetically quiet days (Yamazaki et al., 2012). There is a clear indication of amplitude reduction and phase-shifts at mid-latitude observatories of ESK, DOU, HER, and CZT as well as the equatorial observatory of MBO from the magnetograms in Figure 4.12 (b). Regional IHFACs excursions ground and satellite records show anomalous IHFACs excursions (retardation or unexpected local-time maxima) in some months, coincident with atmospheric forcing patterns consistent with SSW-related tidal changes (Owolabi et al., 2018). SSW can amplify lunar tides and atmospheric planetary waves, further influencing IHFAC formation (Lühr et al., 2019, 2015). In summary, the IHFACs were modulated by SSWs on 23 January 2009, thereby affecting the Sq foci latitudes and most likely causing the APQDs observed.

5.2 Conclusion

The intricate relationship between solar activity and geomagnetic field parameters highlights the importance of understanding the dynamics of the ionosphere and its associated currents. The E-region dynamo plays a crucial role in generating electric currents that significantly influence geomagnetic variations, particularly the quiet-time Sq currents. The improved methodology of sifting the QDs using the SYM-H index and the calculation of Sq variations was crucial for the identification of NQDs and APQDs. The Sq variations exhibit both normal and abnormal variations, which have been analyzed regarding their behaviors and trends under changing solar conditions. The cyclical nature of solar activity, characterized by the solar cycle, is essential in modulating these effects, with sunspot activity directly linked to variations in geomagnetic parameters. The main results are highlighted below:

1. A high APQDs occurrence rate, globally as well as regionally, was observed in the D seasons of all phases and hemispheres of the solar cycle. However, a general trend of high occurrence rate of regional and global APQDs was observed in the Northern Hemisphere's low-latitudes (43.4% & 36.7%) and in the Southern Hemisphere's mid-latitudes (31% and 31.4%), respectively. The highest occurrence of APQDs was observed in the NH during the solar minimum phase (37%) and in the SH during the solar maximum phase (35%). Conversely, the lowest occurrence was noted in the NH during the solar ascending phase (27%) and in the SH during the solar minimum phase (31.2%).

2. APQDs occurrence is higher in Northern Hemisphere low latitude stations and Southern Hemisphere mid-latitudes. The low-latitude observatory KNY in the Asia-Australian sector and the mid-latitude observatory CZT in the Africa-European sector showed higher APQDs occurrences throughout solar cycle 24. Asymmetry for conjugate magnetic observatory pairs was observed when KNY (60.2%) as compared to CTA (30%) in the

Asia-Australia sector and SJG (42.44%) as compared to VSS (7.4%) in the America sector experienced consistently higher APQDs occurrence rates for the low-latitudes of the Northern Hemisphere for all phases of the solar cycle. Similar occurrence rates were observed compared to the conjugate observatories in the Southern Hemisphere for mid-latitude observatories, CZT (58.5%) HER (40.5%) in the Africa-Europe sector, and AMS (44.4%), PAF (51.05%) in the Asia-Australia sector. The behaviour was more or less similar in all phases of the solar cycle.

3. Generally, NQDs occurred during 08:30-13:30 SLT and 10:30-13:30 SLT for low- and mid-latitude observatory pairs in Northern and Southern Hemispheres. Higher APQDs occurrence occurred in morning hours (06:30-09:30 SLT) at low-latitudes, especially in the D season, and afternoon hours (15:30-16:30 SLT) for mid-latitudes across seasons. Afternoon APQD occurrences for CZT were observed at 14:30 SLT with the highest in the D season (16%). The highest morning APQDs occurrences for KNY were observed at 08:30 SLT in the D season (9%) as well.

4. Sq foci variability on QDs and polar transits were observed for the D- and J seasons for the Northern Hemisphere of America and Africa-Europe sectors in 2009. Moreover, the Southern Hemisphere transits of the Sq foci latitudes were observed in the D- and J seasons. The Sq focus was calculated at a polar latitude of 71°S on June 17, 2009 in the Asia-Australia sector. Similar polar transits of the Sq foci latitudes were observed for the J season in 2014 at the America and Asia-Australia sectors and all the seasons at the Africa-Europe sector.

5. The SSW event of 23 January 2009 seemed to influence the IHFACs and shift the Sq foci latitudes to 55°N and 54°S. Moreover, localized APQDs were caused at the mid-latitude observatories of ESK, DOU, HER, and CZT in both hemispheres and at the equatorial observatory of MBO.

5.3 Future Work

This study was limited to the analysis of ground magnetic observatory data in the extraction of APQDs. Future work needs to incorporate the data from satellite instrumentation with the atmospheric or ionosphere-thermosphere coupled models. Detailed analysis of IHFACs from satellite data and E-region data from ionosondes or radars can provide insight into the dynamics of the localized APQDs to ascertain the impact of IHFACs on their causal mechanisms. By comparing Sq foci latitudes calculations in other phases, asserting substorms occurrences and orientation of IMF B_y, checking connections with sporadic-E or E-layer anomalies, calculation of Sq foci conductivity, horizontal winds, assessing connection with seismic activity and

magnetotellurics on QDs, storm recovery influence on QDs, the causal mechanisms behind the APQDs can be assessed in detail.

Appendix A

List of Observatories

The lists of observatory data using H, X, and Y components considered for this study are presented for three longitude sectors.

Table A.1: List of observatories in American sector

S. No.	Observatory Location	IAGA Code	Geog Lat (°)	Geog Long (°)	Geom Lat (°)	Geom Long (°)
1	Victoria	VIC	48.5	-123.42	53.54	-63.02
2	Fredericksberg	FRD	38.21	-77.37	48.42	-1.25
3	Fresno	FRN	37.09	-119.72	42.77	-55.78
4	Bay St.Louis	BSL	30.35	-89.64	40.82	-18.52
5	Honolulu	HON	21.32	-158	20.91	-89.62
6	San Juan	SJG	18.11	-66.15	26.98	10.88
7	Kourou	KOU	5.21	-52.73	9.08	22.14
8	Huancayo	HUA	-12.05	-75.33	0.10	-3
9	Apia	API	-13.81	-171.78	-15.77	-96.98
10	Pamataai	PPT	-17.567	-149.57	-16.5	-74.18
11	Vassouras	VSS	-22.4	-43.65	-19.07	22.38
12	Port Stanley	PST	-51.7	-57.89	-38.73	10.75
13	Faraday Islands	AIA	-65.24	-64.258	-50.64	9.3

Table A.2: List of observatories in African-European sector

S. No.	Observatory Location	IAGA Code	Geog Lat (°)	Geog Long (°)	Geom Lat (°)	Geom Long (°)
1	Eskdalemuir	ESK	55.31	-3.206	52.37	76.87
2	Kiev	KIV	50.7	30.3	46.3	104.45
3	Dourbes	DOU	50.1	4.6	45.8	81.79
4	Ebro	EBR	40.957	0.3	34.9	76.49
5	Guimar	GUI	28.32	-16.44	20.41	-60.29
6	Tamanrasset	TAM	22.79	5.53	13.01	-80.00
7	Mbour	MBO	14.38	16.96	3.89	57.63
8	Ascension Island	ASC	-7.95	-14.38	-19.05	-55.48
9	Tsumeb	TSU	-19.2	17.58	-30.72	88.28
10	Keetmanshoop	KMH	-26.54	18.11	-36.7	86.26
11	Hartebeesthoek	HBK	-25.88	27.7 E	-36.1	96.3
12	Hermanus	HER	-34.4	19.23	-42.48	83.86
13	Port Alfred	CZT	-46.4	51.86	-53.12	107.3

Table A.3: List of observatories in Asian-Australian sector

S. No.	Observatory Location	IAGA Code	Geog Lat (°)	Geog Long (°)	Geom Lat (°)	Geom Long (°)
1	Novorsibirsk	NVS	54.85	83.23	50.62	156.52
2	Irkutsk	IRT	52.27	104.45	47.56	177.95
3	Alma Ata	AAA	43.25	76.92	38.61	149.82
4	Memambetsu	MMB	43.91	144.19	36.91	-143.96
5	Kanoya	KNY	31.42	130.88	24.58	-156.57
6	Jaipur	JAI	26.92	75.80	21.10	148.59
7	Sonmiani	SON	25.19	66.75	19.56	139.23
8	Phuthuy	PHU	21.03	105.95	14.39	178.32
9	Alibag	ABG	18.63	72.87	12.20	145.61
10	Guam	GUA	13.59	144.87	6.08	-143.54
11	Gan	GAN	0.649	73.153	-7.31	145.70

S. No.	Observatory Location	IAGA Code	Geog Lat (°)	Geog Long (°)	Geom Lat (°)	Geom Long (°)
12	Cocos (Keeling Island)	CKI	-12.19	96.83	-21.83	168.95
13	Kakadu	KDU	-12.69	132.47	-21.69	-154.74
14	Charters Towers	CTA	-20.09	146.26	-28.98	-139.17
15	Alice Springs	ASP	-23.76	133.88	-33.75	-152.37
16	Canberra	CNB	-35.32	149.36	-45.11	-132.80
17	Martin de Vivies	AMS	-37.80	77.57	-48.86	139.78
18	Eyrewell	EYR	-43.47	172.40	-50.00	-103.25
19	Port-aux-Francais	PAF	-49.35	70.25	-58.76	135.14

The data was available for the observatories of GAN and CKI was available from 2011 and 2013 till 2019, respectively. The data for TSU and SON was missing in 2008 and 2014, respectively. The data for MBO, PHU and CZT was missing for the year 2019.

Bibliography

Abbas, M., Jusoh, M. H., & Abidin, Z. Z. (2019). Solar quiet (Sq) and conductivity-depth structure of Asia sub-region using solar quiet field variation. *Journal of Physics: Conference Series*, *1152*(1), 012034. https://doi.org/10.1088/1742-6596/1152/1/012034

Adhikari, B., Adhikari, R., Chapagain, N. P., Sapkota, N., Dahal, S., & Pandit, D. (2017). Daily, seasonal and monthly variation of middle-low latitudes magnetic field during low solar activity. *Discovery*, *53*(255), 181–190.

Ahmad, N., & Widyanto, S. (2023). Detection of satellite anomalies using the Dst index. *AIP Conference Proceedings*, *2941*(1), 040001. https://doi.org/10.1063/5.0181386

Alken, P., & Maus, S. (2010). Relationship between the ionospheric eastward electric field and the equatorial electrojet. *Geophysical Research Letters*, *37*(4). https://doi.org/10.1029/2009GL041989

Amm, O., Fujii, R., Kauristie, K., Aikio, A., Yoshikawa, A., Ieda, A., & Vanhamäki, H. (2011). A statistical investigation of the Cowling channel efficiency in the auroral zone. *Journal of Geophysical Research: Space Physics*, *116*(A2). https://doi.org/10.1029/2010JA015988

Amory-Mazaudier, C. (2005). On the scientific contributions of Pierre-Noël Mayaud [Submitted in Hal Archives on 19 May 2014]. *IAGA Assembly 2005*. http://hal.upmc.fr/hal-00993108

Anad, F., Amory-Mazaudier, C., Hamoudi, M., Bourouis, S., Abtout, A., & Yizengaw, E. (2016). Sq solar variation at Medea Observatory (Algeria), from 2008 to 2011. *Advances in Space Research*, *58*(9), 1682–1695. https://doi.org/10.1016/j.asr.2016.06.029

Anderson, D., Anghel, A., Chau, J., & Veliz, O. (2004). Daytime vertical E × B drift velocities inferred from ground-based magnetometer observations at low latitudes. *Space Weather*, *2*(11). https://doi.org/10.1029/2004SW000095

Annadurai, N. M. N., Hamid, N. S. A., Yamazaki, Y., & Yoshikawa, A. (2018). Investigation of unusual solar flare effect on the global ionospheric current system. *Journal of Geophysical Research: Space Physics*, *123*(10), 8599–8609. https://doi.org/https://doi.org/10.1029/2018JA025601

Archana, R., & Arora, K. (2022). Variations of Sq foci position from the Indian longitudes and its influence on Equatorial Electrojet. *Journal of Atmospheric and Solar-Terrestrial Physics*, *236*, 105911. https://doi.org/10.1016/j.jastp.2022.105911

Archana, R., & Arora, K. (2024). Variations of inter-hemispheric field-aligned currents: Observations from ground geomagnetic measurements. *Journal of Geophysical Research: Space Physics*, *129*(3), e2023JA032254. https://doi.org/10.1029/2023ja032254

Archana, R., Lingala, M., & Arora, K. (2023). Re-visiting EEJ and CEJ occurrences pattern under the influence of Sq variations of both hemispheres. *Journal of Geophysical Research: Space Physics*, *128*(6), e2023JA031406. https://doi.org/10.1029/2023ja031406

Arinze, O. F., Chigozie, O. N., & Chukwelu, E. (2016). Statistical characterization of geomagnetic variation in Nigeria. *IOSR Journal of Applied Geology and Geophysics*, *4*, 1–20. https://doi.org/10.9790/0990-0406020120

Aruliah, A. L., Farmer, A. D., Fuller-Rowell, T. J., Wild, M. N., Hapgood, M., & Rees, D. (1996). An equinoctial asymmetry in the high-latitude thermosphere and ionosphere. *Journal of Geophysical Research: Space Physics*, *101*(A7), 15713–15722. https://doi.org/https://doi.org/10.1029/95JA01102

Axford, W. I., & Hines, C. O. (1961). A unifying theory of high-latitude geophysical phenomena and geomagnetic storms. *Canadian Journal of Physics*, *39*(10), 1433–1464. https://doi.org/10.1139/p61-172

Baker, W. G. (1953). Electric currents in the ionosphere. II. The atmospheric dynamo. *Philosophical Transactions of the Royal Society of London.*, *246*(913), 295–305. https://doi.org/10.1098/rsta.1953.0017

Baker, W. G., & Martyn, D. F. (1953). Electric currents in the ionosphere. I. The conductivity. *Philosophical Transactions of the Royal Society of London*, *246*(913), 281–294. https://doi.org/10.1098/rsta.1953.0016

Bello, O., Rabiu, A., Yumoto, K., & Yizengaw, E. (2014). Mean solar quiet daily variations in the Earth's magnetic field along East African longitudes. *Advances in Space Research*, *54*(3), 283–289. https://doi.org/10.1016/j.asr.2013.11.058

Bengtson, M. T. (2017). *Solar wind-magnetosphere coupling: A global perspective of reconnection in the magnetotail* [Master's thesis]. Embry-Riddle Aeronautical University. https://commons.erau.edu/edt/320

Bespalov, P., & Savina, O. (2012). Equatorial electrojet and its response to external electromagnetic effects. *Radiophysics and Quantum Electronics*, *55*(4), 215–231. https://doi.org/10.1007/S11141-012-9361-5

Bhardwaj, S., Rao, P. S., & Veenadhari, B. (2015). Abnormal quiet day variations in Indian region along 75° E meridian. *Earth, Planets and Space*, *67*, 1–15. https://doi.org/10.1186/s40623-015-0292-1

Blanc, M., & Richmond, A. D. (1980). The ionospheric disturbance dynamo., *85*(A4), 1669–1686. https://doi.org/10.1029/JA085iA04p01669

Bolaji, O. S., Adimula, I. A., Adeniyi, J. O., & Yumoto, K. (2013). Variability of horizontal magnetic field intensity over Nigeria during low solar activity. *Earth, Moon, and Planets*, *110*(1-2), 91–103. https://doi.org/10.1007/s11038-012-9412-0

Bolaji, O. S., Rabiu, A. B., Bello, O. R., Yoshikawa, A., Yumoto, K., Odeyemi, O. O., & Ogunmodimu, O. (2015). Spatial variability of solar quiet fields along 96° magnetic

meridian in Africa: Results from MAGDAS. *Journal of Geophysical Research: Space Physics*, *120*(5), 3883–3898. https://doi.org/10.1002/2014ja020728

Bolaji, O. S., Rabiu, A. B., Oyeyemi, E. O., & Yumoto, K. (2012). Climatology of the inter-hemispheric field-aligned currents system over the Nigeria ionosphere. *Journal of Atmospheric and Solar-Terrestrial Physics*, *89*(1), 144–153. https://doi.org/10.1016/j.jastp.2012.07.008

Brown, G. M. (1974). A new solar–terrestrial relationship. *Nature*, *251*(5476), 592–594. https://doi.org/10.1038/251592a0

Brown, G. M. (1975). Sq variability and aeronomic structure. *Journal of Atmospheric and Terrestrial Physics*, *37*(1), 107–117. https://doi.org/10.1016/0021-9169(75)90093-8

Brown, G. M. (1986). The change in Sq(H) amplitude on Abnormal Quiet Days. *Geophysical Journal International*, *86*(2), 467–473. https://doi.org/10.1111/j.1365-246X.1986.tb03838.x

Brown, G. M., & Williams, W. R. (1969). Some properties of the day-to-day variability of Sq (H). *Planetary and Space Science*, *17*(3), 455–470. https://doi.org/10.1016/0032-0633(69)90076-2

Butcher, E. C. (1982). On the latitude of the Sq(H) focus at sunspot minimum. *Geophysical Journal International*, *69*(1), 113–120. https://doi.org/10.1111/j.1365-246x.1982.tb04938.x

Butcher, E. C. (1986). Magnetic quiet daily variation: Variations in the magnetic declination on abnormal quiet days. *Exploration Geophysics*, *17*(1), 16–17. https://doi.org/https://doi.org/10.1071/EG986016

Butcher, E. C. (1987). Currents associated with abnormal quiet days in Sq (H). *Geophysical Journal International*, *88*(1), 111–123. https://doi.org/10.1111/j.1365-246x.1987.tb01371.x

Butcher, E. C. (1989). Abnormal Sq Behaviour. In W. H. Campbell (Ed.), *Quiet Daily Geomagnetic Fields* (pp. 463–483). https://doi.org/10.1007/978-3-0348-9280-3_10

Butcher, E. C., & Brown, G. M. (1980). Abnormal quiet days and the effect of the interplanetary magnetic field on the apparent position of the Sq focus. *Geophysical Journal International*, *63*(3), 783–789. https://doi.org/10.1111/j.1365-246x.1980.tb02652.x

Butcher, E. C., & Brown, G. M. (1981a). On the nature of abnormal quiet days in Sq (H). *Geophysical Journal International*, *64*(2), 513–526. https://doi.org/10.1111/j.1365-246x.1981.tb02680.x

Butcher, E. C., & Brown, G. M. (1981b). The variability of Sq(H) on normal quiet days. *Geophys. J. R. astr. SOC.*, *64*(2), 527–537. https://doi.org/10.1111/j.1365-246x.1982.tb04938.x

Butcher, E. C., McCreadie, H., & Schlapp, D. M. (1993). A worldwide study of the H, D and Z variation on abnormal quiet days (AQDs). *Geophysical Journal International*, *114*(1), 175–184. https://doi.org/10.1111/j.1365-246x.1993.tb01477.x

Calabia, A., Anoruo, C., Shah, M., Amory-Mazaudier, C., Yasyukevich, Y., Owolabi, C., & Jin, S. (2022). Low-latitude ionospheric responses and coupling to the February 2014 multiphase geomagnetic storm from GNSS, magnetometers, and space weather data. *Atmosphere*, *13*(4), 518. https://doi.org/10.3390/atmos13040518

Campbell, W. H. (2003). *Introduction to Geomagnetic Fields*. https://doi.org/10.1017/CBO9781139165136

Campbell, W. H. (2012). *Quiet Daily Geomagnetic Fields*. https://doi.org/10.1007/978-3-0348-9280-3

Campbell, W. H., Arora, B. R., & Schiffmacher, E. R. (1993). External Sq currents in the India-Siberia region. *Journal of Geophysical Research: Space Physics*, *98*(A3). https://doi.org/10.1029/92ja02552

Campbell, W. H., Barton, C. E., Chamalaun, F. H., & Welsh, W. (1998). Quiet-day ionospheric currents and their application to upper mantle conductivity in Australia. *Earth, Planets and Space*, *50*(4), 347–360. https://doi.org/10.1186/BF03352121

Campbell, W. H., & Schiffmacher, E. R. (1985). Quiet ionospheric currents of the northern hemisphere derived from geomagnetic field records. *Journal of Geophysical Research: Space Physics*, *90*(A7), 6475–6486. https://doi.org/10.1029/ja090ia07p06475

Campbell, W. H., & Schiffmacher, E. R. (1987). Quiet ionospheric currents and Earth conductivity profile computed from quiet-time geomagnetic field changes in the region of Australia. *Australian Journal of Physics*, *40*(1), 73–88. https://doi.org/10.1071/ph870073

Campbell, W. H., & Schiffmacher, E. R. (1988). Quiet ionospheric currents of the southern hemisphere derived from geomagnetic records. *Journal of Geophysical Research: Space Physics*, *93*(A2), 933–944. https://doi.org/10.1029/ja093ia02p00933

Campbell, W. H., Schiffmacher, E. R., & Kroehl, H. W. (1989). Global quiet day field variation model WDCA/SQ1. *Eos, Transactions American Geophysical Union*, *70*(5), 66–74. https://doi.org/10.1029/89eo00039

Cardus, J. C., & Romana, A. (1962). *Geomagnetic rapid variations during IGY and IGC* (Vol. 17). https://ui.adsabs.harvard.edu/abs/1962JPSJS..17B..47C

Case, N. (2014). *Solar Wind-Magnetosphere Interactions: A Statistical Analysis of Spacecraft Measurements* [PhD thesis, Lancaster University]. https://eprints.lancs.ac.uk/id/eprint/69143/

Casey, J. P. (2005). *Overview of the Equatorial Electrojet and related Ionospheric Current Systems* (Technical Report No. ADA436210). Naval Undersea Warfare Center Division, Newport, RI. https://apps.dtic.mil/sti/pdfs/ADA436210.pdf

Chandrasekhar, E., & Fontes, S. L. (2004). A study of the ionospheric source current systems of equinoctial (E-) season over the 120°-150°E longitude region. *I Simpósio Brasileiro de Geofísica*, cp–216. https://doi.org/10.22564/1simbgf2004.058

Chapman, S. (1951). The equatorial electrojet as detected from the abnormal electric current distribution above Huancayo, Peru, and elsewhere. *Archiv Fuer Meteorologie, Geophysik und Bioklimatologie, Serie A*, *4*(1), 368–390. https://doi.org/10.1007/BF02246814

Chapman, S., & Stagg, J. (1929). On the variability of the quiet-day diurnal magnetic variation at Eskdalemuir and Greenwich. *Proceedings of the Royal Society of London*, *123*(791), 27–53. https://doi.org/10.1098/rspa.1929.0054

Chemin, Y.-H. H. (2023). *Ionosphere-New Perspectives*. IntechOpen. https://doi.org/10.5772/intechopen.1001520

Chen, G. X., Xu, W. Y., Du, A. M., Wu, Y. Y., Chen, B., & Liu, X. C. (2007). Statistical characteristics of the day-to-day variability in the geomagnetic Sq field. *Journal of Geophysical Research: Space Physics*, *112*(A6). https://doi.org/10.1029/2006JA012059

Chen, S. S., Yamazaki, Y., Denardini, C. M., Resende, L. C. A., Chagas, R. A. J., & Stolle, C. (2024). Tidal composition analysis of global sq current system. *Journal of Geophysical Research: Space Physics*, *129*(5). https://doi.org/10.1029/2023JA032382

Chen, S., Denardini, C. M., Resende, L. C. A., Chagas, R. A. J., Moro, J., da Silva, R. P., do Carmo, C. d. S., & Picanço, G. A. d. S. (2021). Evaluation of the Solar Quiet Reference Field (SQRF) model for space weather applications in the South America Magnetic Anomaly. *Earth, Planets and Space*, *73*(1), 61. https://doi.org/10.1186/s40623-021-01382-8

Chertok, I. M., & Belov, A. V. (2017). Long- and mid-term variations of the soft X-ray flare type in solar cycles. *Solar Physics*, *292*(10). https://doi.org/10.1007/s11207-017-1169-1

Clette, F., & Lefèvre, L. (2015, July). International sunspot number v2.0. https://doi.org/10.24414/qnza-ac80

Clette, F., Svalgaard, L., Vaquero, J. M., & Cliver, E. W. (2014). Revisiting the sunspot number: A 400-year perspective on the solar cycle. *Space Science Reviews*, *186*, 35–103. https://doi.org/10.1007/S11214-014-0074-2

Cliver, E. W., Kamide, Y., Ling, A. G., & Yokoyama, N. (2001). Semiannual variation of the geomagnetic Dst index: Evidence for a dominant nonstorm component. *Journal of Geophysical Research: Space Physics*, *106*(A10), 21297–21304. https://doi.org/https://doi.org/10.1029/2000JA000358

Courtillot, V., Valet, J.-P., Hulot, G., & Le Mouël, J.-L. (1992). The Earth's magnetic field: Which geometry? *Eos, Transactions American Geophysical Union*, *73*(32), 337–342. https://doi.org/10.1029/91eo00260

Cranmer, S. R. (2009). Coronal holes. *Living Reviews in Solar Physics*, *6*(1), 3. https://doi.org/10.12942/lrsp-2009-3

Curto, J. J. (2019). Uncertainty in hourly mean data from classical magnetometers. *Earth, Planets and Space*, *71*(1), 139. https://doi.org/10.1186/s40623-019-1119-2

D'Angelo, G., Battiston, R., Bertello, I., Cicone, A., Follega, F. M., Iuppa, R., Neubüser, C., Papini, E., Parmentier, A., Recchiuti, D., et al. (2022). Investigation of the magnetospheric-ionospheric-lithospheric coupling on occasion of the 14 August 2021 Haitian earthquake. *44th COSPAR Scientific Assembly. Held 16-24 July*, *44*, 750. https://doi.org/10.5194/egusphere-egu22-1329

de Haro Barbas, B. F., Elias, A. G., Cnossen, I., & Zossi de Artigas, M. (2013). Long-term changes in solar quiet (Sq) geomagnetic variations related to Earth's magnetic field secular variation. *Journal of Geophysical Research: Space Physics*, *118*(6), 3712–3718. https://doi.org/10.1002/jgra.50352

de Wit, R. J., Hibbins, R. E., Espy, P. J., Orsolini, Y. J., Limpasuvan, V., & Kinnison, D. E. (2014). Observations of gravity wave forcing of the mesopause region during the January 2013 major Sudden Stratospheric Warming. *Geophysical Research Letters*, *41*(13), 4745–4752. https://doi.org/10.1002/2014GL060501

Dorelli, J. C. (2019). Does the solar wind electric field control the reconnection rate at Earth's subsolar magnetopause? *Journal of Geophysical Research: Space Physics*, *124*(4), 2668–2681. https://doi.org/https://doi.org/10.1029/2018JA025868

Driel-Gesztelyi, L. v., & Owens, M. J. (2020). Solar cycle. https://doi.org/10.1093/acrefore/9780190871994.013.9

Echer, E., Tsurutani, B. T., & Gonzalez, W. D. (2011). Extremely low geomagnetic activity during the recent deep solar cycle minimum. *Proceedings of the International Astronomical Union*, *7*(S286), 200–209. https://doi.org/10.1017/s174392131200484x

Erick, O. G., Paul, B., & Boniface, N. (2016). Quiet time geomagnetic field variations in the equatorial East African region during the inclining phase of solar cycle 24. *International Journal of Astrophysics and Space Science*, *4*, 21–25. https://doi.org/10.11648/j.ijass.20160402.11

Eshtemirovich, E. H., Toshniyozovich, A. U., Xasanovich, X. Y., & Raxmatovich, S. A. (2023). Study of dielectric permittivity and conductivity in the ionosphere. *American Journal of Applied Science and Technology*, *3*(03), 58–64.

Falayi, E. (2014). Equinoctial asymmetry of horizontal component of solar quiet variation Sq(H). *Advances in Physics Theories and Applications*, *38*, 22–29. https://core.ac.uk/download/pdf/234688372.pdf

Fang, T.-W., Akmaev, R., Fuller-Rowell, T., Wu, F., Maruyama, N., & Millward, G. (2013). Longitudinal and day-to-day variability in the ionosphere from lower atmosphere tidal forcing., *40*(11), 2523–2528. https://doi.org/10.1002/grl.50550

Feldstein, Y. I., & Levitin, A. E. (1986). Solar wind control of electric fields and currents in the ionosphere. *Journal of Geomagnetism and Geoelectricity*, *38*(11), 1143–1182. https://doi.org/10.5636/jgg.38.1143

Feldstein, Y. I., & Zaitzev, A. N. (1968). Quiet and disturbed solar-daily variations of magnetic field at high latitudes during the IGY. *Tellus*, *20*(2), 338–366. https://doi.org/10.1111/j.2153-3490.1968.tb00376.x

Fillion, M., Hulot, G., Alken, P., & Chulliat, A. (2023). Modeling the climatology of low- and mid-latitude f-region ionospheric currents using the SWARM constellation. *Journal of Geophysical Research: Space Physics*, *128*(5). https://doi.org/10.1029/2023JA031344

Fleetham, A. L., Milan, S. E., Imber, S. M., & Vines, S. K. (2023). Solar wind control of hemispherically-integrated field-aligned currents at Earth. *Journal of Geophysical Research: Space Physics*, *128*(8), e2023JA031540. https://doi.org/https://doi.org/10.1029/2023JA031540

Forbes, J. M. (1981). Atmospheric tides: A review. *Journal of Atmospheric and Terrestrial Physics*, *43*, 737–766. https://doi.org/10.1016/0021-9169(81)90111-2

Forbes, J. M., & Garrett, H. B. (1979). Solar tidal wind structures and the E-region dynamo. *Journal of Geomagnetism and Geoelectricity*, *31*(3), 173–182. https://doi.org/10.5636/jgg.31.173

Francia, P., Lepidi, S., Villante, U., Di Giuseppe, P., & Lazarus, A. J. (1999). Geomagnetic response at low latitude to continuous solar wind pressure variations during northward interplanetary magnetic field. *Journal of Geophysical Research: Space Physics*, *104*(A9), 19923–19930. https://doi.org/https://doi.org/10.1029/1999JA900229

Friis-Christensen, E., Lühr, H., & Hulot, G. (2006). SWARM: A constellation to study the Earth's magnetic field. *Earth, Planets and Space*, *58*, 351–358. https://doi.org/10.1186/bf03351933

Fukushima, N. (1979). Electric potential difference between conjugate points in middle latitudes caused by asymmetric dynamo in the ionosphere. *Journal of Geomagnetism and Geoelectricity*, *31*(3), 401–409. https://doi.org/10.5636/jgg.31.401

Fukushima, N. (1994). Some topics and historical episodes in geomagnetism and aeronomy. *Journal of Geophysical Research: Space Physics*, *99*, 19113–19142. https://doi.org/10.1029/94ja00102

Gasda, S., & Richmond, A. D. (1998). Longitudinal and interhemispheric variations of auroral ionospheric electrodynamics in a realistic geomagnetic field. *Journal of Geophysical Research: Space Physics*, *103*(A3), 4011–4021. https://doi.org/10.1029/97JA03243

Georgieva, K. (2011). Why the sunspot cycle is double peaked. *International Scholarly Research Notices*, *2011*(1), 437838. https://doi.org/10.5402/2011/437838

Gerontidou, M., Mavromichalaki, H., & Daglis, T. (2018). High-speed solar wind streams and geomagnetic storms during solar cycle 24. *Solar Physics*, *293*, 1–18. https://doi.org/10.1007/s11207-018-1348-8

Gjerloev, J. (2012). The SuperMAG data processing technique. *Journal of Geophysical Research: Space Physics*, *117*(A9). https://doi.org/10.1029/2012JA017683

Glatzmaiers, G. A., & Roberts, P. H. (1995). A three-dimensional self-consistent computer simulation of a geomagnetic field reversal. *Nature*, *377*(6546), 203–209. https://doi.org/10.1201/b12581-24

Gnevyshev, M. (1967). On the 11-years cycle of solar activity. *Solar Physics*, *1*, 107–120. https://doi.org/10.1007/BF00150306

Gold, T. (1959). Motions in the magnetosphere of the Earth. *Journal of Geophysical Research*, *64*(9), 1219–1224. https://doi.org/10.1029/jz064i009p01219

Gonzalez, W. D., Joselyn, J. A., Kamide, Y., Kroehl, H. W., Rostoker, G., Tsurutani, B. T., & Vasyliūnas, V. M. (1994). What is a geomagnetic storm?, *99*(A4), 5771–5792. https://doi.org/10.1029/93JA02867

Gopalswamy, N. (2006). Coronal mass ejections of solar cycle 23. *Journal of Astrophysics and Astronomy*, *27*(2-3), 243–254. https://doi.org/10.1007/BF02702527

Gupta, J. C. (1973). Movement of the Sq foci in 1958. *Pure and Applied Geophysics*, *110*, 2076–2084. https://doi.org/10.1007/bf00876572

Gvishiani, A., & Soloviev, A. (2020). *Observations, Modeling and Systems Analysis in Geomagnetic Data Interpretation*. Springer. https://doi.org/10.1007/978-3-030-58969-1

Gyébré, A. M. F., Gnabahou, D. A., & Ouattara, F. (2018). The geomagnetic effects of solar activity as measured at Ouagadougou station. *International Journal of Astronomy and Astrophysics*, *08*(02), 178–190. https://doi.org/10.4236/ijaa.2018.82013

Haberle, V., Marchaudon, A., Chambodut, A., & Blelly, P. L. (2022). Direct determination of geomagnetic baselines during quiet periods for low- and mid-latitude observatories. *Journal of Geophysical Research: Space Physics*, *127*(8). https://doi.org/10.1029/2022JA030407

Hady, A. A., Mostafa, M. H., & Samwel, S. W. (2015). Descriptive study of X-class flares released in the year 2014, during the double peak of SC-24. *Proceedings of the International Astronomical Union*, *11*(S320), 330–332. https://doi.org/10.1017/S1743921316000405

Hall, S. H. (1966). The magnetic field of the ionospheric dynamo. *Contemporary Physics*, *7*(6), 430–439. https://doi.org/10.1080/00107516608205485

Hamid, N. S. A., Liu, H., Uozumi, T., & Yumoto, K. (2013). Brief study of equatorial electrojet and global Sq currents at Southeast Asia region. *2013 IEEE International Conference on Space Science and Communication (IconSpace), Melaka, Malaysia (pp. 194-197). IEEE.* https://doi.org/10.1109/ICONSPACE.2013.6599463

Hamid, N. S. A., Liu, H., Uozumi, T., Yumoto, K., Veenadhari, B., Yoshikawa, A., & Sanchez, J. A. (2014). Relationship between the equatorial electrojet and global Sq currents at the dip equator region. *Earth, Planets and Space*, *66*, 1–11. https://doi.org/10.1186/S40623-014-0146-2

Hasegawa, M. (1960). On the position of the focus of the geomagnetic Sq current system. *Journal of Geophysical Research*, *65*(5), 1437–1447. https://doi.org/10.1029/jz065i005p01437

Hathaway, D. H. (2015). The solar cycle. *Living Reviews in Solar Physics*, *12*(1), 4. https://doi.org/10.1007/lrsp-2015-4

Hayakawa, M., Izutsu, J., Schekotov, A., Yang, S.-S., Solovieva, M., & Budilova, E. (2021). Lithosphere–atmosphere–ionosphere coupling effects based on multiparameter precursor observations for February–March 2021 earthquakes (M7) in the offshore of Tohoku area of Japan. *Geosciences*, *11*(11). https://doi.org/10.3390/geosciences11110481

Heilig, B., & Lühr, H. (2018). Quantifying the relationship between the plasmapause and the inner boundary of small-scale field-aligned currents, as deduced from SWARM observations. *Annales Geophysicae*, *36*(2), 595–607. https://doi.org/10.5194/angeo-36-595-2018

Herrmann, F., & Vorbach, T. (2020). The Geodynamo for Non-Geophysicists. *European Journal of Physics*, *41*(4), 045803. https://doi.org/10.1088/1361-6404/ab8780

Hibberd, F. H. (1981). Day-to-day variability of the Sq geomagnetic field variation. *Aust. J. Phys.*, *34*(1), 81–90. https://doi.org/10.1071/PH810081

Hobbs, B. A. (1981). A comparison of Sq analyses with model calculations. *Geophysical Journal International*, *66*(2), 435–444. https://doi.org/10.1111/J.1365-246X.1981.TB05965.X

Hwang, J., Kim, H.-P., & Park, Y.-D. (2012). Diurnal and seasonal variations in mid-latitude geomagnetic field during international quiet days: BOH magnetometer. *Journal of Astronomy and Space Sciences*, *29*(4), 329–336. https://doi.org/10.5140/jass.2012.29.4.329

Imajo, S., Matsuoka, A., Toh, H., & Iyemori, T. (2022). *Mid-latitude geomagnetic indices ASY and SYM(ASY/SYM indices)* (tech. rep.). World Data Center for Geomagnetism, Kyoto. https://doi.org/10.14989/267216

Iyemori, T. (1990). Storm-time magnetospheric currents inferred from mid-latitude geomagnetic field variations. *Journal of Geomagnetism and Geoelectricity*, *42*(11), 1249–1265. https://doi.org/10.5636/jgg.42.1249

Jacobs, J. (Ed.). (1987). *Geomagnetism, Volume 1*. Academic Press.

Jadhav, A. P., Yamazaki, Y., Gurubaran, S., Stolle, C., Conte, J. F., Batista, P. P., & Buriti, R. A. (2024). Quasi 16-day wave signatures in the interhemispheric field aligned currents: A new perspective toward atmosphere-ionosphere coupling. *Journal of Geophysical Research: Space Physics*, *129*(6). https://doi.org/10.1029/2023JA032383

Jankowski, J., & Sucksdorff, C. (1996). *IAGA Guide for Magnetic Measurements and Observatory Practice*. International Association of Geomagnetism & Aeronomy (IAGA).

Jault, D., Cardin, P., & Nataf, H. C. (1999). Geodynamo and M.H.D. In A. Alemany, P. Marty, & J. P. Thibault (Eds.), *Transfer Phenomena in Magnetohydrodynamic and Electroconducting Flows: Selected papers of the PAMIR Conference held in Aussois, France, 22–26 September 1997* (pp. 17–30). Springer. https://doi.org/"10.1007/978-94-011-4764-4_2"

Javaraiah, J., Rozelot, J. P., & Bertello, L. (2012). The solar cycle. *Advances in Astronomy*, *1*(470631). https://doi.org/10.1155/2012/470631

Jin, H., Miyoshi, Y., Fujiwara, H., Shinagawa, H., Terada, K., Terada, N., Ishii, M., Otsuka, Y., & Saito, A. (2011). Vertical connection from the tropospheric activities to the ionospheric longitudinal structure simulated by a new Earth's whole atmosphere-ionosphere coupled model. *Journal of Geophysical Research: Space Physics*, *116*(A1). https://doi.org/10.1029/2010JA015925

Joselyn, J. A. (1989). Geomagnetic quiet day selection. *Pure and Applied Geophysics*, *131*, 333–341. https://doi.org/10.1007/bf00876832

Kane, R. (1974). Relation between the strength of the Sq current system and its focus position. *Proceedings of the Indian Academy of Sciences-Section A*, *80*(1), 17–25. https://doi.org/10.1007/BF03046669

Kane, R. (1975). Day-to-day variability of ionospheric electron content at mid-latitudes. *Journal of Geophysical Research*, *80*(22), 3091–3099. https://doi.org/10.1029/JA080i022p03091

Kane, R. (2007). Latitude dependence of the "Gnevyshev" peaks and gaps. *Solar Physics*, *245*, 415–421. https://doi.org/10.1007/S11207-007-9031-5

Kaplan, K. (2024). The characteristic properties of solar activity in solar cycle 24. *Kinematics and Physics of Celestial Bodies*, *40*(2), 105–115. https://doi.org/10.3103/S0884591324020041

Kato, S. (1957). Horizontal wind systems in the ionospheric E region deduced from the dynamo theory of the geomagnetic Sq variation part IV. *Journal of Geomagnetism and Geoelectricity*, *9*(2), 107–115. https://doi.org/10.5636/jgg.9.107

Kawano-Sasaki, K., & Miyahara, S. (2008). A study on three-dimensional structures of the ionospheric dynamo currents induced by the neutral winds simulated by the Kyushu-GCM. *Journal of Atmospheric and Solar-Terrestrial Physics*, *70*(11-12), 1549–1562. https://doi.org/10.1016/j.jastp.2008.05.004

Kilpua, E., Koskinen, H. E. J., & Pulkkinen, T. I. (2017). Coronal mass ejections and their sheath regions in interplanetary space. *Living Reviews in Solar Physics*, *14*(1), 83. https://doi.org/10.1007/s41116-017-0009-6

Kivelson, M. G., & Russell, C. T. (1995). *Introduction to Space Physics*. Cambridge University Press.

Koch, S., & Kuvshinov, A. (2015). Does the South Atlantic Anomaly influence the ionospheric Sq current system? Inferences from analysis of ground-based magnetic data. *Earth, Planets and Space*, *67 (10)*. https://doi.org/10.1186/s40623-014-0172-0

Konik, R. M., Lanzerotti, L. J., Maclennan, C. G., Wolfe, A., & Venkatesan, D. (1995). Cusp latitude magnetic impulse events: 3. Associated low-latitude signatures. *Journal of Geophysical Research: Space Physics*, *100*(A5), 7731–7743. https://doi.org/https://doi.org/10.1029/94JA02327

Krainev, M., & Webber, W. (2004). The solar cycle in the heliospheric parameters and galactic cosmic ray intensity. *Proceedings of the International Astronomical Union*, *2004*(IAUS223), 81–84. https://doi.org/10.1017/S1743921304005150

Lanza, R., & Meloni, A. (2006). *The Earth's Magnetism: An Introduction for Geologists*. Springer. https://doi.org/10.1007/978-3-540-27980-8

Last, B. J., Emilia, D. A., & Outhred, A. K. (1976). AQD occurrence at Addis Ababa, Trivandrum and Alibag. *Planetary and Space Science*, *24*(6), 567–572. https://doi.org/10.1016/0032-0633(76)90134-3

Le Mouel, J. L., & Menvielle, M. (1982). Geomagnetic variation anomalies and deflection of telluric currents. *Geophysical Journal International*, *68*(3), 575–587. https://doi.org/10.1111/j.1365-246X.1982.tb04916.x

Le Sager, P., & Huang, T. (2002). Ionospheric currents and field-aligned currents generated by dynamo action in an asymmetric Earth magnetic field. *Journal of Geophysical Research: Space Physics*, *107*(A2), SIA–4. https://doi.org/10.1029/2001ja000211

Levitin, A. E., Afonina, R. G., Belov, B. A., & Feldstein, Y. A. (1982). Geomagnetic variation and field-aligned currents at Northern high-latitudes, and their relations to the solar wind parameters. *Philosophical Transactions of the Royal Society of London*, *304*, 253–301. https://doi.org/10.1098/rsta.1982.0013

Li, M., Yao, L., Wang, Y., Parrot, M., Hayakawa, M., Lu, J., Tan, H., & Xie, T. (2019). Anomalous phenomena in DC–ULF geomagnetic daily variation registered three days before the 12 May 2008 Wenchuan MS 8.0 earthquake. *Earth and Planetary Physics*, *3*(4), 330–341. https://doi.org/10.26464/epp2019034

Li, Y., Fraser, B. J., Menk, F. W., Webster, D. J., & Yumoto, K. (1998). Properties and sources of low and very low latitude Pi2 pulsations. *Journal of Geophysical Research: Space Physics*, *103*(A2), 2343–2358. https://doi.org/10.1029/97JA02921

Lindzen, R. S., & Chapman, S. (1969). Atmospheric tides. *Space Science Reviews*, *10*, 3–188. https://doi.org/10.1007/BF00171584

Liu, H. L., Wang, W., Richmond, A. D., & Roble, R. G. (2010). Ionospheric variability due to planetary waves and tides for solar minimum conditions. *Journal of Geophysical Research: Space Physics*, *115*(A6). https://doi.org/10.1029/2009JA015188

Liu, H.-L., Yudin, V. A., & Roble, R. G. (2013). Day-to-day ionospheric variability due to lower atmosphere perturbations. *Geophysical Research Letters*, *40*(4), 665–670. https://doi.org/10.1002/grl.50125

Liu, X., Han, P., Liu, Y., Xu, J., Hattori, K., Chen, H., Jiao, L., & Tu, J. (2025). North-South asymmetry of Sq variations at geomagnetically conjugate area. *Journal of Geophysical Research: Space Physics*, *130*(2). https://doi.org/10.1029/2024JA033507

Liu, Y., & Lu, C. (2010). The influence of the 11-year sunspot cycle on the atmospheric circulation during winter. *Chinese Journal of Geophysics*, *53*(3), 354–364. https://doi.org/10.1002/cjg2.1504

Liu, Y., Ren, Z., Wei, Y., & Zhou, X. (2024). A simulation study of the modulation of the geomagnetic field configuration on the seasonal variation of ionospheric Sq currents. *Journal of Geophysical Research: Space Physics*, *129*(3), e2023JA032180. https://doi.org/10.1029/2023ja032180

Lloyd, H. (1874). *A Treatise on Magnetism: General and Terrestrial*.

Love, J. J. (2008). Magnetic monitoring of Earth and space. *Physics Today*, *61*(2), 31–37. https://doi.org/10.1063/1.2883907

Love, J. J., & Rigler, E. J. (2014). The magnetic tides of Honolulu. *Geophysical Journal International*, *197*, 1335–1353. https://doi.org/10.1093/gji/ggu090

Lühr, H., & Maus, S. (2010). Solar cycle dependence of quiet-time magnetospheric currents and a model of their near-Earth magnetic fields. *Earth, planets and space*, *62*, 843–848. https://doi.org/10.5047/EPS.2010.07.012

Lühr, H., Kervalishvili, G., Michaelis, I., Rauberg, J., Ritter, P., Park, J., Merayo, J. M., & Brauer, P. (2015). The interhemispheric and F region dynamo currents revisited with the Swarm constellation. *Geophysical Research Letters*, *42*(9), 3069–3075. https://doi.org/10.1002/2015gl063662

Lühr, H., Kervalishvili, G. N., Stolle, C., Rauberg, J., & Michaelis, I. (2019). Average characteristics of low-latitude interhemispheric and F region dynamo currents deduced from the swarm satellite constellation. *Journal of Geophysical Research: Space Physics*, *124*(12), 10631–10644. https://doi.org/10.1029/2019JA027419

Lühr, H., Rother, M., Häusler, K., Alken, P., & Maus, S. (2008). The influence of nonmigrating tides on the longitudinal variation of the equatorial electrojet. *Journal of Geophysical Research: Space Physics*, *113*(A8). https://doi.org/10.1029/2008JA013064

Lyatskaya, S., Khazanov, G. V., & Zesta, E. (2014a). Interhemispheric field-aligned currents: Simulation results. *Journal of Geophysical Research: Space Physics*, *119*(7), 5600–5612. https://doi.org/10.1002/2013JA019558

Lyatskaya, S., Lyatsky, W., & Khazanov, G. V. (2014b). Effect of interhemispheric field-aligned currents on region-1 currents. *Geophysical Research Letters*, *41*(11), 3731–3737. https://doi.org/10.1002/2014GL060413

MacDougall, J. (1979). Equatorial electrojet and Sq current system-part II. *Journal of Geomagnetism and Geoelectricity*, *31*(3), 359–372. https://doi.org/10.5636/jgg.31.359

Maeda, H. (1955). Horizontal wind systems in the ionospheric E region deduced from the dynamo theory of the geomagnetic Sq variation. *Journal of Geomagnetism and Geoelectricity*, *7*(4), 121–132. https://doi.org/10.5636/jgg.7.121

Maeda, H. (1974). Field-aligned current induced by asymmetric dynamo action in the ionosphere. *Journal of Atmospheric and Terrestrial Physics*, *36*(8), 1395–1401. https://doi.org/10.1016/0021-9169(74)90216-5

Malin, S., & Gupta, J. (1977). The Sq current system during the International Geophysical Year. *Geophysical Journal International*, *49*(2), 515–529. https://doi.org/10.1111/j.1365-246x.1977.tb03720.x

Mandea, M., Korte, M., Mozzoni, D., & Kotzé, P. (2007). The magnetic field changing over the southern African continent: A unique behaviour. *South African Journal of Geology*, *110*(2-3), 193–202. https://doi.org/10.2113/gssajg.110.2-3.193

Mandea, M., Korte, M., Yau, A., & Petrovsky, E. (Eds.). (2019). *Geomagnetism, aeronomy and space weather: A journey from the earth's core to the sun* (Vol. 4). Cambridge University Press. https://doi.org/10.1017/9781108290135

Marchetti, D., Zhu, K., Piscini, A., Ghamry, E., Shen, X., Yan, R., He, X., Wang, T., Chen, W., Wen, J., Zhang, Y., Cheng, Y., Fan, M., Zhang, D., Zhang, H., & Ventura, G. (2024). Changes in the lithosphere, atmosphere, and ionosphere before and during the Mw = 7.7 Jamaica 2020 earthquake. *Remote Sensing of Environment*, *307*, 114146. https://doi.org/10.1016/j.rse.2024.114146

Martin, S. F. (2024). Observations key to understanding solar cycles: a review. *Frontiers in Astronomy and Space Sciences*, *10*. https://doi.org/10.3389/fspas.2023.1177097

Matsushita, S. (1967). Solar quiet and lunar daily variation fields. In S. Matsushita & W. H. Campbell (Eds.), *Physics of Geomagnetic Phenomena* (Vol. I). Academic Press.

Matsushita, S., & Maeda, H. (1965). On the geomagnetic solar quiet daily variation field during the IGY. *Journal of Geophysical Research*, *70*(11), 2535–2558. https://doi.org/10.1029/jz070i011p02535

Maus, S. (2016). International Geomagnetic Reference Field (IGRF) [Slide 3/17, PDF format]. https://cedarscience.org/sites/default/files/workshops/2016/igrf-2016.pdf

Mayaud, P. N., Menvielle, M., Berthelier, A., & Chambodut, A. (2023). Am geomagnetic index [dataset]. eost. https://doi.org/10.25577/et43-6h78

Mayaud, P.-N. (1965). Analyse morphologique de la variabilité jour-à-jour de la variation journalière régulière SR du champ magnétique terrestre, ii – le système de courants CM (régions non-polaires). *Annales de Géophysique*, 514–544.

Mayaud, P., & IAGA. (1967). IAGA bulletin no. 21: Atlas of K indices, text and figures. https://doi.org/10.25577/gb4j-zn77

McKenna, S. M. P. (1965). The International Years of the Quiet Sun. *Irish Astronomical Journal*, *7*, 4.

Menk, F. W., Waters, C. L., & Fraser, B. J. (2000). Field line resonances and waveguide modes at low latitudes: 1. Observations. *Journal of Geophysical Research: Space Physics*, *105*(A4), 7747–7761. https://doi.org/10.1029/1999JA900268

Menvielle, M., & Berthelier, A. (1991). The K-derived planetary indices: Description and availability. *Reviews of Geophysics*, *29*(3), 415–432. https://doi.org/https://doi.org/10.1029/91RG00994

Menvielle, M., Iyemori, T., Marchaudon, A., & Nosé, M. (2010). Geomagnetic indices. In M. Mandea & M. Korte (Eds.), *Geomagnetic Observations and Models* (pp. 183–228, Vol. 5). Springer. https://doi.org/10.1007/978-90-481-9858-0_8

Moldwin, M. (2008). *An Introduction to Space Weather*. Cambridge University Press. https://doi.org/10.1017/9781108866538

Moro, J., Denardini, C. M., Resende, L. C. A., Chen, S., & Schuch, N. J. (2016). Equatorial E region electric fields at the dip equator: 1. Variabilities in eastern Brazil and Peru. *Journal of Geophysical Research: Space Physics*, *121*(10), 10–220. https://doi.org/10.1002/2016JA022751

Morozova, A., Rebbah, R., & Pais, M. (2020). The solar quiet variation observed near the vortex focus: Effect of the geomagnetic activity and vortex dynamics on the Sq extraction. *ESS Open Archive*. https://doi.org/10.1002/essoar.10504878.1

Nicholls, R. W. (1993). The Upper Atmosphere and the Ionosphere. In R. N. DeWitt, D. Duston, & A. K. Hyder (Eds.), *The Behavior of Systems in the Space Environment* (pp. 103–116). Springer. https://doi.org/10.1007/978-94-011-2048-7_5

Nopper, R. W., Jr. (1978, January). *Ionospheric Electric Fields and Currents of Magnetospheric Origin.* [Doctoral dissertation, Boston College, Massachusetts].

Okeke, F. N., & Obiora, D. N. (2016). Application of solar quiet day (Sq) current in determining mantle electrical-depth conductivity structure: A review. *Journal of African Earth Sciences*, *114*, 54–62. https://doi.org/10.1016/j.jafrearsci.2015.11.015

Olsen, N. (1993). The solar cycle variability of lunar and solar daily geomagnetic variations. *Annales Geophysicae*, *11*(4), 254–262.

Olsen, N. (1997). Ionospheric F region currents at middle and low latitudes estimated from Magsat data. *Journal of Geophysical Research: Space Physics*, *102*(A3), 4563–4576. https://doi.org/10.1029/96ja02949

Olsen, N., & Kotsiaros, S. (2010). Magnetic Satellite Missions and Data. In M. K. M. Mandea (Ed.), *Geomagnetic Observations and Models* (pp. 27–44). Springer. https://doi.org/10.1007/978-90-481-9858-0_2,

Olsen, N., & Stolle, C. (2017). Magnetic signatures of ionospheric and magnetospheric current systems during geomagnetic quiet conditions—An overview. *Space Science Reviews*, *206*(1-4), 5–25. https://doi.org/10.1007/s11214-016-0279-7

Onovughe, E. (2015). *Geomagnetic diurnal variation studies using global models & observatory data at quiet & moderately disturbed times.* [Doctoral dissertation, University of Liverpool]. https://doi.org/10.17638/02032947

Onwumechili, A. (1992). Study of the return current of the equatorial electrojet. *Journal of Geomagnetism and Geoelectricity*, *44*(1), 1–42. https://doi.org/10.5636/JGG.44.1

Onwumechili, A., & Akasofu, S.-I. (1972). On the abnormal depression of Sq (H) under the equatorial electrojet in the afternoon. *Journal of Geomagnetism and Geoelectricity*, *24*(2), 161–173. https://doi.org/10.5636/jgg.24.161

Ouattara, F., & Amory-Mazaudier, C. (2012). Statistical study of the equatorial F_2 layer critical frequency at Ouagadougou during solar cycles 20, 21 and 22, using Legrand and Simon's classification of geomagnetic activity. *Journal of Space Weather and Space Climate*, *2*, A19. https://doi.org/10.1051/swsc/2012019

Owens, M. J., & Forsyth, R. J. (2013). The heliospheric magnetic field. *Living Reviews in Solar Physics*, *10*. https://doi.org/10.12942/lrsp-2013-5

Owolabi, C., Ruan, H., Yamazaki, Y., Kaka, R., Akinola, O., & Yoshikawa, A. (2022). Ionospheric current variations by empirical orthogonal function analysis: Solar activity dependence and longitudinal differences. *Journal of Geophysical Research: Space Physics*, *127*(1), e2021JA029903. https://doi.org/10.1029/2021JA029903

Owolabi, O. P., Bolaji, O. S., Adeniyi, J. O., Oyeyemi, E. O., Rabiu, A. B., & Habarulema, J. B. (2018). Excursions of interhemispheric field-aligned currents in Africa. *Journal of Geophysical Research: Space Physics*, *123*(7). https://doi.org/10.1029/2017JA025083

Panovska, S. (2024). Long-term changes of the geomagnetic field: Recent progress, challenges and applications. *EGU General Assembly 2024 Abstracts*. https://doi.org/10.5194/egusphere-egu24-10977

Park, J., Lühr, H., & Min, K. W. (2011). Climatology of the inter-hemispheric field-aligned current system in the equatorial ionosphere as observed by CHAMP. *Annales Geophysicae*, *29*(3), 573–582. https://doi.org/10.5194/angeo-29-573-2011

Park, J., Stolle, C., Yamazaki, Y., Rauberg, J., Michaelis, I., & Olsen, N. (2020). Diagnosing low-/mid-latitude ionospheric currents using platform magnetometers: CryoSat-2 and GRACE-FO. *Earth, Planets and Space*, *72*(1). https://doi.org/10.1186/s40623-020-01274-3

Parker, E. N. (1958). Dynamics of the interplanetary gas and magnetic fields. *Astrophysical Journal*, *128*, 664. https://doi.org/10.1086/146579

Patil, A., Arora, B. R., & Rastogi, R. G. (1983). Daily variation of the geomagnetic field near the focus of Sq-current system in Indian longitude. *Proceedings of the Indian Academy of Sciences - Earth and Planetary Sciences*, *92*(3), 239–245. https://doi.org/10.1007/bf02854592

Pedatella, N., Forbes, J., & Richmond, A. (2011). Seasonal and longitudinal variations of the solar quiet (Sq) current system during solar minimum determined by CHAMP satellite magnetic field observations. *Journal of Geophysical Research: Space Physics*, *116*(A4). https://doi.org/10.1029/2010JA016289

Pesnell, W. D. (2008). Predictions of solar cycle 24. *Solar Physics*, *252*(1), 209–220. https://doi.org/10.1007/s11207-008-9252-2

Pfaff, R. F., Jr., Acuña, M. H., Marionni, P. A., & Trivedi, N. B. (1997). DC polarization electric field, current density, and plasma density measurements in the daytime equatorial electrojet., *24*(13), 1667–1670. https://doi.org/10.1029/97GL01536

Pomerantz, M. A. (1964). Something new under the quiet sun. *Physics Today*, *17*(10), 19–31. https://doi.org/10.1063/1.3051171

Price, A. T. (1963). The noncyclic variation during quiet days. *Journal of Geophysical Research*, *68*(24), 6383–6389. https://doi.org/10.1029/jz068i024p06383

Price, A. T., & Wilkins, G. A. (1963). New methods for the analysis of geomagnetic fields and their application to the Sq field of 1932-3. *Philosophical Transactions of the Royal Society of London*, *256*(1066), 31–98. https://doi.org/10.1098/rsta.1963.0016

Pulkkinen, T. (2007). Space weather: Terrestrial perspective. *Living Reviews in Solar Physics*, *4*(1), 1. https://doi.org/10.12942/lrsp-2007-1

Rabiu, A., Mamukuyomi, A., & Joshua, E. (2007). Variability of equatorial ionosphere inferred from geomagnetic field measurements. *Bulletin of the Astronomical Society of India*, *35*(4), 607–618.

Rabiu, B., Ogunjo, S., Dare-Idowu, O., & Fuwape, I. (2025). Longitudinal variability of complexities associated with equatorial electrojet and its coupling with solar quiet daily variation Sq field. *Advances in Space Research*, *75*(1), 864–875. https://doi.org/10.1016/j.asr.2024.07.075

Ranasinghe, M., Fujimoto, A., Yoshikawa, A., & Jayaratne, C. (2021). Seasonal variation of inter-hemispheric field-aligned currents deduced from time-series analysis of the equatorial geomagnetic field data during solar cycle 23–24. *Earth, Planets and Space*, *73*(1). https://doi.org/10.1186/s40623-021-01481-6

Raouafi, N. E., Vourlidas, A., & Yongliang Zhang, L. (Eds.). (2021). *Solar Physics and Solar Wind*. https://doi.org/10.1002/9781119815600

Rasson, J. L. (2007). Observatories, Instrumentation. In D. Gubbins & E. Herrero-Bervera (Eds.), *Encyclopedia of Geomagnetism and Paleomagnetism* (pp. 710–717). Springer. https://doi.org/10.1007/978-1-4020-4423-6

Rastogi, R., & Crandra, H. (1996). On the disintegration of the vortex structure of ionospheric current system along Asian longitude sector. *Journal of Geomagnetism and Geoelectricity*, *48*(12), 1481–1488. https://doi.org/10.5636/jgg.48.1481

Rastogi, R., & Patil, A. (1992). On certain aspects of daily variation of geomagnetic field at low latitudes. *Journal of Geomagnetism and Geoelectricity*, *44*(7), 495–503. https://doi.org/10.5636/jgg.44.495

Rees, D. (1979). Mid-latitude winds and electric fields in the lower thermosphere and their relationship with the global Sq ionospheric current system. *Journal of Geomagnetism and Geoelectricity*, *31*, 267–285. https://doi.org/10.5636/jgg.31.267

Richards, P., & Torr, D. (1986). Thermal coupling of conjugate ionospheres and the tilt of the Earth's magnetic field. *Journal of Geophysical Research: Space Physics*, *91*(A8), 9017–9021. https://doi.org/10.1029/ja091ia08p09017

Richardson, I. G. (2018). Solar wind stream interaction regions throughout the heliosphere. *Living Reviews in Solar Physics*, *15*(1), 95. https://doi.org/10.1007/s41116-017-0011-z

Richmond, A. D. (1979). Ionospheric wind dynamo theory: A review. *Journal of Geomagnetism and Geoelectricity*, *31*(3), 287–310. https://doi.org/10.5636/jgg.31.287

Richmond, A. D. (1995). The Ionospheric Wind Dynamo: Effects of Its Coupling With Different Atmospheric Regions. In R. M. Johnson & T. L. Killeen (Eds.), *The Upper Mesosphere and Lower Thermosphere: A Review of Experiment and Theory* (pp. 49–65). American Geophysical Union (AGU). https://doi.org/10.1029/GM087p0049

Richmond, A. D. (2011). Electrodynamics of Ionosphere–Thermosphere Coupling. In M. A. Abdu & D. Pancheva (Eds.), *Aeronomy of the Earth's Atmosphere and Ionosphere* (pp. 191–201). Springer. https://doi.org/10.1007/978-94-007-0326-1_13

Richmond, A. D., Matsushita, S., & Tarpley, J. D. (1976). On the production mechanism of electric currents and fields in the ionosphere. *Journal of Geophysical Research: Space Research*, *81*(4), 547–555. https://doi.org/10.1029/JA081I004P00547

Richmond, A. D., & Roble, R. G. (1987). Electrodynamic effects of thermospheric winds from the NCAR Thermospheric General Circulation Model. *Journal of Geophysical Research: Space Physics*, *92*(A11), 12365–12376. https://doi.org/10.1029/ja092ia11p12365

Ripka, P. (2021). *Magnetic Sensors and Magnetometers*. Artech House.

Rourke, G. F. (1964). Magnetic quiet day relationships. *Nature*, *202*(4935), 891–891. https://doi.org/10.1038/202891a0

Russell, C. T. (2002). The solar wind interaction with the Earth's magnetosphere: A tutorial. *IEEE Transactions on Plasma Science*, *28*(6), 1818–1830. https://doi.org/10.1109/27.902211

Santos, Â. M., Abdu, M. A., Souza, J. R., Batista, I. S., & Sobral, J. H. (2017). Unusual behavior of quiet-time zonal and vertical plasma drift velocities over Jicamarca during the recent extended solar minimum of 2008. *Annales Geophysicae*, *35*(6), 1219–1229. https://doi.org/10.5194/angeo-35-1219-2017

Santos, Â. M., Brum, C. G., Batista, I. S., Sobral, J. H., Abdu, M. A., & Souza, J. R. (2022). Responses of intermediate layers to geomagnetic activity during the 2009 deep solar minimum over the Brazilian low-latitude sector. *Annales Geophysicae*, *40*(3), 259–269. https://doi.org/10.5194/angeo-40-259-2022

Sastri, J. H. (1982). Phase variability of Sq (H) on normal quiet days in the equatorial electrojet region. *Geophysical Journal International*, *71*(1), 187–197. https://doi.org/10.1111/j.1365-246x.1982.tb04992.x

Sato, S., Goto, T.-n., & Koike, K. (2020). Spatial gradients of geomagnetic temporal variations causing the instability of inter-station transfer functions. *Earth, Planets and Space*, *72*(1), 105. https://doi.org/10.1186/s40623-020-01231-0

Scheepers, G. L. M. (1978). Seasonal variation of the Sq focus over Southern Africa. *South African Journal of Science*, *74*(1), 15–21. https://doi.org/10.10520/AJA00382353_4900

Schieldge, J., Venkateswaran, S., & Richmond, A. D. (1973). The ionospheric dynamo and equatorial magnetic variations. *Journal of Atmospheric and Terrestrial Physics*, *35*(6), 1045–1061. https://doi.org/10.1016/0021-9169(73)90004-4

Schlapp, D., Mann, R., & Butcher, E. (1988). On the relation between days of small amplitude of Sq (H) and abnormal quiet days. *Geophysical Journal International*, *95*(3), 633–639. https://doi.org/10.1111/j.1365-246x.1988.tb06709.x

Schmucker, U. (1999). A spherical harmonic analysis of solar daily variations in the years 1964–1965: Response estimates and source fields for global induction: II. Results. *Geophysical Journal International*, *136*(2), 455–476. https://doi.org/10.1046/j.1365-246x.1999.00743.x

Schnepf, N. R., Nair, M., Maute, A., Pedatella, N. M., Kuvshinov, A., & Richmond, A. D. (2018). A comparison of model-based ionospheric and ocean tidal magnetic signals with observatory data. *Geophysical Research Letters*, *45*(15), 7257–7267. https://doi.org/10.1029/2018gl078487

Schwenn, R. (2006). Space weather: The solar perspective. *Living Reviews in Solar Physics*, *3*(1), 2. https://doi.org/10.12942/lrsp-2006-2

Shahzad, R., Shah, M., Tariq, M. A., Calabia, A., Melgarejo-Morales, A., Jamjareegulgarn, P., & Liu, L. (2023). Ionospheric–thermospheric responses to geomagnetic storms from multi-instrument space weather data. *Remote Sensing*, *15*(10), 2687. https://doi.org/10.3390/rs15102687

Sharma, S. S., Singh, R. P., Pundhir, D., & Singh, B. (2021). Lithospheric electromagnetic emissions associated with some major earthquakes occurred in Indian subcontinent. *Geomagnetism and Aeronomy*, *61*(4), 619–631. https://doi.org/10.1134/S0016793221040150

Shinbori, A., Koyama, Y., Nosé, M., Hori, T., & Otsuka, Y. (2017). Characteristics of seasonal variation and solar activity dependence of the geomagnetic solar quiet daily variation. *Journal of Geophysical Research: Space Physics*, *122*(10), 10–796. https://doi.org/10.1002/2017ja024342

Shinbori, A., Koyama, Y., Nose, M., Hori, T., Otsuka, Y., & Yatagai, A. (2014). Long-term variation in the upper atmosphere as seen in the geomagnetic solar quiet daily variation. *Earth, Planets and Space*, *66*, 1–20. https://doi.org/10.1186/s40623-014-0155-1

Shiraki, M. (1973). Variations of focus latitude and intensity of overhead current system of Sq with the solar activity. *Memoirs of the Kakioka Magnetic Observatory*, *15*(2). https://cir.nii.ac.jp/crid/1570291225069797376

Singh, A., & Patel, K. (2021). Statistical study of solar activity parameters of solar cycle 24. *Journal of Scientific Research*, *65*, 197–200. https://doi.org/10.37398/JSR.2021.650125

Sinha, A., P, V., & BM, P. (2010). Solar wind-magnetosphere-ionosphere coupling: Pi2 observations. *Indian Journal of Radio Space Physics*, *39*, 257–264.

Smit, J. (2007). In A. Moliton (Ed.), *Basic Electromagnetism and Materials* (pp. 89–118). Springer New York. https://doi.org/10.1007/978-0-387-49368-8_3

Soloviev, A., Smirnov, A., Gvishiani, A., Karapetyan, J., & Simonyan, A. (2019). Quantification of Sq parameters in 2008 based on geomagnetic observatory data. *Advances in Space Research*, *64*(11), 2305–2320. https://doi.org/10.1016/j.asr.2019.08.038

Sreenivasan, B. (2010). Modelling the geodynamo: Progress and challenges. *Current Science*, *99*(12), 1739–1750. Retrieved July 20, 2025, from http://www.jstor.org/stable/24073497

Stacey, F. D., & Davis, P. M. (2008). *Physics of the Earth*. Cambridge University Press.

Stening, R., Reztsova, T., Ivers, D., Turner, J., & Winch, D. (2005). A critique of methods of determining the position of the focus of the Sq current system. *Journal of Geophysical Research: Space Physics*, *110*. https://doi.org/10.1029/2004JA010784

Stening, R. J. (1977). Field-aligned currents driven by the ionospheric dynamo. *Journal of Atmospheric and Terrestrial Physics*, *39*(8), 933–937. https://doi.org/10.1016/0021-9169(77)90175-1

Stening, R. J. (1989). A calculation of ionospheric currents due to semidiurnal antisymmetric tides. *Journal of Geophysical Research: Space Physics*, *94*(A2), 1525–1531. https://doi.org/10.1029/ja094ia02p01525

Stening, R. J. (1995). Variations in the strength of the Sq current system. *Annales Geophysicae*, *13*, 627–632. https://doi.org/10.1007/s00585-995-0627-5

Stening, R. J. (2008). The shape of the Sq current system. *Annales Geophysicae*, *26*(7), 1767–1775. https://doi.org/10.5194/ANGEO-26-1767-2008

Stening, R. J., & Winch, D. E. (2013). The ionospheric Sq current system obtained by spherical harmonic analysis. *Journal of Geophysical Research: Space Physics*, *118*(3), 1288–1297. https://doi.org/10.1002/jgra.50194

Sugiura, M., & Poros, D. J. (1971). *Hourly values of equatorial Dst for the years 1957 to 1970* (tech. rep. No. NASA-TM-X-65645). NASA Goddard Space Flight Center. Greenbelt, MD. https://ntrs.nasa.gov/api/citations/19710022962/downloads/19710022962.pdf

Svalgaard, L. (2016). Reconstruction of solar extreme ultraviolet flux 1740–2015. *Solar Physics*, *291*(9), 2981–3010. https://doi.org/10.1007/s11207-016-0921-2

Takeda, M. (2016). Long-term variation of Ampère force by geomagnetic Sq currents and their relation to ionospheric conductivity. *Journal of Geophysical Research: Space Physics*, *121*, 11407–11412. https://doi.org/10.1002/2016JA022845

Takeda, M. (1982). Three dimensional ionospheric currents and field aligned currents generated by asymmetrical dynamo action in the ionosphere. *Journal of Atmospheric and Terrestrial Physics*, *44*(2), 187–193. https://doi.org/10.1016/0021-9169(82)90122-2

Takeda, M. (1990). Geomagnetic field variation and the equivalent current system generated by an ionospheric dynamo at the solstice. *Journal of Atmospheric and Terrestrial Physics*, *52*(1), 59–67. https://doi.org/10.1016/0021-9169(90)90115-4

Takeda, M. (1993). Geomagnetic field variation on the ground by the electric currents in the oceans induced by the geomagnetic Sq field. *Journal of Geomagnetism and Geoelectricity*, *45*(6), 487–493. https://doi.org/10.5636/jgg.45.487

Takeda, M. (1999). Time variation of global geomagnetic Sq field in 1964 and 1980. *Journal of Atmospheric and Solar-Terrestrial Physics*, *61*(10), 765–774.

Takeda, M. (2002). The correlation between the variation in ionospheric conductivity and that of the geomagnetic sq field. *Journal of Atmospheric and Solar-Terrestrial Physics*, *64*(15), 1617–1621.

Takeda, M. (2013). Contribution of wind, conductivity, and geomagnetic main field to the variation in the geomagnetic Sq field. *Journal of Geophysical Research: Space Physics*, *118*(7), 4516–4522. https://doi.org/10.1002/JGRA.50386

Takeda, M., & Maeda, H. (1980). Three-dimensional structure of ionospheric currents 1. Currents caused by diurnal tidal winds. *Journal of Geophysical Research: Space Physics*, *85*(A12), 6895–6899. https://doi.org/10.1029/JA085iA12p06895

Takeda, M., & Yamada, Y. (1989). Quasi two-day period variation of the geomagnetic field. *Journal of Geomagnetism and Geoelectricity*, *41*(5), 469–478. https://doi.org/10.5636/jgg.41.469

Talha, M., Murtaza, G., Rasson, J. L., Ahmed, N., & Peerzada, M. (2021). Sq (H) field variations at Sonmiani geomagnetic observatory, Pakistan for solar cycle 24. *Advances in Space Research*, *67*(1), 66–74. https://doi.org/10.1016/j.asr.2020.09.013

Tarpley, J. (1973). Seasonal movement of the Sq current foci and related effects in the equatorial electrojet. *Journal of Atmospheric and Terrestrial Physics*, *35*(6), 1063–1071. https://doi.org/10.1016/0021-9169(73)90005-6

Telford, W. M., Geldart, L. P., & Sheriff, R. E. (1990). *Applied Geophysics*. Cambridge University Press. https://doi.org/10.1017/CBO9781139167932

Temmer, M. (2021). Space weather: The solar perspective. *Living Reviews in Solar Physics*, *18*(1), 80. https://doi.org/10.1007/s41116-021-00030-3

Tenfjord, P., Østgaard, N., Strangeway, R., Haaland, S., Snekvik, K., Laundal, K. M., Reistad, J. P., & Milan, S. E. (2017). Magnetospheric response and reconfiguration times following IMF B_y reversals. *Journal of Geophysical Research: Space Physics*, *122*(1), 417–431. https://doi.org/10.1002/2016ja023018

Thébault, E., Finlay, C. C., Beggan, C. D., Alken, P., Aubert, J., Barrois, O., Bertrand, F., Bondar, T., Boness, A., Brocco, L., et al. (2015). International Geomagnetic Reference Field: The 12th Generation. *Earth, Planets and Space*, *67*, 1–19. https://doi.org/10.1186/s40623-015-0228-9

Tian, L., Du, A., Huang, S., Luo, H., Xu, W., & Ge, Y. (2022). Effect of the non-dipole field on the seasonal variation of the geomagnetic Sq(Y). *Journal of Geophysical Research: Space Physics*, *127*(10). https://doi.org/10.1029/2022JA030441

Titheridge, J. E. (1995). Winds in the ionosphere - A review. *Pergamon Journal of Atmospheric and Terrestrial Physics*, *57*(14), 1681–1714. https://doi.org/10.1016/0021-9169(95)00091-7

Torta, J. M., Curto, J. J., & Bencze, P. (1997). Behavior of the quiet day ionospheric current system in the European region. *Journal of Geophysical Research: Space Physics*, *102*(A2), 2483–2494. https://doi.org/10.1029/96ja03463

Trenkin, A. A. (2015). Possible influence of telluric current on seismicity of the Earth's crust in seismoactive zones. *Geomagnetism and Aeronomy*, *55*(1), 133–138. https://doi.org/10.1134/S0016793215010119

Tsunomura, S. (1999). Numerical analysis of global ionospheric current system including the effect of equatorial enhancement. *Annales Geophysicae*, *17*(5), 692–706. https://doi.org/10.1007/s00585-999-0692-2

Tsurutani, B. T., Gonzalez, W. D., Tang, F., Akasofu, S. I., & Smith, E. J. (1988). Origin of interplanetary southward magnetic fields responsible for major magnetic storms near solar maximum (1978–1979). *Journal of Geophysical Research: Space Physics*, *93*(A8), 8519–8531. https://doi.org/10.1029/JA093iA08p08519

Tsurutani, B. T., & Lakhina, G. S. (1997). Some basic concepts of wave-particle interactions in collisionless plasmas. *Reviews of Geophysics*, *35*(4), 491–501. https://doi.org/10.1029/97RG02200

Ugwu, E. B. I., & Okeke, C. E. (2021). On the variation of geomagnetic H-component during solar quiet days. *European Journal of Applied Physics*, *3*(2), 11–15. https://doi.org/10.24018/ejphysics.2021.3.2.35

Van Sabben, D. (1964). North-south asymmetry of Sq. *Journal of Atmospheric and Terrestrial Physics*, *26*(12), 1187–1195. https://doi.org/10.1016/0021-9169(64)90127-8

Van Sabben, D. (1966). Magnetospheric currents, associated with the N-S asymmetry of Sq. *Journal of Atmospheric and Terrestrial Physics*, *28*(10), 965–982. https://doi.org/10.1016/s0021-9169(17)30026-0

Van Sabben, D. (1969). The computation of magnetospheric currents, caused by dynamo action in the ionosphere. *Journal of Atmospheric and Terrestrial Physics*, *31*(3), 469–474. https://doi.org/10.1016/0021-9169(69)90072-5

Van Sabben, D. (1970). Solstitial Sq-currents through the magnetosphere. *Journal of Atmospheric and Terrestrial Physics*, *32*(7), 1331–1336. https://doi.org/10.1016/0021-9169(70)90064-4

Vasiljeva, I., & Pishkalo, M. (2021). History of sunspot research and forecast of the maximum of solar cycle 25. *Kinematics and Physics of Celestial Bodies*, *37*(4), 200–211. https://doi.org/10.3103/S0884591321040073

Vasyliūnas, V. M. (1970). Mathematical Models of Magnetospheric Convection and Its Coupling to the Ionosphere. In B. M. McCormack & A. Renzini (Eds.), *Particles and field in the magnetosphere* (p. 60, Vol. 17). https://doi.org/10.1007/978-94-010-3284-1_6

Vasyliūnas, V. M. (2012). The physical basis of ionospheric electrodynamics. *Annales Geophysicae*, *30*(2), 357–369. https://doi.org/10.5194/angeo-30-357-2012

Veenadhari, B., & Alex, S. (2006). Space weather effects on low latitude geomagnetic field and ionospheric plasma response. In N. Gopalswamy & A. Bhattacharya (Eds.), *Proceedings of the ILWS Workshop on Solar Influence on the Heliosphere and Earth's Environment: Recent Progress and Prospects* (pp. 395–398). Quest Publications. https://cdaw.gsfc.nasa.gov/publications/ilws_goa2006/395_Veenadhari.pdf

Vervelidou, F. (2013). *Contribution à la modélisation et à l'interprétation multi-échelle du champ magnétique de la lithosphère terrestre* [PhD thesis]. Université Paris Diderot, Paris Institute of Global Physics (IPGP). http://www.theses.fr/2013PA077261

Vichare, G., Rawat, R., Hanchinal, A., Sinha, A. K., Dhar, A., & Pathan, B. M. (2012). Seasonal evolution of Sq current system at sub-auroral latitude. *Earth, Planets and Space*, *64*, 1023–1031. https://doi.org/10.5047/eps.2012.04.007

Vichare, G., Rawat, R., Jadhav, M., & Sinha, A. K. (2017). Seasonal variation of the Sq focus position during 2006–2010. *Advances in Space Research*, *59*(2), 542–556. https://doi.org/10.1016/j.asr.2016.10.009

Vieira, L. E. A., Gonzalez, W. D., Echer, E., Guarnieri, F. L., Prestes, A., Gonzalez, A. L. C., Santos, J. C., Dal Lago, A., & Schuch, N. J. (2003). Multi-scale analysis of the geomagnetic symmetric index (sym). *Solar Physics*, *217*(2), 383–394. https://doi.org/10.1023/B:SOLA.0000006858.86646.9f

Viljanen, A., Juusola, L., Vanhamäki, H., & Smirnov, M. (2020). Telluric currents play a big role in interpreting geomagnetic variations. *EGU General Assembly Conference Abstracts*, 2020–2309. https://doi.org/10.5194/egusphere-egu2020-2309

Wagner, C.-U., Möhlmann, D., Schäfer, K., Mishin, V., & Matveev, M. (1980). Large-scale electric fields and currents and related geomagnetic variations in the quiet plasmasphere. *Space Science Reviews*, *26*(4), 391–446. https://doi.org/10.1007/bf00217388

Wang, F., Lühr, H., Xiong, C., Park, J., & Zhou, Y. (2023). Global characteristics of improved interhemispheric field-aligned currents and of F-region meridional currents observed by the Swarm dual-spacecraft. *Journal of Geophysical Research: Space Physics*, *128*(2). https://doi.org/10.1029/2022JA031096

Wang, J., Yang, D., Zhang, S., & Zhu, R. (2011). Research on the distribution of geomagnetic daily variation along some station chains in China. *Data Science Journal*, *10*, IAGA183–IAGA191. https://doi.org/10.2481/dsj.IAGA-26

Wanliss, J. (2005). Fractal properties of SYM-H during quiet and active times. *Journal of Geophysical Research: Space Physics*, *110*(A3). https://doi.org/10.1029/2004JA010544

Wanliss, J., & Showalter, K. M. (2006). High-resolution global storm index: Dst versus SYM-H. *Journal of Geophysical Research: Space Physics*, *111*(A2). https://doi.org/10.1029/2005JA011034

Wickramasinghe, N., Steele, E. J., Wainwright, M., Tokoro, G., Fernando, M., & Qu, J. (2017). Sunspot cycle minima and pandemics: The case for vigilance. *Astrobiol Outreach*, *5*(2), 2332–2519. https://doi.org/10.4172/2332-2519.1000159

Wolf, R. (1859). *Mittheilungen über die Sonnenflecken* (Vol. 9). https://ngzh.ch/wp-content/uploads/2024/07/5_3.pdf

Wu, Y., Liu, L., & Ren, Z. (2021). Equinoctial asymmetry in solar quiet fields along the 120° E meridian chain. *Applied Sciences*, *11*(19). https://doi.org/10.3390/app11199150

Yacob, A., & Sen, A. (1974). On quiet-day maximum minimum and range in H. *Pure and Applied Geophysics*, *112*, 464–471. https://doi.org/10.1007/bf00876154

Yamashita, S., & Iyemori, T. (2002). Seasonal and local time dependences of the interhemispheric field-aligned currents deduced from the Ørsted satellite and the ground geomagnetic observations. *Journal of Geophysical Research: Space Physics*, *107*(A11), SIA–11. https://doi.org/10.1029/2002ja009414

Yamazaki, A., Shigeno, N., & Yamamoto, T. (2011a). Magnetic anomaly caused by soil excavation and its long-term stability: Case study of a magnetic anomaly in the absolute observation house at Kanoya Magnetic Observatory. *Technical Report of the Kakioka Magnetic Observatory*, *10*(1,2), 1–12. https://www.kakioka-jma.go.jp/publ/journal_DB/abstract?no=1137&

Yamazaki, Y., & Maute, A. (2017). Sq and EEJ - A review on the daily variation of the geomagnetic field caused by ionospheric dynamo currents. *Space Science Reviews*, *206*, 299–405. https://doi.org/10.1007/s11214-016-0282-z

Yamazaki, Y., Yumoto, K., Cardinal, M. G., Fraser, B. J., Hattori, P., Kakinami, Y., Liu, J. Y., Lynn, K. J. W., Marshall, R., McNamara, D., Nagatsuma, T., Nikiforov, V. M., Otadoy, R. E., Ruhimat, M., Shevtsov, B. M., Shiokawa, K., Abe, S., Uozumi, T., & Yoshikawa, A. (2011b). An empirical model of the quiet daily geomagnetic field variation. *Journal of Geophysical Research: Space Physics*, *116*(A10). https://doi.org/10.1029/2011JA016487

Yamazaki, Y. (2015). Introduction to geomagnetic Sq variations [Slide 18/21, PDF format].

Yamazaki, Y., Häusler, K., & Wild, J. (2016). Day-to-day variability of midlatitude ionospheric currents due to magnetospheric and lower atmospheric forcing. *Journal of Geophysical Research: Space Physics*, *121*(7), 7067–7086. https://doi.org/10.1002/2016JA022817

Yamazaki, Y., Richmond, A., Maute, A., Liu, H.-L., Pedatella, N., & Sassi, F. (2014). On the day-to-day variation of the equatorial electrojet during quiet periods. *Journal of Geophysical Research: Space Physics*, *119*(8), 6966–6980. https://doi.org/10.1002/2014JA020243

Yamazaki, Y., & Richmond, A. D. (2013). A theory of ionospheric response to upward-propagating tides: Electrodynamic effects and tidal mixing effects. *Journal of Geophysical Research: Space Physics*, *118*(9), 5891–5905. https://doi.org/10.1002/jgra.50487

Yamazaki, Y., Richmond, A. D., Liu, H., Yumoto, K., & Tanaka, Y. (2012). Sq current system during stratospheric sudden warming events in 2006 and 2009. *Journal of Geophysical Research: Space Physics*, *117*(A12). https://doi.org/10.1029/2012JA018116

Yu, Y., Cao, J., Pu, Z., Jordanova, V. K., & Ridley, A. (2022). Meso-scale electrodynamic coupling of the Earth magnetosphere-ionosphere system. *Space Science Reviews*, *218*(8), 74. https://doi.org/10.1007/s11214-022-00940-0

Zhang, P., Sun, Y.-Y., Chen, C.-H., Yisimayili, A., & Mao, Z. (2024). Non-migrating thermospheric tides shift and deform the solar quiet current vortex over Asia. *Journal of Geophysical Research: Space Physics*, *129*(12). https://doi.org/10.1029/2023JA032381

Zhang, R., Liu, L., Chen, Y., Le, H., & Li, W. (2023). The Stratosphere-Ionosphere-Protonosphere coupling: Evidence from the ion composition observations during the 2009 Sudden Stratospheric Warming. *Geophysical Research Letters*, *50*(2). https://doi.org/10.1029/2022GL101707

Zhang, X., & Zhao, Y. (2008). Analysis of key technologies in geomagnetic navigation. *Proceedings SPIE 7128, Seventh International Symposium on Instrumentation and Control Technology: Measurement Theory and Systems and Aeronautical Equipment*, *7128*, 571–576. https://doi.org/10.1117/12.807129

Zhao, X., He, Y., Wu, Y., & Li, Q. (2022). Equivalent current systems of quiet ionosphere during the 24th solar cycle derived from the geomagnetic records in China. *Atmosphere*, *13*(11), 1843. https://doi.org/10.3390/atmos13111843

Zhao, X.-D., Yang, D.-M., He, Y.-F., Yu, P.-Q., Liu, X.-C., Zhang, S.-Q., Luo, K.-Q., & Hu, X.-J. (2014). The study of Sq equivalent current during the solar cycle. *Chinese Journal of Geophysics*, *57*(11), 3777–3788. https://doi.org/10.6038/cjg20141131

Zou, Z., Huang, H., Zuo, P., Ni, B., San, W., Yuan, Q., Hu, J., & Wei, J. (2024). A forecast model of geomagnetic indices from the solar wind fluids observations based on long short-term memory neural network. *Physics of Fluids*, *36*(2). https://doi.org/10.1063/5.0196284